

Old Dominion University

ODU Digital Commons

Engineering Management & Systems
Engineering Theses & Dissertations

Engineering Management & Systems
Engineering

Summer 2012

Response Surface Optimization of Electron Beam Freeform Fabrication Depositions Using Design of Experiments

Patricia A. Quigley
Old Dominion University

Follow this and additional works at: https://digitalcommons.odu.edu/emse_etds



Part of the [Applied Statistics Commons](#), [Mathematics Commons](#), [Probability Commons](#), [Structures and Materials Commons](#), and the [Systems Engineering and Multidisciplinary Design Optimization Commons](#)

Recommended Citation

Quigley, Patricia A.. "Response Surface Optimization of Electron Beam Freeform Fabrication Depositions Using Design of Experiments" (2012). Master of Science (MS), Thesis, Engineering Management & Systems Engineering, Old Dominion University, DOI: 10.25777/2ytc-7298
https://digitalcommons.odu.edu/emse_etds/224

This Thesis is brought to you for free and open access by the Engineering Management & Systems Engineering at ODU Digital Commons. It has been accepted for inclusion in Engineering Management & Systems Engineering Theses & Dissertations by an authorized administrator of ODU Digital Commons. For more information, please contact digitalcommons@odu.edu.

RESPONSE SURFACE OPTIMIZATION OF
ELECTRON BEAM FREEFORM FABRICATION DEPOSITIONS USING
DESIGN OF EXPERIMENTS

by

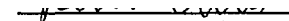
Patricia A. Quigley
B.S. May 2007, Strayer University

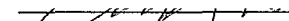
A Thesis Submitted to the Faculty of
Old Dominion University in Partial Fulfillment of the
Requirements for the Degree of


MASTER OF SCIENCE
ENGINEERING MANAGEMENT

OLD DOMINION UNIVERSITY
August 2012

Approved by:


Resit Unal (Advisor)


Ariel Pinto (Member)


Charles Daniels (Member)

ABSTRACT

RESPONSE SURFACE OPTIMIZATION OF ELECTRON BEAM FREEFORM FABRICATION DEPOSITIONS USING DESIGN OF EXPERIMENTS

Patricia Quigley
Old Dominion University, 2012
Director: Dr. C. Ariel Pinto

The Electron Beam Freeform Fabrication (EBF³) System is a material depositing, layer additive technique that produces three dimensional (3D) parts out of a wide range of metals in high vacuum, using an electron beam and wire feedstock. Screening deposition trials on a titanium alloy, Ti-6Al-4V, at the National Aeronautics Space Administration (NASA) revealed selective vaporization of the aluminum content of linear prototypes when subjected to chemical analysis. In this study, the aluminum content, bead height and bead width output responses were analyzed from a systematic study of the effects that the interactions of the EBF³ processing parameters had on the finished parts. Results were derived from mathematical models (equations) using regression and the Analysis of Variance (ANOVA) statistics. These models were used to predict the optimum values of the processing parameters to promote the maximum aluminum content and optimal bead geometry to support future validation experiments. Optimization of EBF³ processing is vital to realizing the vision of manufacturing high quality and reliable replacement parts for space transportation.

Copyright, 2012, by Patricia A. Quigley, All Rights Reserved.

This thesis is dedicated to my parents, Alfred and Barbara Visciarelli, in love and appreciation for encouraging me to achieve my dreams.

ACKNOWLEDGEMENTS

My sincere thanks are extended to the many people who made the development of this thesis possible.

I would first like to thank Cynthia L. Lach of the Advanced Materials and Processes Branch (AMPB) at National Aeronautics and Space Administration (NASA) Langley Research Center (LaRC) for dedicating many months of scientific guidance and technical expertise as my mentor, for training me in the use of Design-Expert ®, for reviewing the drafts of this thesis, and for becoming a great friend.

Thanks also to Lawrence Green of the Vehicle Analysis Branch at NASA LaRC for guidance on the use of Design of Experiments, and especially with the Design-Expert ® software and Response Surface Method (RSM) modeling techniques. Thank you also for thoroughly reviewing my drafts.

I am sincerely grateful to Dr. Resit Unal of Old Dominion University, for offering to be my advisor and for the suggestion to take the Robust Engineering Design course during my work on the EBF³ experiment analysis. The course proved to be invaluable in working with the optimization techniques necessary for this project. I would also like to thank him for being available for meetings and for attending the EBF³ deposition at NASA LaRC, and for the timely and patient responses to all of my questions.

My thanks are also extended to Karen Taminger of the AMPB at NASA LaRC for welcoming me to the AST community as a student, and for authorizing the purchase of the much needed Design-Expert ® software used in the computational analyses.

I am so grateful for the suggestions and comments on this thesis offered by Bill Seufzer, PhD, Computational Scientist of the AMPB, NASA LaRC. In addition, the

career and educational discussions we have had over the years have been invaluable. I consider him one of my role models.

I would also like to thank Richard Martin, Lead Engineering Technician, of the Fabrication Processes section at NASA LaRC for his time in explaining the features, functions and settings of the EBF³ machine and the associated computer system.

Thank you to Dr. Charlie Daniels, Professor at Old Dominion University, for accepting my request to serve as a member on my committee and for the time dedicated to reviewing this thesis.

Thank you to Dr. C. Pinto for all of the sound advice given during the thesis planning and consultation, and especially for introducing me to Dr. Resit. The connection was perfectly timed with the course he was teaching and perfectly aligned with the interests of my NASA colleagues and the project.

I would also like to express my sincere gratitude to the Virginia Air National Guard for fully funding my entire Master's degree.

Thanks also to my employer, Science Systems Applications, Inc., SSAI, for funding my undergraduate degree making graduate studies possible. I hold Om Bahethi, President of SSAI, in the highest regard for his work ethic, and offer my sincere gratitude for the generosity and kindness he bestows on his employees.

My appreciation extends also to Strayer University for accepting credits I earned from colleges all over the world while I was serving on active duty with the United States Air Force. The degree served as a sound platform for acceptance into the Old Dominion University Engineering Management degree program.

Thank you to my children, Renee, Jennifer and Sara for their support and patience during my study times. I hope that through my efforts on this degree that they understand how important education is to a successful life and that by continually challenging my potential, I have set an example for them to follow.

Last, but most importantly, thank you God, for directing the paths of my life.
Where You lead, I will follow.

NOMENCLATURE

df	degrees of freedom (units)
mm	millimeters (length)
ipm	inches per minute (speed)
kW	kilowatt (power)
torr	Torr (pressure)
wt %	percent of total weight (weight)
in	inches (length)
ss	sum of squares (units)

TABLE OF CONTENTS

	Page
NOMENCLATURE	viii
LIST OF TABLES	xii
LIST OF FIGURES	xiv
1. INTRODUCTION	1
1.0 Background	1
1.1 Scope	2
1.2 Purpose	4
1.3 Research Problem	5
1.4 Analysis Strategy	6
2. LITERATURE REVIEW	8
2.0 Introduction	8
2.1 EBF ³ System	9
2.2 Benefits of EBF ³	11
2.3 EBF ³ Application	12
2.4 EBF ³ Limitations	13
2.5 Ti-6Al-4V Alloy	13
2.6 Design of Experiment (DOE)	13
2.7 Math Models	18
2.8 Transformations	18
2.9 Validation	19
2.10 Literature Review Summary	19
3. METHODOLOGY	21
3.0 Experimental Method	21

	Page
3.1 System Design	22
3.2 Initiate EBF3	24
3.3 EBF ³ Cool-Down Process	25
3.4 Extract Finished EBF ³ Deposits	25
3.5 Chemical Analysis.....	25
3.6 Observation	26
3.7 Proposed Solution.....	27
3.8 Analysis Methodology	31
 4. ANALYSIS and RESULTS.....	 35
4.0 Analysis Overview	35
4.1 Analysis Approach	35
4.2 Assumptions	36
4.3 Analysis of Visual Inspection of Deposit Samples	36
4.4 Regression Analysis for Non-Transformed Response Data	41
4.5 Math Models for Response Data	50
4.6 Processing Levels for Response Data	52
4.7 Contour Plots for Response Data	53
4.8 Transformation Overview	56
4.9 SQRT(x) Transformation and Regression of BH Response Data	58
4.10 Math Model for SQRT Transformed BH Response Data	63
4.11 Processing Levels for Square Root Transformed BH Response Data	63
4.12 Contour Plot for Square Root Transformed BH Response Data	63
4.13 Log(x) Transformation and Regression of Response Data	64
4.14 Math Models for Log(x) Transformed Response Data	68
4.15 Processing Levels for Log(x) Transformed Response Data	69
4.16 Box-Cox Plots for Log(x) Transformed Response Data	70
4.17 Contour Plots for Log(x) Transformed Response Data.....	72
4.18 Analysis Conclusion.....	76
 5. CONCLUSION.....	 79
5.0 Conclusion of Visual Examination.....	79

	Page
5.1 Conclusion of Regression Analyses	79
5.2 Summary of Transformation	80
5.3 Summary of Optimization	80
5.4 Validation Testing	82
5.5 Future Work	83
5.6 Applications in Aerospace.....	83
5.7 Future Work Potential	85
 BIBLIOGRAPHY.....	 86
 APPENDICES	
Single Bead DOE Experiments – Macro Images of Ti-6Al-4V Deposits.....	90
Calculation Matrix for Aluminum, Bead Height	103
and Bead Width Response Data	103
Log (x) and Square Root Transformed Aluminum, Bead Height	104
and Bead Width Response Data	104
Box-Behnken Design Matrix	105
 VITA.....	 106

LIST OF TABLES

Table	Page
1. Yates Algorithm Matrix.....	17
2. Modified Yates Algorithm Matrix.....	17
3. Computation of Degrees of Freedom.....	21
4. The AL Content of the Final Deposits.....	26
5. Melting Points of Ti-6Al-4V Elements.....	26
6. BH of the Final Deposits.....	28
7. BW of the Final Deposits.....	29
8. Observation of 27 Samples	37
9. AL Content and Processing Levels.....	38
10. BH Values and Processing Levels.	39
11. BW Values and Processing Levels.	39
12. Calculations for R Square Values of Response Variables.....	42
13. F Statistics for AL, BH and BW Responses.	42
14. Standard Deviations for AL, BH and BW Responses.	42
15. Coefficients for the Processing Parameters for AL Responses	45
16. P-Values for the AL Response Coefficients	46
17. Coefficients for the Processing Parameters of BH Responses.....	48
18. P-Values for the BH Coefficients	48
19. Coefficients for the Processing Parameters for BW Responses	50
20. P-Values for the BW Response Coefficients	50

Table	Page
21. Coefficients for AL, BH and BW Responses.	51
22. Optimized Responses for AL, BH and BW	52
23. Processing Levels for BP, TS and WF Rate.	53
24. Summary of Statistics for BH before and after SQRT Transformation.....	60
25. Coefficients for Square Root Transformed BH Responses	62
26. Processing Levels for Square Root Transformed BH Responses	63
27. Statistics and ANOVA Results for Non-Transformed and Log(x) Transformed	66
28. Coefficients for Log(x) Transformed AL, BH and BW Responses.....	69
29. Processing Levels for Log(x) Transformed BP, TS and WF Responses.....	70

LIST OF FIGURES

Figure	Page
1. Electron Beam Freeform Fabrication.....	8
2. Example of Curvilinear Structure (Lach, 2007)	9
3. Electron Beam Freeform Fabrication System (Lach, 2007)	10
4. Full Factorial Design Cube	15
5. Distribution Curve for AL Content (Wt %) Responses	27
6. Distribution Curve for BH (mm) Responses	30
7. Distribution Curve for BW (mm) Responses.....	30
8. Box-Cox Plot for Power Transforms	32
9. Distribution Curve for Square Root Transformed BH Responses.....	33
10. Predicted vs. Actual Values for AL Responses	43
11. Predicted vs. Actual Values for BH Responses.....	43
12. Predicted vs. Actual Values for BW Responses	44
13. AL Response Data Evaluated Optimized When BP = +1, TS = -1, WF = -1.....	54
14. BH Response Data Optimized When BP = +1, TS = -1, WF = +1	55
15. BW Response Data Optimized When BP = +1, TS = -1, WF = +1.....	56
16. Box-Cox Plot for Power Transforms – AL Responses	57
17. Box-Cox Plot for Power Transforms – BH Responses.....	58
18. Box-Cox Plot for Power Transforms – BW Responses.....	58
19. Box-Cox Plot for Power Transforms – BH Responses Square Root Transformation.....	59
20. Distribution of the Square Root Transformed BH Responses	60
21. Predicted vs. Actual Values for Non-Transformed BH Responses	61
22. Predicted vs. Actual Values for Square Root Transformed BH Responses	61

Figure	Page
23. BH with SQRT Transformation Optimized when BP = +1, TS = -1, WF = +1	64
24. AL Responses Transformed with Log(x)	65
25. BH Responses Transformed with Log(x)	65
26. BW Responses Transformed with Log(x)	66
27. Predicted vs. Actual Values for Log(x) Transformed AL Responses.	67
28. Predicted vs. Actual Values for Log(x) Transformed BH Responses.	68
29. Predicted vs. Actual Values Log(x) Transformed BW Responses.	68
30. Log(x) Transformed Box-Cox Plot for AL.....	70
31. Log(x) Transformed Box-Cox Plot for BH	71
32. Log(x) Transformed Box-Cox Plot for BW.....	72
33. Log(x) Transformed AL Response Data Optimized BP = +1, TS = -1, WF = +1	73
34. Log(x) Transformed BH Response Data Optimized when BP = +1,	74
35. Log(x) Transformed BW Response Data Optimized BP = +1, TS = -1, WF = +1	75
36. Power Transformed BW Response Data Optimized BP = +1, TS = -1, WF = +1	75
37. EBF ³ Ti-6Al-4V - Sample 7 [BH = +1, TS = -1, BW = +1]	78
38. Example Box-Behnken Design Cube	82
39. EBF ³ Ti-6Al-4V - Sample 1 (left) and Sample 3 (right)	90
40. EBF ³ Ti-6Al-4V - Sample 4 (left) and Sample 5 (right)	91
41. EBF ³ Ti-6Al-4V - Sample 6 (left) and Sample 7 (right)	92
42. EBF ³ Ti-6Al-4V - Sample 8 (left) and Sample 9 (right)	93
43. EBF ³ Ti-6Al-4V - Sample 10 (left) and Sample 11 (right)	94
44. EBF ³ Ti-6Al-4V - Sample 12 (left) and Sample 13 (right)	95
45. EBF ³ Ti-6Al-4V - Sample 14 (left) and Sample 15 (right)	96

Figure	Page
46. EBF ³ Ti-6Al-4V - Sample 16 (left) and Sample 17 (right)	97
47. EBF ³ Ti-6Al-4V - Sample 18 (left) and Sample 19 (right)	98
48. EBF ³ Ti-6Al-4V - Sample 20 (left) and Sample 21 (right)	99
49. EBF ³ Ti-6Al-4V - Sample 22 (left) and Sample 23 (right)	100
50. EBF ³ Ti-6Al-4V - Sample 24 (left) and Sample 25 (right)	101
51. EBF ³ Ti-6Al-4V - Sample 26 (left) and Sample 27 (right)	102

1. INTRODUCTION

1.0 Background

Electron beam freeform fabrication (EBF³) is used for high energy welding. It is a layer additive process that builds three dimensional metallic parts by focusing an electron beam (e-beam) onto a substrate plate creating a molten pool of the plate material. Wire feedstock is then fed through dual wire feeder nozzles into the leading edge of the pool where it melts. As the deposit hardens, it becomes the base for the next pass in the layer-additive rapid manufacturing process of fabricating 3D metallic parts. This experiment was conducted on an industrial sized unit, but NASA has patented a smaller unit capable of quick mobilization to remote regions on Earth and in space.

Some key features of NASA's unique design include the potential for automated process control for consistent depositions, a versatile part envelope and a reduction in voltage requirements. The accelerating voltage was reduced from 60–200 kV, typically seen in industrial size machines, to 20 kV making it smaller, lighter, safer, and portable (NASA, 2012). This is due to the unique ion/e-beam deflection system. The data collection for this thesis was done on a machine capable of 60kV, according to Bill Seufzer (personal communication, August 7, 2012).

The EBF³ process proves to be an attractive alternative to conventional machining for use in both the commercial and space industries as it requires no tooling. Waste material is minimized as lightweight, precision, cost-effective components can be manufactured on demand. Computer aided design (CAD) modeling software contains commands to guide the rapid building of complex parts including curvilinear structures that can be dynamically scaled to near-net, design specified, dimensions (Lach, 2007).

The portability of the patented EBF³ system is extremely beneficial to the military and aerospace communities as it is capable of mobilization anywhere including remote regions on earth or in space.

The aerospace industry has been using an alloy known as Ti-6Al-4, sometimes referred to as Ti64 (titanium alloyed with aluminum 6 wt % and vanadium 4 wt %), for component manufacturing. Ti-6Al-4V is the alloy of choice because it has an outstanding strength-to-weight ratio, good fatigue strength and toughness, low elastic modulus, good biocompatibility and corrosion resistance and anti-magnetic properties (Hussein, et. al, 2012). Some of these benefits, however, are overshadowed by the high cost of honing titanium parts by conventional machining methods due to the volumes of cutting fluid used in production and the excess scrap material upon completion. For example, a 300 pound part may have started as a 6,000 pound block of titanium before machining. That yields approximately 5,700 pounds of scrap that would need to be recycled. With EBF³ the same part can be built using 350 pounds of titanium with only 50 pounds of material needing to be machined away to achieve the final configuration (NASA, 2009).

1.1 Scope

Material scientists at NASA LaRC were interested in testing EBF³ manufactured Ti-6Al-4V components in order to produce parts with all of the robust characteristics of traditionally tempered metallic products, but at the reduced cost EBF³ affords due to reduced parts and less waste. The approach was a Design of Experiment (DOE) that included systematic trials of the entire processing envelope, followed by a compositional analysis (Lach, 2007). While many variables can be considered significant to the

production of high quality finished parts, this DOE exclusively studied the beam power (BP), translation speed (TS) and the wire feed rate (WF) during EBF³ processing to observe the combined effects these had on trial depositions.

The experiment involved the collaboration of several specialties. The DOE was conceived by Materials Research Engineers of NASA's Advanced Materials and Processes Branch (AMPB). The Lead Engineering Technician of the Fabrication Processes Section implemented the design by priming the chamber, executing the computer software and monitoring the process. The rest of the unique EBF³ team is comprised of computer specialists who gather data during the process for future closed loop control capability and photographers who capture and process in-situ images of the EBF³ process. The team also conducted metallographic analysis and multi-bead micro-chemical analysis using wavelength dispersive spectroscopy. A team from Spirit AeroSystems, Inc. conducted single-bead bulk chemistry analysis using an inductively coupled plasma technique of the samples provided by NASA LaRC and correlated single bead deposit chemistry with processing parameters (Lach, 2007).

The experiment was intended to be a screening test to find a focused range of processing parameters to use as a baseline for future validation testing. Testing was done at this level strictly to identify the effects of the full range of key processing variables. The DOE was implemented for 27 linear depositions of Ti-6Al-4V wire feedstock onto Ti-6Al-4V substrate. Although the factors (BP, TS and WF) could be varied continuously if desired, they were studied at three discrete levels at the extremes of the processing envelope. There was some space left on one of the plates at the end of the test, so one validation test was done by replicating the processing levels for run 8. This

sample was chosen based on the good geometry of the finished deposit. This replicate is intentionally left out of the analysis as it was not part of the initial design.

1.2 Purpose

After reviewing the results of a chemical analysis of the Ti-6Al-4V alloy depositions, it was discovered that selective vaporization of aluminum (AL) was occurring. Vaporization was expected since EBF³ processing was done at approximately 2300° above the AL vaporization point of approximately 1220⁰F, but the AL loss varied inconsistently. This experiment involved single bead deposits, but when building parts of multiple layers, vaporization can also vary the AL content of each layer. This can cause errors in the finished part that can subsequently propagate to the system level. In addition, components must meet compositional requirements, defined in the Aerospace Material Specification (AMS4999) as being between 5.50 wt % and 6.75 wt % (SAE Aerospace, 2002). Several output responses were found to be outside of that range.

Statistical analysis of errors at the base levels will reveal variances so that the process can be refined to produce consistent results by managing heat flux and cooling rates during deposition through control of the processing parameters (Taminger, 2002). The purpose of this thesis is to study the effects of the processing variables on the output response in order to minimize AL loss and maximize bead height (BH) and bead width (BW) by identifying the processing parameters that will optimize the production of Ti-6Al-4V parts made with the EBF³ system.

The AL responses for the DOE were obtained and input into a full factorial DOE calculation matrix using Microsoft ® Excel as shown in Appendix B in the column labeled Al (wt %). The processing values (BP, TS and WF) in this matrix are coded as

high (+1), medium (0) and low (-1) to protect unpublished NASA data. The full factorial design chosen is, by definition, a screening design and is typically the first stage in process optimization so it is ideal for this experiment (Ferreira, et al., 2007). It allows the effects of all of the factors to be studied simultaneously for each response. A regression analysis which included Analysis of Variance (ANOVA) to assess the interaction of the processing variables was then run on the calculation matrix using Microsoft® Excel and a response surface (RS) that computed the predicted AL content for the three parameters was obtained. ANOVA is a robust method for analysis of individual factors to determine variation of output (Schmider, et al., 2010) and is a statistical technique which compartmentalizes sources of variation for hypothesis testing of the model parameters (Stat-Ease®, 2011). ANOVA diagnostics and summary statistics from the regression indicated that the resulting RS model was not a good fit for the data. In addition, the AL content of the 27 depositions showed very little overall variability compared to the wide range of processing levels. This was evident in the non-normal distribution of the response data. A study of other responses to include the BH and BW was then recommended. These critical responses were chosen because each layer becomes the support for the next layer. The measurements for BH and BW are also shown in the calculation matrix in Appendix B. If the results of the analysis are feasible, they will be recommended in validation testing to further define a more focused region of the design space.

1.3 Research Problem

EBF³ operates in high vacuum as it cannot propagate through an atmosphere. This makes it ideal for use in space, but temperature control is complicated by the slow

cooling rate in vacuum. This could affect the thickness of the bead walls and the chemical properties of the finished part as heat increases with each layer so the processing inputs control geometry of the deposit and prevent it from spreading. It is generally expected that the bead be of high quality such that it forms a good base for each subsequent level of the deposit. Tight control of the processing variables will keep the BH, BW and penetration depth of the electron beam predictable. The penetration depth, not included in this study, refers to how much of the previous layer is warped or changed by the electron beam of the depositing layer. The technical performance measures (TPM) for the bead morphology are explained in detail in section 4.3 of this paper, but generally wall BH and BW are determined by the part being manufactured and must be uniform with a symmetric structure with which to build upon. The TPM for AL content is the range 5.50 wt% – 6.75 wt% as previously discussed. This analysis should predict optimum processing levels that conform to these requirements.

1.4 Analysis Strategy

The models chosen for this DOE utilize Response Surface Methodology (RSM) tools developed in the 1960's for the purpose of optimizing operating conditions (Myers, 1989). These tools, by design, aid in the construction of models which serve to reduce the number of experiments needed for testing and to provide an analytic means to achieve process optimization. The reduced need for testing translates into less work in the laboratory and the potential for a smarter allocation of resources within a project. Tools used in this study include regression analysis, ANOVA, Microsoft ® Excel Solver optimization, and RSM optimization techniques available in Design-Expert ® software from Stat-Ease ®. The regression analysis provided numerical computation of the

response surface (RS), while plots generated using the Design-Expert ® software provided graphical representations of the models. Transformations of the data, discussed in the next section of this paper, were conducted to improve the RS fit and normality of the data about the mean value surface.

Visual observations and measurements of the BH and BW, as compared with the calculated wt % of the AL content were also analyzed. The visual observation analysis was used to compare the bead geometries with the resulting AL contents by studying the effects of individual and two-way coupling of factors on the responses through the use of RS models. RS models also provided sensitivity information to reveal which parameters had the greatest effect on the final deposition at specific points within the design space.

The goal with RSM is to identify processing variables that detract from or contribute to the optimization of a process. In this study, AL responses should yield maximum levels of wt % while maintaining the integrity of the chemical composition of the Ti-6Al-4V depositions. The analytical RS form of the processing parameter inputs (factors) and output variables (responses), derived from the ANOVA, determined optimal processing conditions, that can lead to production repeatability and enable the quantification of uncertainty associated with the process.

2. LITERATURE REVIEW

2.0 Introduction

The EBF³ process is an advanced layer-additive rapid manufacturing process that uses an electron beam and wire to fabricate 3D metallic structures in high vacuum. In this DOE, titanium alloy substrate plates are fastened to a moveable table within the vacuum chamber of the machine. The electron beam is focused onto the plate creating a molten pool of substrate material. Wire is then fed into the leading edge of a molten pool where it melts. The layering process is seen in Figure 1 as the wire laden molten pool of hardens on top of the previous deposit. The process continues layer-by-layer in the z direction in an additive process that builds up the part until it conforms to the x and y model specifications.

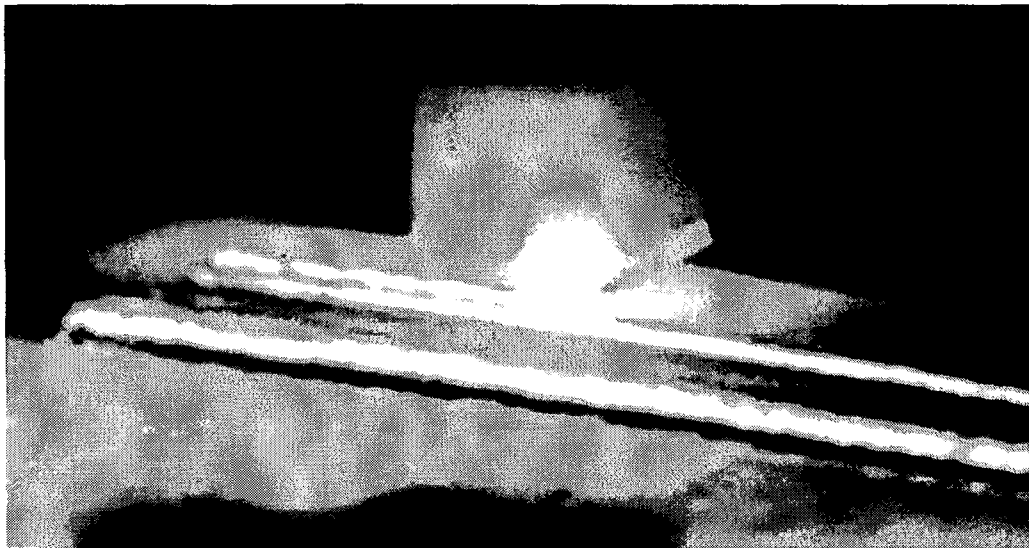


Figure 1. Electron Beam Freeform Fabrication.

The EBF³ is a cost effective process as complex parts such as curvilinear unitized structures such as that shown in Figure 2 (Lin, et al., 2007), on-demand precision

components, and experimental prototypes can be manufactured more efficiently than traditional machining. EBF³ minimizes time, materials, waste, equipment and space while maximizing design efficiency. The process efficiencies of the electron beam and the solid wire feedstock make EBF³ attractive for use in commercial and space applications where machining and raw materials are not available, and cargo space on transporter vehicles is restricted (NASA, 2009).

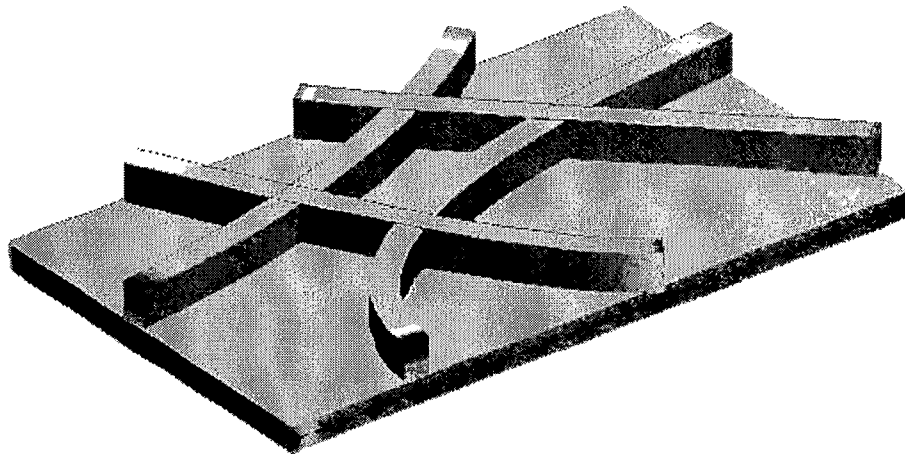


Figure 2. Example of Curvilinear Structure (Lach, 2007).

2.1 EBF³ System

The EBF³ system used at NASA LaRC is comprised of an external computer control system, and a 42 kW electron beam [EB] gun, dual wire feeders, a wire feed nozzle, and a tilt/rotate table enclosed in a vacuum chamber. Figure 3 (Lin, et al., 2007) shows the system as set up at NASA LaRC. The metallic substrate is secured to the table. Wire feedstock is passed through the wire feeder nozzle. The computer control

system uses a Computer Aided Design (CAD) model of 2D slices, x and y specifications of the component to be fabricated, to drive the EB gun and direct the translation speed and angle of the table. The 42kW EB gun focuses an electron beam onto the substrate plate and then wire is fed into the electron beam through the wire feeder nozzle creating a molten pool of material on the substrate in the shape of computerized specifications (Lin, et al, 2007). The envelope is 1.8m x .6m x .6m.

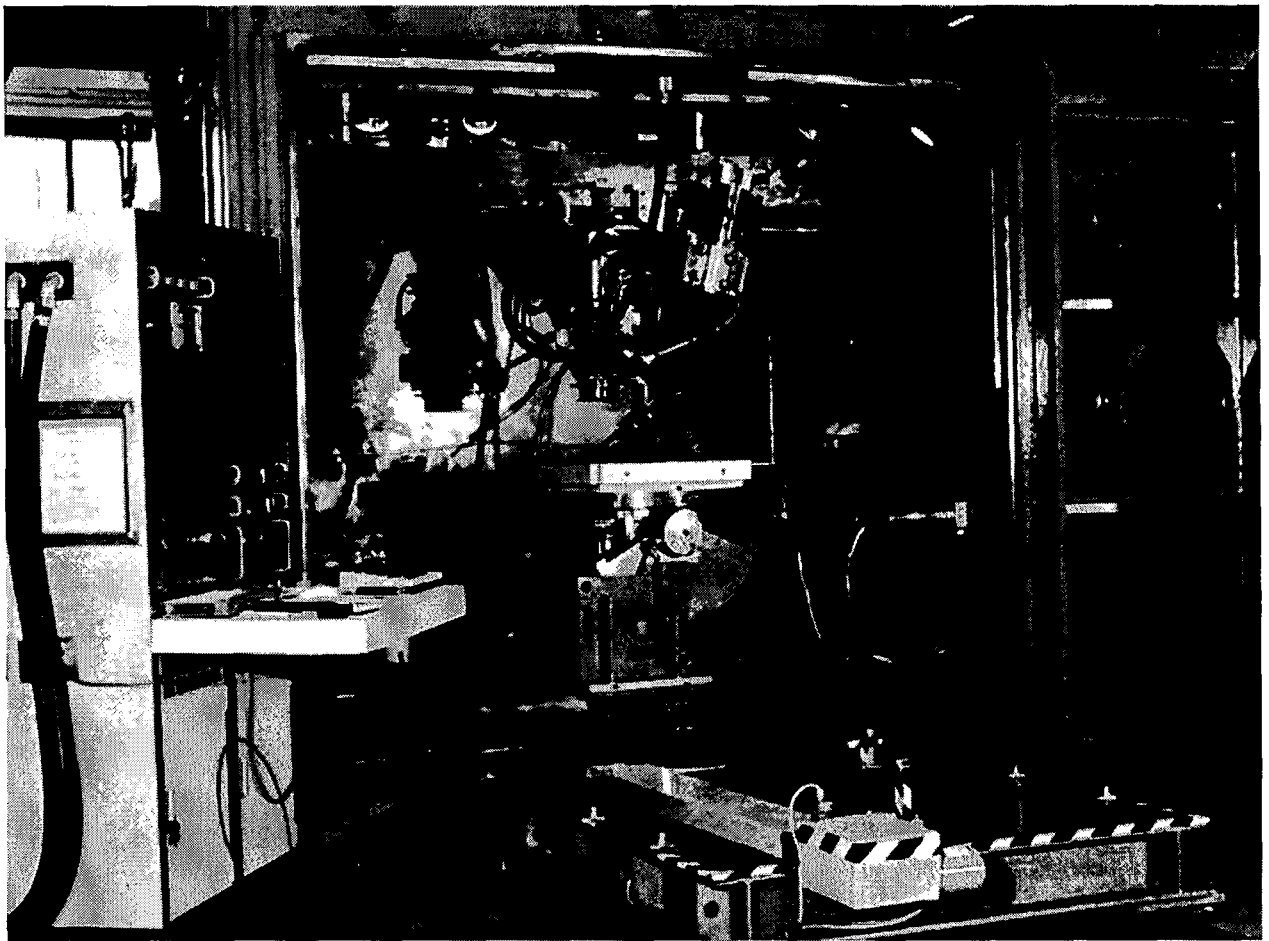


Figure 3. Electron Beam Freeform Fabrication System (Lach, 2007).

2.2 Benefits of EBF³

Additive processes have been used for prototyping for over 15 years (Levy, et al., 2007), but the demand for rapid manufacturing is increasing where production of small quantities of complex parts in minimal time is desired (Ratnadeep, 2011). EBF³ provides near-net shaped parts needing little or no final machining, and functionally graded components. This means that composition and structure can be varied by introducing different wire feedstock transitioning to new alloys as the microstructure of the part in whole evolves with each added layer (Domack, et al., 2006).

The list of benefits is not restrictive:

- Space Reduction: The EBF³ equipment used at NASA Langley Research Center is large, but the system has been scaled down and tested on a NASA jet (NASA, 2009). Although there are cases where material can be forged to net shape using dies which does not involve cumbersome apparatus, heat treatment of such materials may be necessary. Gantry-type atmosphere furnaces are needed for this. The furnaces are large and have an endothermic (energy absorbing) atmosphere which must be maintained by a gas generator (MacKenzie, 2008). This would pose enormous complications for use in space. The EBF³ system can be scaled down to a lightweight, portable machine for quick mobilization on earth or in space.
- On-orbit Applications: Structures can be repaired and maintained independently in the naturally ambient vacuum of space, reducing the need for shipping heavy parts (Hillier, et al., 2009).
- Cost Reduction: Loss of material due to refinement is negligible and system cost is significantly less than conventional machining methods. The EBF³ process uses less electricity (NASA, 2009).
- Waste Reduction: Excess material is not generated as in conventional machining. Parts are near net-shaped (Lach, et al., 2007).
- Efficiency: Geometry of design is not limited (Hague, et al., 2003) or restricted by the availability of materials.
- Scalability: During the additive layering process, material can be changed. (Taminger, et al., 2004).

- Versatility: Capable of working in microgravity (Taminger, et al., 2004).
- Material Reduction: Use of wire feedstock reduces material needed for building quality parts (Lach, et al., 2007).
- Importance Sampling: Properties, microstructures and chemistry typically can be calculated from any layer of the process using tools such as scanning electron microscopes (Lach, 2007).
- Process Monitoring: Sensors can be installed for process monitoring (Taminger, et al., 2004).

2.3 EBF³ Application

EBF³ technology is prescribed for use in government and commercial applications in areas of land, sea, and air-based vehicles such as fighter jets and support aircraft, medical devices, motorcycle parts, sports equipment (designer golf clubs, rackets, baseball bats), tool and die, automobile parts (fenders, exhaust systems, headers, designer rims), jewelry, bicycle parts, household appliances, and replacement parts in remote or hostile locations (military forward-operating locations, seafaring ships, offshore oil rigs and polar research stations) (NASA, 2009). Aircraft weight reduction is also achieved through advanced fabrication techniques because traditional construction of parts such as wing panels consist of multiple panels enforced with individually affixed stiffeners (Richardson, 2009, p1). The EBF³ enables integration of stiffeners within the build requiring fewer parts such as fasteners during assembly.

Other considerations include landing gear to eliminate the time consuming manufacture of conventional landing gear. This process presently consists of forging high strength alloys in dies to produce a general shape. Parts are then transported to another facility where they are machined to net shape and then heat treated. The heat

treatment causes distortion in the shape which results in an iterative process of inspections and machining before being honed and finally surface coated (MacKenzie, 2008).

2.4 EBF³ Limitations

Interactions between BP, TS and WF must be strictly controlled to maintain chemical and mechanical properties as problems including porosity, delamination, thermal stresses and crack formation have been noted (Alimardani, et al., 2009). The geometrical and structural integrity of parts may be compromised by operating conditions and parameters (Wanjara, et al., 2006), particularly due to the slow cooling rate between layering passes in high vacuum. For this reason screenings are done to examine the extreme range of the processing envelope to identify successes and failures.

2.5 Ti-6Al-4V Alloy

Ti-6Al-4V is distinguished among alloys as the workhorse of the aerospace industry. Setting the world standard for its light weight, strength and corrosion resistant properties, it is the alloy of choice for land, sea and air vehicles. These qualities make it desirable for use in the EBF³ process provided that finished components satisfy rigorous performance requirements for safety and reliability. Qualification of EBF³ over conventional manufacturing requires maintainability of the established compositional range of Ti-6Al-4V and mechanical properties.

2.6 Design of Experiment (DOE)

The purpose of this DOE is to identify variability that can lead to undesirable features during processing that can also propagate to the system level thus inducing risk and uncertainty into finished products. With respect to this DOE, material scientists and

process engineers analyzed the finished depositions using visual observation and measurement as well as techniques to verify the chemistry and microstructure. The prediction RS was based on conclusions drawn from these observations and calculations. Controlled experiments are then constructed using the observed results of the ANOVA. Once test points are defined as suggested by the ANOVA results, the experiment is run again and new data is acquired. ANOVA is then used again to analyze the data with RSM. This technique is valuable because extreme conditions can first be modeled using known and unknown data in the safety of virtual testing sometimes using repeated random number generation sampling tools such as Monte Carlo. Designs are set up according to established design models. Those used in this study are discussed.

2.6.0 Full Factorial Design

Each of the three processing factors was considered at discrete high, medium and low values for each of the three control variables. Using three levels allows for a nonlinear, quadratic relationship to be exposed between the factors and the response(s). This provided three factors and three levels to examine, therefore, the model used in this DOE was a three level three factorial design with higher order interactions studied. This is also known as a full factorial design. In contrast to space filling designs such as a Box-Behnken design, the full factorial is a screening design providing specific test points including the corners and centers of the faces and edges of the design as illustrated in Figure 4.

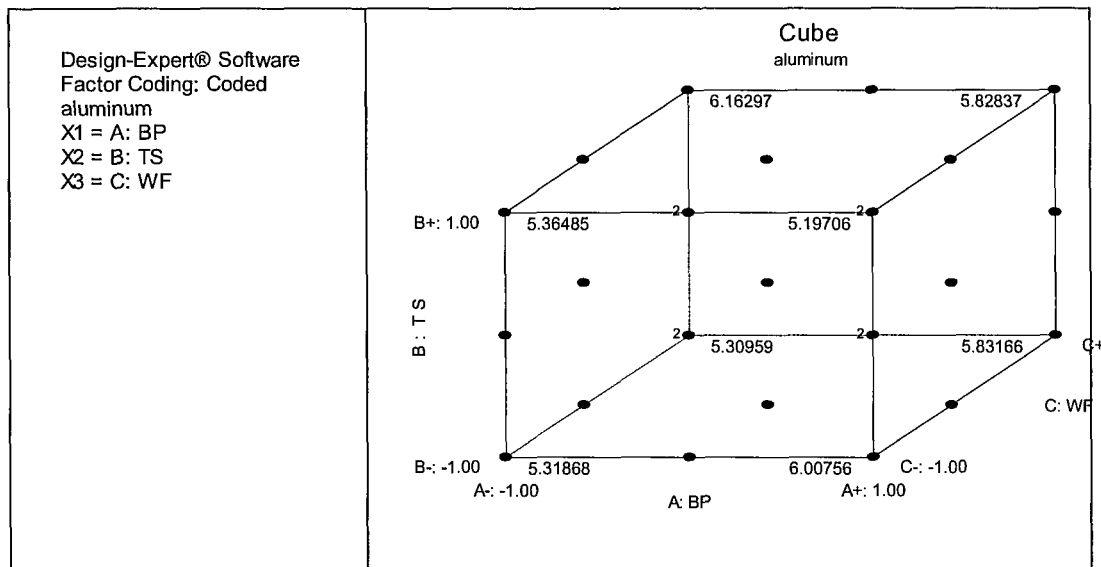


Figure 4. Full Factorial Design Cube.

Figure 4 also illustrates the orthogonality or mathematical independence of the design proven when the sum of the columns in the calculation matrix, as shown in Appendix B, is zero (Unal, 2012). The design cube shows the possible combinations of effects and levels that can be studied. Ronald Fisher introduced factorial designs in 1926 (Marengo, et al., 1995). His premise was that even small effects due to changes can be revealed (Ek, 2005). Fisher's goal was to identify variables that contribute to optimum processing (Ek, 2005). The full factorial design method was superior to the method previously used known as the one variable at a time method (OVAT). Using the OVAT, also referred to as the one factor at a time (OFAT) method, factors that affect the responses, or experiment results, are studied independently ignoring any possible interactions between these factors. This method bore high costs because many experiments were needed, and also bore high risk because interaction effects were not exposed (Unal, 2012). It should be noted that the selection of processing factors to be

studied in this thesis was decided by subject matter experts; these factors typically reflect the controlled variables and the primary, or expected, sources of uncertainty.

2.6.1 Response Surface Methodology (RSM)

“The [RSM] method is a collection of statistical techniques in which a response of interest is influenced by several variables” (Ghasemi, et. al, 2008). For RSM to be practical, conditions must be controlled as much as possible in order to certify that variability is induced by the processing variables. During the EBF³ of the Ti-6Al-4V alloy, variations in the chemical deposition of material were observed. To restrict chemical decomposition of the AL in the alloy to a value between 5.50 wt% and 6.75 wt %, as is required to maintain chemical integrity, factors affecting these variations are studied to obtain optimum processing levels. RSM works within the optimization framework yield to identify processing variables that most affects the process (Myers, et al., 2009).

2.6.2 Yates Algorithm

Frank Yates was considered a pioneer in the field of statistics. He developed an algorithm known as the Yates Algorithm which is a full factorial, orthogonal design. When the level of a variable changes, the Yates Algorithm is used to obtain a quantitative estimate of the effects the change has on the system. The decision for how many experiments to conduct is found in the formula $2^{(n-1)}$ where n is equal to the number of factors studied. The process of setting up a calculation matrix using the Yates Algorithm is shown in Table 1. The values refer to coded values that represent the high and low physical values of the various factors.

Experimentents	FACTOR 1	FACTOR 2	FACTOR 3
1	-1	-1	-1
2	+1	-1	-1
3	-1	+1	-1
4	+1	+1	-1
5	-1	-1	+1
6	+1	-1	+1
7	-1	+1	+1
8	+1	+1	+1

Table 1. Yates Algorithm Matrix.

This procedure works well for factors studied at two levels. When three levels are studied, a modified Yates Algorithm is used where low, medium and high are repeated at 1, 3, 9 and 27 intervals respectively for each factor (Unal, 2012). As with the Yates Algorithm, the number of experiments can become unwieldy. Table 2 illustrates this pattern for 9 experiments at three levels with three factors.

Experiments	FACTOR 1	FACTOR 2	FACTOR 3
1	-1	-1	-1
2	0	-1	-1
3	+1	-1	-1
4	-1	0	-1
5	0	0	-1
6	+1	0	-1
7	-1	+1	-1
8	0	+1	-1
9	+1	+1	-1

Table 2. Modified Yates Algorithm Matrix.

When the number of factors increases to the point of making the number of experiments unfeasible, other design matrices such as partial fractional,

minimum point or space filling designs should be considered especially if time and cost reduction are to be minimized (Franceschini, et al., 2007).

2.7 Math Models

2.7.0 Polynomial Models

First order models study second order main and interaction effects of the main processing variables (Unal, 2012). The math equation is called a two factor interaction and represents a linear RS. It is written as:

$$Y=b_0+ b_1A+ b_2B+ b_3C+ b_4AB+ b_5BC+ b_6AC+ b_7ABC$$

The factors A, B and C are examined independently and as interactions by multiplying them, as either actual values or coded values, by the coefficients obtained in the regression analysis, represented by $b_{(x)}$.

2.7.1 Quadratic Models

RSM models use a second order approximation model (Unal, 2006). Quadratic models include the squared terms that allow interactions of every variable to be studied (Unal, 2012). The A*B*C interaction is excluded as the results of this interaction are most always insignificant (Unal, 2012). The equation includes squared terms to account for non-linearity of the data:

$$Y=b_0+ b_1A+ b_2B+ b_3C+ b_4AB+ b_5BC+ b_6AC+ b_7A^2+ b_8 B^2+ b_9C^2$$

2.8 Transformations

Transformations are used for the purpose of normalizing the curve of the distribution about the mean value surface. A commonly preferred transformation is to apply $\log(x)$ to the data written by the equation $y= \log(x)$ where x is the output response variable. This technique will smooth the data to a normal shape (van Albada, et al.,

2006). Other transformations include Square Root, Base 10 Log, Inverse Square Root, Inverse, Power, Logit, Log(x), Reciprocal and ArcSin Square Root. Transformations normalize the distribution curve by reducing the range and standard deviation of the data relative to the mean value surface. Transformations used in this study were Log(x) and Square Root.

2.9 Validation

Choosing the correct model is crucial to predicting the output responses. It also serves to reduce cost by minimizing the number of experiments needed to validate the effects of the variables and their interactions (Unal, 2006). After a design has passed through the conceptual phase and a preliminary design is implemented, such as a screening test, results should be run through a rigorous process of validation (Blanchard, et al., 2001). “Validation can be defined as the process of ensuring that a model provides a good representation of a real system (Usunoff, et al., 1992).” Validation is accomplished through statistical analysis methods such as ANOVA and RSM of a validation DOE. The validation DOE should prove that the results of the statistical analyses predicted processing levels that can be used in production designs. If it does not, a new design is conceived and the cycle of design, testing, evaluating and validating is continued until the process is sufficiently improved. In EBF³ processing, the quality of each layer determines the quality of each subsequent layer.

2.10 Literature Review Summary

“Electron beam freeform fabrication (EBF³) of titanium alloy, Ti-6Al-4V, requires molten pool processing in high vacuum where parameter selection is critical to avoid selective vaporization of AL. For repeatable mechanical performance and to

qualify an EBF³ component the composition must meet ASM4999A requirements” (Lach, et al., 2012, p.1). The multitude of benefits and applications derived from components manufactured with EBF³ justify focus on models that will enable optimization of this process. Optimization will also reduce or eliminate risks and uncertainties resulting from unknown interaction effects of the processing parameters on the finished product and prevent compounded errors at the system level by conserving mechanical and chemical properties. DOE has been proven to produce models that identify variability that leads to uncertainty. Full factorial designs, specifically the Yates Algorithm, are robust designs valued in the statistical community for reliability in yielding a quadratic polynomial mathematical equation that best describes non-linear data. In the event that the data is not a good fit for the model, the data can be transformed to produce a more normalized distribution curve. If the model is proved credible through validation testing, it can be used to derive consistent EBF³ components that meet industry standards.

3. METHODOLOGY

3.0 Experimental Method

To determine optimum processing conditions, all combinations of the factors should be studied (Unal, 2010). A DOE was therefore constructed for 27 single-bead width linear EBF³ depositions of Ti-6Al-4V on titanium substrate plates. One replicate, mentioned in this analysis, was not studied. Each deposit used process schedules that varied discrete level values of BP, TS and WF and an alternating plate sequence to maintain as close to uniform heating of the plates as possible. The plates were kept below 65° C prior to conducting the next deposit (Lach, 2007).

The full factorial DOE was based on the degrees of freedom (df) computed as shown in Table 3. The df are the number of samples in the design that are free to vary and identify how many samples will be needed to adequately predict the RS. There were 27 output responses in the initial design. Three processing variables, beam power (BP), translation speed (TS) and wire feed rate (WF) were studied at three coded levels [high = +1, medium = 0, and low -1] and calculated as $3^3 = 27$. The degrees of freedom, therefore, cannot exceed 27.

	Degrees of Freedom
Mean	1
Main (BP, TS, WF)	$3(3-1)=6$
Interactions	$3(3-1)(3-1)=12$
Total	19

Table 3. Computation of Degrees of Freedom.

Using the chemically analyzed AL weight percent output obtained at steady state conditions defined as being the center of the deposit length, and BH and BW geometry response outputs of the final depositions, the full factorial design matrix using the modified Yates algorithm shown in Appendix B was constructed. This allowed for the three processing factors to be studied at high, medium and low levels. It also enabled the interactions of all effects at all three levels and the non-linearity to be modeled within the quadratic RS.

The BP is the value in kW of the electron beam as it focuses on the wire. The TS is measured in inches per minute (ipm) and corresponds to the velocity of the table. The WF is the speed at which the wire is fed through the wire feeder nozzle and is also measured in ipm. These three main independent input parameters were originally examined to observe the influence they had on the AL and Vanadium (V) content of the final depositions for the purpose of providing insight into uniformity over the process and future closed loop control for real-time adjustments to the processing levels (Lach, 2007). Concern about the AL vaporization then focused analysis on reduction of AL loss and maximization of the bead geometry.

3.1 System Design

3.1.0 Conceptual Design

Consistent with systems engineering procedure, a conceptual design preceded the initiation of the experiment (Blanchard, et al., 2011). Material Scientists were tasked with evaluating the effects BP, TS and WF had on the AL and V content of the final

depositions of Ti-6Al-4V as a single bead deposit onto titanium substrate plates. The DOE was designed so that the entire range of BP, TS and WF could be observed.

3.1.1 Preliminary Design

The preliminary design consisted of a screening test using the extreme range of discrete levels for each of the processing factors (BP, TS and WF) in steady state to satisfy the conditions of the conceptual design. The objective of the screening test was to narrow the processing parameter ranges and predict processing levels for validation testing.

3.1.2 Equipment Setup

The EBF³ system process was described by Richard Martin, (personal communication, June 26, 2012).

3.1.2.0 Computer System Coding

Once the design specifications for the deposits are chosen, they are translated into computer instructions call G codes. G codes are an element of the Computer Numerical Control (CNC) language used for driving machines to make parts. The CAD software stores each G code which corresponds to an action for the EBF³ to follow such as direction (linear or circular) depending on 2D specifications of width, height, and radius to build the part in the z direction. G codes are also input for the main effects (BP, TS and WF). G codes make it possible to adjust the settings by stepping up and stepping down the processing schedules layer by layer.

3.1.2.1 EBF³ Chamber Setup

Plates or substrates made of Ti-6Al-4V were orientated within the EBF³ chamber. The plates are arranged according to the design of the beam pass so that the deposit is

along the length of the rolling direction of the plate. They are also aligned so that the beam focus can be alternated between passes to avoid overheating of the substrate. Strategic placement of material on sections of the plate helps to reduce temperature variability on the substrate. The temperature is continually monitored by the operator using thermocouples on the top and bottom of the substrate plate.

3.1.2.2 Create High Vacuum Environment

Air tends to scatter electron beam particles so the process must be run in high vacuum. Once the door is closed, the chamber is rough pumped down to a pressure of 1^{-1} torr. When this level is achieved, the operator initiates a diffusion pump that brings the chamber atmosphere down to the desire level of 10^{-6} torr.

3.1.2.3 Cleaning Pass

The first pass of the fabrication is called the cleaning pass. No wire is fed through at this time. This is a low power pass of the beam for the purpose of removing oxides from the substrate in addition to preheating the substrate.

3.2 Initiate EBF3

The electron beam is aligned to the starting position on the plate and wire is fed through a wire feeder nozzle to a point under the focus of the beam. The wire is fed into the leading edge of the molten pool created on the substrate plate by the electron beam. The wire is then melted into the pool on the plate. The plate has 6-axis rotational capability and can translate during this operation (Lach, 2007). This process is repeated layer by layer until the final design is achieved.

3.3 EBF³ Cool-Down Process

When the layering is completed, the chamber is allowed to cool down slowly. Opening the chamber too soon will cause oxygen to be sucked into the chamber and oxidize the titanium alloy causing a rainbow effect on the deposits. This is significant because oxidation (removal of electrons) caused by the heated metals sudden interaction with oxygen indicates that the part measurement is reduced. When this happens, the part may also be brittle as the chemical composition of the part will have changed.

3.4 Extract Finished EBF³ Deposits

When the chamber is sufficiently cooled, the door is opened and the deposits are removed. Photomicrographs of the actual plates showing the cross-sections of the full deposits at steady state for the Ti-6Al-4V run can be seen in Appendix A.

3.5 Chemical Analysis

The samples were examined at steady state by cutting them at the center of the deposit length. An elemental analysis was then done by an independent laboratory on the finished samples using Direct Current Plasma Atomic Emission Spectrometry to determine the wt % of AL and V (Matusiewicz1, et al., 1984). This method of analysis is commonly used for analyzing elements in alloys. The sample is first dissolved in a solution and is then vaporized. The vapors are then atomized. After excitation of the resulting vapors, a spectrometer measures the amount of ambient radiation and is compared to the known radiation of the Ti-6Al-4V elements. Table 4 summarizes the AL wt % content of the final depositions, also staged in columnar form, in the calculation matrix in Appendix B.

Runs	Aluminum (wt %)				
1 - 5	5.95	5.35	5.05	5.58	5.5
6-10	5.40	6.12	5.93	5.87	6.05
11-15	5.37	5.39	4.96	5.83	5.36
16-20	5.13	5.42	5.67	6.54	5.07
21-25	5.32	5.36	5.32	5.58	5.71
26-27	5.26	4.96			

Table 4. The AL Content of the Final Deposits.

3.6 Observation

The chemical analysis of the 27 depositions showed little varying weight percentages of AL, however, vaporization of AL was selective. Several of the samples were below the required range indicating degradation of Ti-6Al-4V composition. Visual observation also proved that the integrity of the finished parts was compromised as the AL loss varied with changing processing schedules. High heat caused aluminum to reach its boiling point sooner than the other metals in the alloy. For this reason, AL became the main focus of study. The melting points and vaporization temperatures of the three elements in the Ti-6Al-4V alloy illustrate the problem. The approximate values, as shown in Table 5, prove that aluminum reaches these points much sooner than the other elements.

Element	Melting Point	Vaporization Temperature
Aluminum	1220 ⁰ F	4220 ⁰ F
Titanium	3000 ⁰ F	5900 ⁰ F
Vanadium	3434 ⁰ F	6116 ⁰ F
Ti-6Al-4V	2920 ⁰ F – 3020 ⁰ F	5507 ⁰ F

Table 5. Melting Points of Ti-6Al-4V Elements.

Normality of the data was also discovered to be problematic. The Central Limit Theorem states that $n \geq 3$ or 4 random variables from the same distribution are distributed normally (Montgomery, 2009). The AL responses provided by the chemical analysis were sorted in ascending order and then processed using the Microsoft® Excel NORMDIST function to test for normality. The results showed that the distribution of AL responses does not follow a normal curve. The results were plotted as shown by the dashed lines in Figure 5. When data such as this does not follow a normal distribution, as shown by the solid line in Figure 5, the regression analysis will present statistics that do not meet expected values. Numerous outputs from the regression analysis and ANOVA statistics discussed in the analysis section of this paper validated this problem.

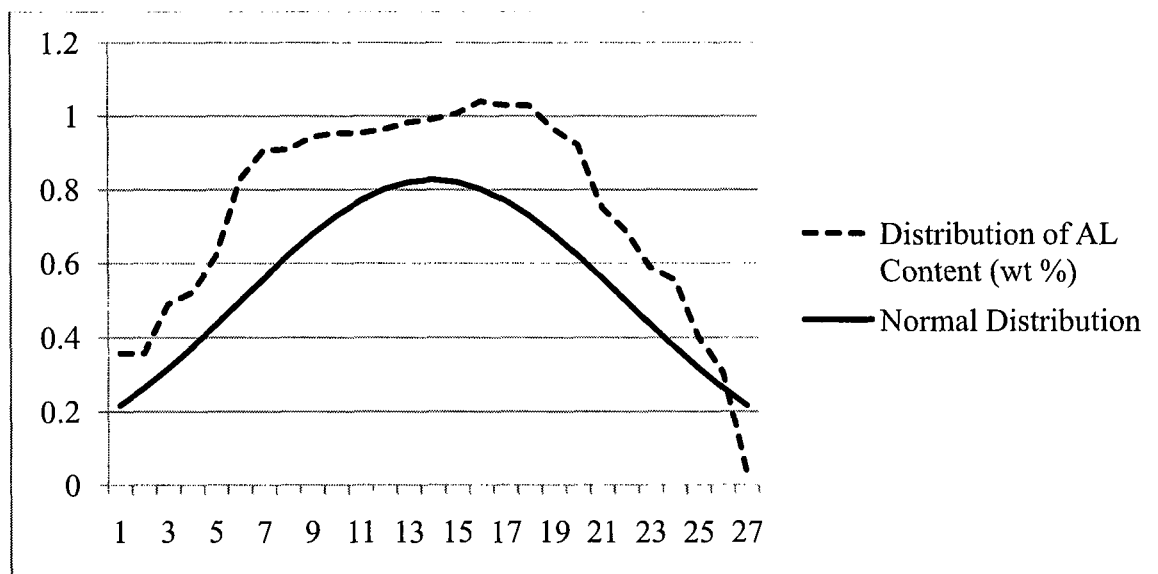


Figure 5. Distribution Curve for AL Content (Wt %) Responses.

3.7 Proposed Solution

Non-normal distributions can be a symptom that the response variables are being affected by more than one process (Montgomery, 2009). One solution is to study other

factors. Measurements of the BH and BW were taken in order to create response values for a regression analysis. The measurement process is described next.

Two engineers took independent BH measurements from photomicrographs with an approximate scale of 9.5 mm, as shown in Appendix A (incidentally reduced in size during arrangement of two samples per page), from the top of the substrate plate to the centerline of the deposit bead. Some samples, like Sample 5 in Figure 40 of Appendix A, had multiple peaks. In such cases, two independent measurements were taken at the centerline and at the highest peak and then averaged. The final calculations from each engineer were then averaged and converted to mm yielding one final bead height measurement for each sample. Specimen 2 was not available as a scaled micrograph so it was measured with digital calipers using the actual deposition and plate. The preliminary height for this sample is defined as measured from the bottom of the substrate to the top of the bead. Six heights from this sample were taken. Three from the front view and three from the back view. The substrate heights were then subtracted from each height and the results averaged. The actual heights as shown in Table 6 were extracted from the calculation matrix in Appendix B.

Runs	Bead Height (mm)				
1 - 5	1.5	0.2	1.0	3.0	1.2
6-10	1.8	5.2	3.6	1.9	0.5
11-15	1.3	0.3	0.7	1.1	0.4
16-20	0.9	2.7	4.0	0.8	1.0
21-25	2.3	0.8	1.2	4.4	1.9
26-27	1.9	1.3			

Table 6. BH of the Final Deposits.

The BW is also a product of two independent measurements that were taken from photomicrographs with an approximate scale of 9.5 mm. Specimen 2 was measured with digital calipers using the actual deposition and plate remnant. Three width measurements from two independent sources were taken for sample 2 at the centerline of the bead, and three at the peak using the true width of the specimen. These three measurements were then averaged. The results from each source were then also averaged. Table 7 shows the resulting BW responses.

Runs	Bead Width (mm)				
	1 - 5	6-10	11-15	16-20	21-25
1 - 5	8.97	0.61	3.60	4.55	4.12
6-10	5.23	11.19	8.58	4.75	3.30
11-15	4.47	3.29	4.44	3.87	4.50
16-20	4.48	7.37	9.30	4.39	4.54
21-25	4.75	3.38	3.38	8.12	7.15
26-27	6.18	5.60			

Table 7. BW of the Final Deposits.

Distribution plots were constructed as shown in Figures 6 and 7. The distributions for BH and BW were also non-normal.

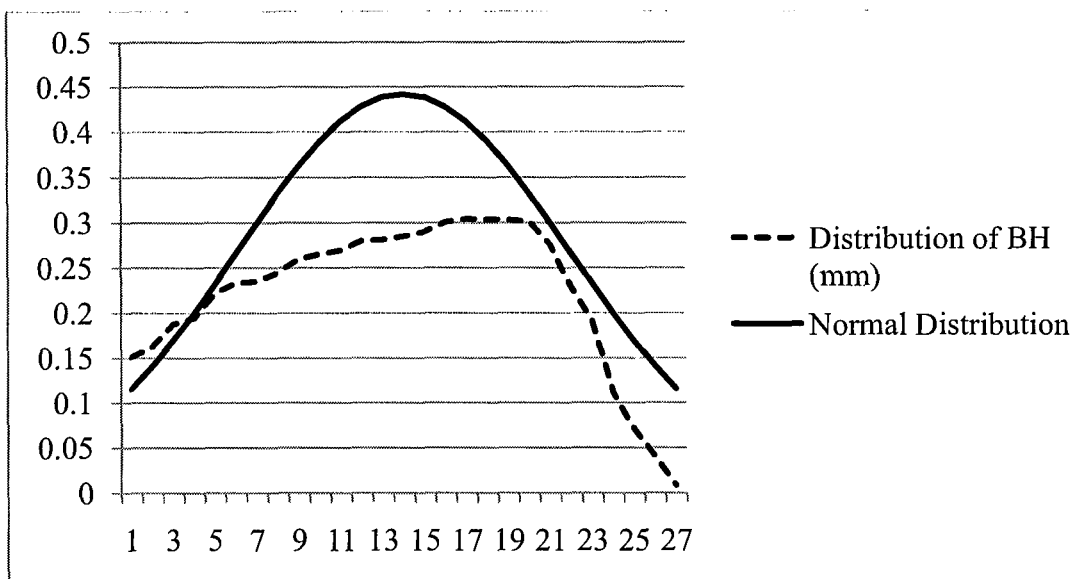


Figure 6. Distribution Curve for BH (mm) Responses.

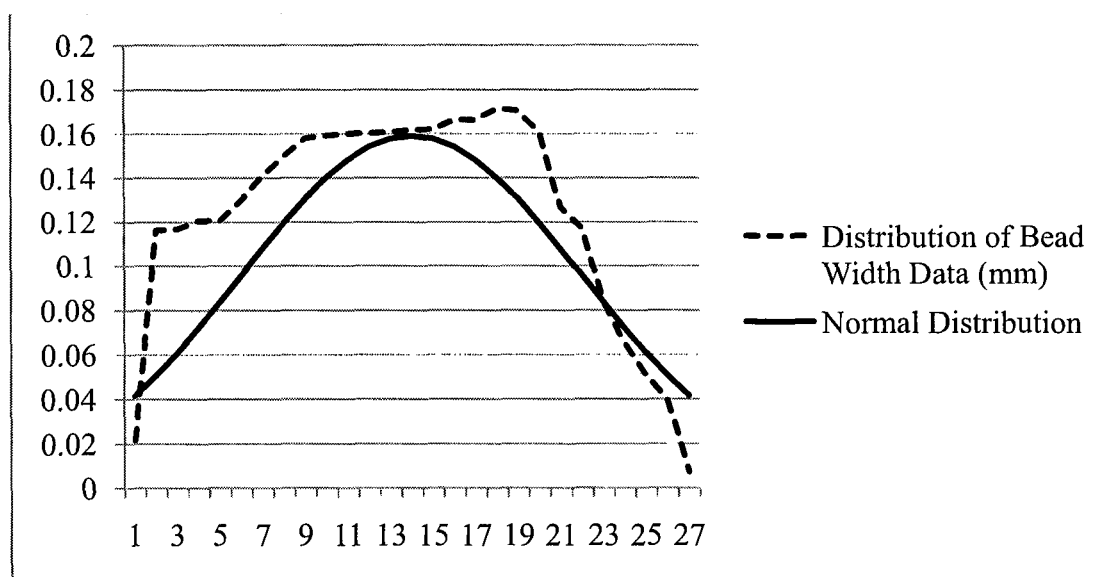


Figure 7. Distribution Curve for BW (mm) Responses.

3.8 Analysis Methodology

3.8.0 Visual Inspection

The samples were examined visually and categorized using criteria that would distinguish good samples from bad samples for the purpose of eliminating deposits that were not acceptable. Several of the deposit specimens had uneven slopes so these were discarded first. Undercuts are described as surfaces where the beam melted into the substrate. They have been known to initiate cracks in worn areas (Nguyen, et. al, 1998). Samples with one or more undercuts were excluded. In some cases, the wire did not completely melt. These were also removed leaving 12 samples which were deemed acceptable based solely on a visual acceptance of the geometric shape as being uniform and free of processing artifact.

Measurements of the BH and BW were then used to perform separate sorts. This identified maximum, tall, wide and uniform bead heights and bead widths. The 12 samples were then sorted by AL content to rank the deposits with the highest AL contents (wt %).

3.8.1 Regression Analysis

Separate regression analyses were run for each of the three output responses. The results of the regression statistics and ANOVA analyses were used to construct RS models of the design spaces. This enabled the prediction of processing variables that best optimized the output responses. Contour plots were also constructed using the strongest independent and interaction factors as identified by the regression to visually confirm the results of the prediction models.

3.8.2 Transformation

A solution to working with non-normal data is to use a transformation. This generally gives the data a more normal appearance. When the data from the calculation matrices were input into separate RSM models using Design-Expert ® to test for normality, no transformations were recommended for the AL or BW responses, but a square root transformation was recommended for the BH responses. A Box-Cox plot for power transforms as shown in Figure 8 supports the recommendation.

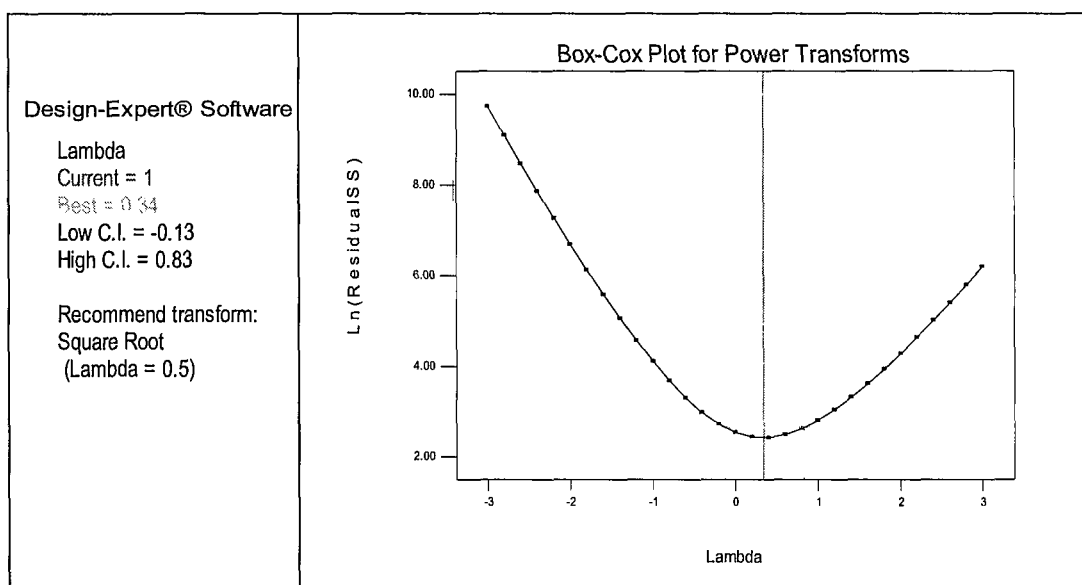


Figure 8. Box-Cox Plot for Power Transforms.

According to Design-Expert ® documentation, the upper and lower confidence intervals shown in the plot key are computed using a chi-square approximation to the likelihood ratio test. The best Lambda is computed by taking the log (x) of the sum of squares of the residuals. If the value Lambda = 1 is not included in the confidence set, no transformation is recommended. In this case, Lambda = 1 fell outside of the interval

range and a square root transformation was recommended to be applied to the BH response data. The distribution curve for the square root transformed bead heights as shown in Figure 9, although not greatly improved, appears to be more normally distributed.

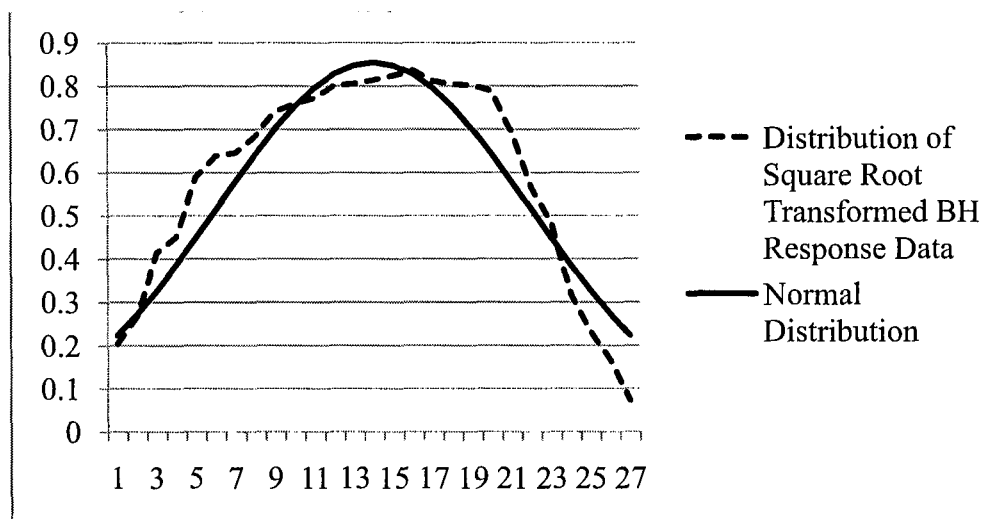


Figure 9. Distribution Curve for Square Root Transformed BH Responses.

When a regression analysis was run on the square root transformed data for BH, the statistics were not improved and the Microsoft ® Excel Solver computed nearly the same RS as the non-transformed data. This will be shown in the next section. No transformations were recommended by Design-Expert ® for AL or BW response data.

A hypothesis was then developed that suggested applying the Log(x) transformation to the AL, BH and BW output responses to achieve normality and a consistent prediction RS. The statistical results were not improved, but the prediction equation and processing levels were consistent with predicted levels of non-transformed

responses. The data used for the transformed regressions are shown in Appendix C and the evaluation is discussed in the analysis section of this paper.

3.8.3 Optimization

Optimization RS models were built from the coefficients output by separate regressions for each of the responses. The coefficients are the result of the sum of squares or a measure of the dispersion of data points about the mean. Using Microsoft® Excel Solver the equations were solved and optimized. The resulting equation or approximation model describes the shape of the curve. The objective of the optimization was to predict maximized values of the AL wt %, BH and BW by discretely varying the three control parameters and then to identify the processing levels that promoted optimization. These results can then be used for validation testing. Features in Design-Expert® were also utilized for optimization.

3.8.4 RSM

Design-Expert® models used for the transformation were also beneficial in illustrating the results graphically. The predicted vs. actual plots provide a visual representation of the normality of the models while contour plots show the trend towards optimization. The software also provided the design cubes and the Box-Cox transformation plots.

4. ANALYSIS and RESULTS

4.0 Analysis Overview

A visual and computational analysis was conducted to identify the processing levels for the sample that exhibited minimum AL content wt % loss and maximum BH and BW geometry. Transformation of the responses was also conducted and the results analyzed.

4.1 Analysis Approach

Since the EBF³ screening experiment had already been conducted, this study begins with an analysis of the finished samples. In order to maximize the capabilities of the statistical tools used and the system design lifecycle the following steps were observed:

1. Examine the samples and choose the best sample based on visual observation and measurement.
2. Examine the samples computationally and choose the best sample based on statistical analysis:
 - i. Build a full factorial calculation matrix consisting of 27 runs with AL, BH and BW measurements in the response columns for each run.
 - ii. Apply a regression analysis for each response set.
 - iii. Build a math, second order approximation, model for each regression analysis set using the coefficients from the ANOVA.
 - iv. Obtain processing levels using Microsoft ® Excel Solver to optimize the objective function.
 - v. Analyze the recommended processing levels for feasibility using the results of the optimization and contour plots.

- vi. Apply a transformation as recommended by the Box-Cox test within the Design-Expert ® software to determine if the transformation improved the response modeling.
- vii. Apply a regression analysis on the transformed data response sets.
- viii. Build a deterministic optimization for each transformed regression analysis.
- ix. Obtain processing levels for transformed data using Microsoft ® Excel solver to optimize the desired objective.
- x. Analyze processing levels for feasibility using the results of the optimization and contour plots.
- xi. Use an alternate transformation to test for a better fit and repeat vii through x.
- xii. Compare the processing levels with the results from the visual inspection.
- xiii. Recommend processing levels for future validation testing.

4.2 Assumptions

It is assumed that steady state fabrication conditions were maintained while varying only the values of the processing variables. It is further assumed that uncertainty is present through imprecise setting of the control variables and through imprecise measurement of the responses. The screening TPM requires a tall, wide bead of consistent thickness and good symmetry with respect to the centerline of the bead. The deposit should contain no wire artifacts or show signs of undercutting. The AL content should range between 5.50 and 6.75 Wt %.

4.3 Analysis of Visual Inspection of Deposit Samples

The visual analysis of the 27 deposits excluded samples with uneven slopes. An example of a deposit with an uneven slope can be seen in Sample 26 in Figure 51 of Appendix A. An example of an undercut event can be seen on the left side of Sample 15

in figure 45 of Appendix A. An example of un-melted wire can be seen in Sample 19 in Figure 47 of Appendix A. Sample 3, shown in Figure 39 of Appendix A was included because the bead was inadvertently truncated by erroneous cutting of the substrate. Sample 9, shown in Figure 42 of Appendix A was not excluded for its comparatively short BH and BW because it was highly symmetrical. Table 8 shows the observations that were made of the samples.

SAMPLE	OBSERVATION
1	Acceptable
2	Poor bead width and height
3	Acceptable
4	Acceptable
5	Uneven slope, wire remnant
6	Acceptable
7	Acceptable
8	Acceptable
9	Acceptable
10	Undercut and wire remnant
11	Undercut, uneven slope and wire remnant
12	Wire remnant, poor bead height and undercut
13	Undercut, poor bead height
14	Uneven slope, wire remnant
15	Undercut, poor bead height
16	Undercut
17	Uneven slope, wire remnant
18	Acceptable
19	Wire remnant
20	Acceptable
21	Acceptable
22	Undercut, wire remnant
23	Undercut
24	Acceptable
25	Uneven slope
26	Uneven slope
27	Acceptable

Table 8. Observation of 27 Samples.

The remaining 12 samples were then sorted by maximum to minimum AL content as shown in Table 9.

SAMPLE	AL CONTENT (wt %)	BP (kw)	TS (ipm)	WF (ipm)
7*	6.12	1	-1	1
1	5.95	1	1	1
8 *	5.93	1	-1	0
9 *	5.87	1	-1	-1
18 *	5.67	0	-1	-1
4 *	5.58	1	0	1
24 *	5.58	-1	0	-1
6	5.40**	1	0	-1
21*	5.32**	-1	1	-1
20*	5.07**	-1	1	0
27*	4.96**	-1	-1	-1
3*	5.05**	1	1	-1

Table 9. AL Content and Processing Levels.

*Most symmetric

**Aluminum content below range (5.5 – 6.75)

Table 10 lists the samples ordered by maximum to minimum BH.

SAMPLE	BH (mm)	BP (kw)	TS (ipm)	WF (ipm)
7*	5.2	1	-1	1
24 *	4.4	-1	0	-1
18 *	4.0	0	-1	-1
8 *	3.6	1	-1	0
4 *	3.0	1	0	1
21*	2.3**	-1	1	-1
9 *	1.9	1	-1	-1
6	1.8**	1	0	-1
1	1.5	1	1	1
27*	1.3**	-1	-1	-1
20*	1.0**	-1	1	0
3*	1.0**	1	1	-1

Table 10. BH Values and Processing Levels.

*Most symmetric

**Aluminum content below range (5.5 – 6.75)

Table 11 lists the samples ordered by maximum to minimum BW.

SAMPLE	BW (mm)	BP (kw)	TS (ipm)	WF (ipm)
7*	11.2	1	-1	1
18 *	9.3	0	-1	-1
1	9.0	1	1	1
8 *	8.6	1	-1	0
24 *	8.1	-1	0	-1
27*	5.6**	-1	-1	-1
6	5.2**	1	0	-1
9 *	4.8	1	-1	-1
21*	4.8**	-1	1	-1
4 *	4.6	1	0	1
20*	4.5**	-1	1	0
3*	3.6**	1	1	-1

Table 11. BW Values and Processing Levels.

*Most symmetric

**Aluminum content below range (5.5 – 6.75)

4.3.0 Visual Analysis Conclusion

The analysis approach first required that the best sample be chosen based on visual observation and measurement. Samples were categorized according to bead structure by removing anomalies such as poor morphology, wire remnants in the deposit and undercuts to the substrate. There were four pairs of duplicate AL compositions which could suggest consistency in processing. The following analysis supports the exclusion of these special case samples.

Samples 4 and 24 had AL weights of 5.58 Wt%, but with different bead heights and widths. In addition, the processing levels conflict. Sample 4 as shown in Figure 40 of Appendix A was run at high BP, medium TS and high WF. Sample 24, as shown in Figure 50 of Appendix A was run at low BP, medium TS and low WF. This could indicate that varying the processing levels is not contributing to the differences in BH and BW. It could also indicate that as the conditions inside the chamber changed as a result of processing or simply that different processing schedules result in the same compositions. In any event, these samples did not visually rank highest with respect to all responses.

Samples 15 and 22 had AL weights of 5.36. Sample 15, as shown in Figure 45 of Appendix A, shows a deep undercut on the left side of the substrate. Sample 22, as shown in Figure 49 of Appendix A, contains wire remnant and deep undercutting on the left side of the substrate. Wire remnants give a false high AL weight percentage.

Samples 21 and 23 had AL weights of 5.32. Sample 21, as shown in Figure 48 of Appendix A, had good bead morphology and AL content and was ranked among the twelve most visually appealing samples, but Sample 23, as shown in Figure 49 of

Appendix A, had a deep undercut on the right side of the substrate so no correlation can be made between these two samples. The same reasoning holds for Samples 13 and 27. Sample 27, as shown in Figure 51 of Appendix A, proved to be adequate, but Sample 13, as shown in Figure 44 of Appendix A, had undercutting on both sides of the substrate and poor bead geometry.

Sample 7, as shown in Figure 41 of Appendix A, ranked highest with respect to BH (5.2 mm) and BW (11.2 mm). It also ranked the highest for AL content (6.12 Wt %). This sample will be considered as ideal for comparison with the results of the regression analysis and optimization.

4.4 Regression Analysis for Non-Transformed Response Data

A regression analysis was run for each response set as required in the next step of the analysis approach using the Microsoft® Excel Regression Data Analysis tool. R Square values were culled from the summary statistics and analyzed. R Square values represent how well the regression line approximates the real data, also referred to as goodness of fit. It explains how the percentage of the variation in one variable may be explained by another variable. R Square values close to 1.0 or 100% are desired. The residuals are the difference between the sample and an expected value. The sum of squares (SS) measures the dispersion of the data points. The R Square value is computed using the Residual Sum of Squares (SS) and Total (SS) from the ANOVA or $R\text{ Square} = 1 - \text{Residual SS} / \text{Total SS}$ (Montgomery, 2009). Table 12 shows the R Square Values for each of the factors. The results deviate significantly from the ideal R Square value of 1.0 and indicate that the model is non-linear.

Responses	AL	BH	BW
R Square	0.47	0.63	0.53

Table 12. Calculations for R Square Values of Response Variables.

The F Statistic is the probability that the math model equation does not explain the variation in Y (Montgomery, 2009). The F statistic should be <0.1 (10%). High values as seen in Table 13 indicate that the model does not explain the variation in the AL, BH and BW responses.

Responses	AL	BH	BW
F Statistic	1.71	3.17	2.14

Table 13. F Statistics for AL, BH and BW Responses.

The standard deviation is the dispersion from the mean (Montgomery, 2009). Standard deviations for AL, BH and BW are shown in Table 14. The response values for AL yielded the least variation which is a rough indication that varying the BP, TS and WF had less impact on the AL content over the bead geometry.

Responses	AL	BH	BW
Standard Deviation	0.38	1.31	2.32

Table 14. Standard Deviations for AL, BH and BW Responses.

Figures 10, 11 and 12 graphically illustrate the non-normality of the data using Predicted vs. Actual plots generated in Design-Expert ®. The points should be split evenly about and along the 45 degree line.

Design-Expert® Software
aluminum

Color points by value of
aluminum
6.54
4.96

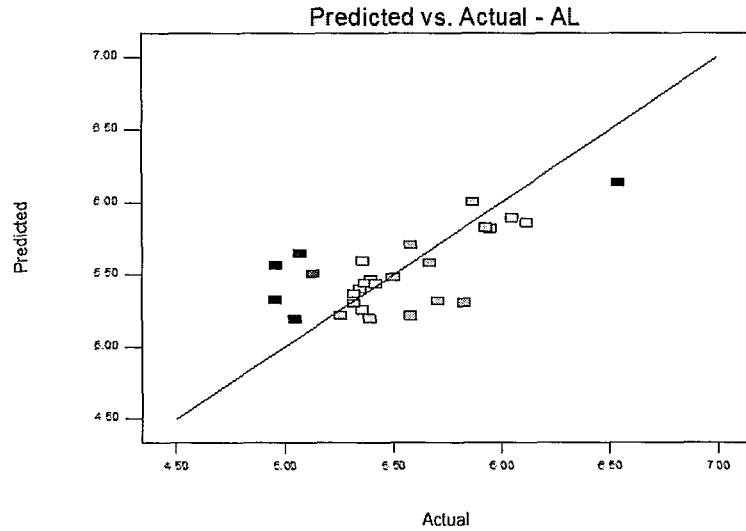


Figure 10. Predicted vs. Actual Values for AL Responses.

Design-Expert® Software
Bead Height

Color points by value of
Bead Height
5.22761
0.182621

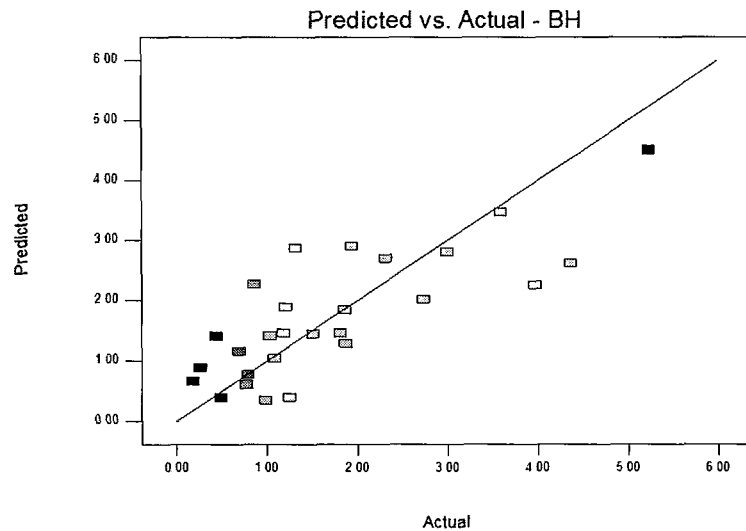


Figure 11. Predicted vs. Actual Values for BH Responses.

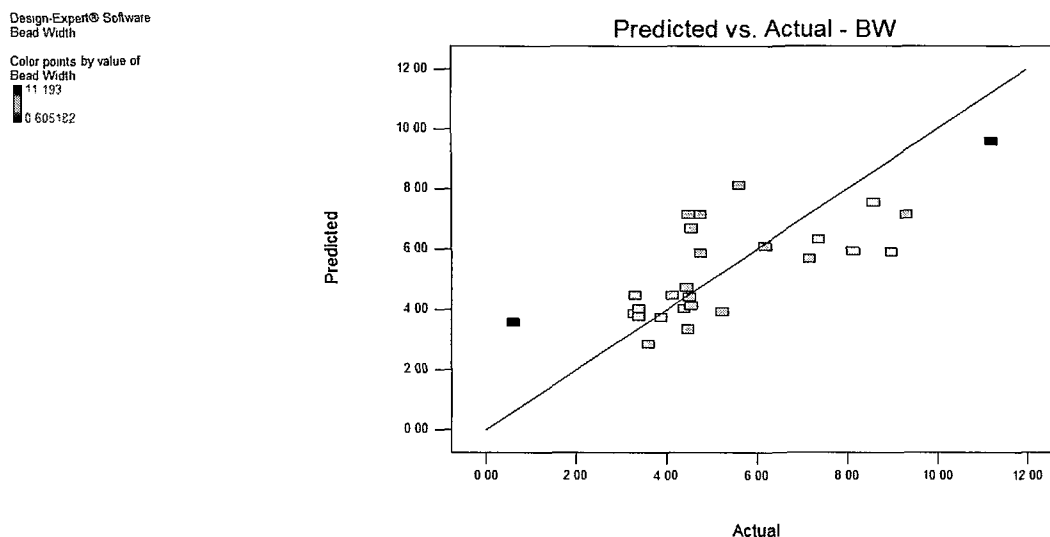


Figure 12. Predicted vs. Actual Values for BW Responses.

4.4.0 Analysis of Regression and ANOVA Statistics for AL Response Data

- Multiple R is the square root of R Square and represents the correlation between the factors and the response. Values close to 1.0 or 100% are desired. A value of 0.69 (69%) does not suggest an adequate R Square.
- R Square represents how well the regression line approximates the real data. Values close to 1.0 or 100% are desired. This value is computed using the Residual and Total SS from the ANOVA. $1 - \text{Residual SS} / \text{Total SS} = 1 - 2.00 / 3.81 = 0.47$. This value (47%) does not suggest an adequate fit.
- Adjusted R Square is adjusted to account for the increase in the R Square with each additional factor. This value is always lower than the R Square value and can be used to compare this model to one where more effects for this experiment are studied. It is computed as $1 - (\text{Total df} / \text{Residual df}) * (\text{Residual SS} / \text{Total SS}) = 1 - (26 / 17) * (2.00 / 3.81) = 0.19$
- Standard Error is an estimate of the standard deviation of the coefficients. The value of 0.34 is due to lack of repetition of the experiment. There is no variability to measure as each processing event was conducted one time.
- Observations are the number of experiments that were conducted which in this case is 27.
- Regression df represents the number of factors that can be varied. The regression allows for 9. This experiment varies only 3.

- Residual df of 20 is the Regression df subtracted from the total df = $(26 - 9) = 17$.
- Total df is 1 subtracted from the total degrees of freedom: Total df = $27 - 1 = 26$.
- Regression SS is the Residual SS subtracted from the Total SS. = $3.81 - 2.00 = 1.81$
- Residual SS for this regression is 2.00. If this model was an exact fit for the actual values then the Residual SS would be zero and R Square would be 1.
- Total SS is calculated as: $(N-1) * (\text{standard deviation}(Y))^2 = (27-1) * (0.38)^2 = 3.81$
- Regression MS is the Regression SS/Regression df. = $1.81/9 = 0.20$ which is used to compute the standard error.
- Residual MS is the Residual SS/Residual df = $2.00/17 = 0.12$. This is used to compute the standard error.
- F Statistic is the probability that the math model equation does not explain the variation in Y so that if there were a fit, it would be by chance. The F statistic should be < 1 (10%). The F Statistic for this model was 1.71 (170%) which is extremely high.
- Significance F for this model was 0.16 (16.0%) meaning that there is a 16% chance that this model is reliable. Values should be closer to 100%.
- Coefficients are the responses for each effect. They represent the mean or intercept of the Y values and the main and interaction effects. Values which are higher represent those having the most influence on the math model. The coefficients indicate that WF was the strongest independent factor affecting the final AL response and BP*TS had the strongest interaction effect. Weakest effects were TS and the BP*WF interaction. These are shown in Table 15 as values with 8 significant digits as output by Microsoft ® Excel.

Processing Parameters	Coefficients
Intercept	5.30592593
BP	0.09055556
TS	0.00111111
WF	0.15555556
BP*TS	-0.21416667
BP*WF	-0.035
TS*WF	0.19333333
BP^2	0.08388889
TS^2	0.13222222
WF^2	0.10555556

Table 15. Coefficients for the Processing Parameters for AL Responses.

- P-values indicate the validity of the coefficients. They should be approximately below .05 to prove that the coefficients are valid. Most are not below .05. The P-values are shown in Table 16 with 8 significant digits as output by Microsoft® Excel.

<i>Processing Parameters</i>	<i>P-value</i>
Intercept	2.98945E-16
BP	0.278532272
TS	0.989201222
WF	0.071407257
BP*TS	0.04520178
BP*WF	0.728234619
TS*WF	0.067692875
BP^2	0.557258914
TS^2	0.358559548
WF^2	0.461548189

Table 16. P-Values for the AL Response Coefficients.

4.4.1 Analysis of Regression and ANOVA Statistics for BH Response Data

- Multiple R is the square root of R Square and represents the correlation between the factors and the response. Values close to 1.0 or 100% are desired. A value of 0.79 (79%) does not suggest an adequate R Square; however it is closer to ideal than AL.
- R Square represents how well the regression line approximates the real data. Values close to 1.0 or 100% are desired. This value is computed using the Residual and Total SS from the ANOVA. $1 - \text{Residual SS} / \text{Total SS} = 1 - 16.62 / 44.54 = 0.63$. This value (63%) does not suggest an adequate fit, but it is closer than AL.
- Adjusted R Square is adjusted to account for the increase in the R Square with each additional factor. This value is always lower than the R Square value and can be used to compare this model to one where more effects for this experiment are studied. It is computed as $1 - (\text{Total df} / \text{Residual df}) * (\text{Residual SS} / \text{Total SS}) = 1 - (26/17) * (16.62/44.54) = 0.43$.
- Standard Error is an estimate of the standard deviation of the coefficients. The value of 0.90 is due to lack of repetition of the experiment. There is no variability to measure as each processing event was conducted one time.
- Observations are 27.

- Regression df is 9.
- Residual df of 20 is the Regression df subtracted from the total df = $(26 - 9) = 17$.
- Total df is 1 subtracted from the total degrees of freedom: Total df = $27 - 1 = 26$.
- Regression SS is the Residual SS subtracted from the Total SS. = $44.54 - 16.62 = 27.92$.
- Residual SS for this regression is 16.62. If this model was an exact fit for the actual values then the Residual SS would be zero and R Square would be 1.
- Total SS is calculated as: $(N-1) * (\text{standard deviation}(Y))^2 = (27-1) * (1.31)^2 = 44.54$.
- Regression MS is the Regression SS/Regression df. = $27.92/9 = 3.10$ which is used to compute the standard error.
- Residual MS is the Residual SS/Residual df = $16.62/17 = 0.98$. This is used to compute the standard error.
- F Statistic is the probability that the math model equation does not explain the variation in Y so that if there were a fit, it would be by chance. The F statistic should be $< .1$ (10%). The F Statistic for this model was 3.17 (~300%) which is extremely high.
- Significance F for this model was 0.019 (2.0%) meaning that there is a 2% chance that this model is reliable. Values should be closer to 100%.
- Coefficients are the responses for each effect. They represent the mean or intercept of the Y values and the main and interaction effects. Values which are higher represent those having the most influence on the math model. The coefficients indicate that TS was the strongest independent factor affecting the final BH response and BP*WF had the strongest interaction effect. Weakest effects were WF and the TS*WF interaction. These are shown in Table 17 as values with 8 significant digits as output by Microsoft® Excel.

<i>Processing Parameters</i>	<i>Coefficients</i>
Intercept	1.033475
BP	0.218582
TS	-0.80819
WF	-0.12224
BP*TS	-0.59607
BP*WF	0.79754
TS*WF	-0.12679
BP^2	0.634344
TS^2	0.169224
WF^2	0.2429

Table 17. Coefficients for the Processing Parameters of BH Responses.

- P-values indicate the validity of the coefficients. They should be approximately below .05 to prove that the coefficients are valid. Most values are above .05. These are shown in Table 18 as values with 8 significant digits as output by Microsoft® Excel.

<i>Processing Parameters</i>	<i>P-value</i>
Intercept	2.98945E-16
BP	0.278532272
TS	0.989201222
WF	0.071407257
BP*TS	0.04520178
BP*WF	0.728234619
TS*WF	0.067692875
BP^2	0.557258914
TS^2	0.358559548
WF^2	0.461548189

Table 18. P-Values for the BH Coefficients.

4.4.2 Analysis of Regression and ANOVA Statistics for BW Response Data

- Multiple R is the square root of R Square and represents the correlation between the factors and the response. Values close to 1.0 or 100% are desired. A value of 0.73 (72%) does not suggest an adequate R Square.
- R Square represents how well the regression line approximates the real data. Values close to 1.0 or 100% are desired. This value is computed using the Residual and Total SS from the ANOVA. $1 - \text{Residual SS} / \text{Total SS} = 1 - 65.79 / 140.46 = 0.53$. This value (53%) does not suggest an adequate fit.

- Adjusted R Square is adjusted to account for the increase in the R Square with each additional factor. This value is always lower than the R Square value and can be used to compare this model to one where more effects for this experiment are studied. It is computed as $1 - (\text{Total df} / \text{Residual df}) * (\text{Residual SS} / \text{Total SS}) = 1 - (26/17) * (65.79/140.46) = 0.28$.
- Standard Error is an estimate of the standard deviation of the coefficients. The value of 1.97 is due to lack of repetition of the experiment. There is no variability to measure as each processing event was conducted one time.
- Observations are 27.
- Regression df is 9.
- Residual df of 17 is the Regression df subtracted from the total df = $(26 - 9) = 17$.
- Total df is 1 subtracted from the total degrees of freedom: Total df = $27 - 1 = 26$.
- Regression SS is the Residual SS subtracted from the Total SS. = $140.46 - 65.79 = 74.67$
- Residual SS for this regression is 65.79. If this model was an exact fit for the actual values then the Residual SS would be zero and R Square would be 1.
- Total SS is calculated as: $(N-1) * (\text{standard deviation}(Y))^2 = (27-1) * (2.32)^2 = 140.46$.
- Regression MS is the Regression SS/Regression df. = $74.67/9 = 8.30$ which is used to compute the standard error.
- Residual MS is the Residual SS/Residual df = $65.79/17 = 3.87$. This is used to compute the standard error.
- F Statistic is the probability that the math model equation does not explain the variation in Y so that if there were a fit, it would be by chance. The F statistic should be < 1 (10%). The F Statistic for this model was 2.14 (214%) which is extremely high.
- Significance F for this model was 0.084 (8.0%) meaning that there is an 8% chance that this model is reliable. Values should be closer to 100%.
- Coefficients are the responses for each effect. They represent the mean or intercept of the Y values and the main and interaction effects. Values which are higher represent those having the most influence on the math model. The coefficients indicate that TS was the strongest independent factor affecting the final AL response and BP*WF had the strongest interaction effect. Weakest effects were WF and the

TS*WF interaction. These are shown in Table 19 as values with 8 significant digits as output by Microsoft ® Excel.

<i>Processing Parameters</i>	<i>Coefficients</i>
Intercept	3.741437
BP	0.227468
TS	-1.48245
WF	0.150674
BP*TS	-0.50874
BP*WF	1.22237
TS*WF	0.153763
BP^2	0.503581
TS^2	1.072966
WF^2	0.818655

Table 19. Coefficients for the Processing Parameters for BW Responses.

- P-values indicate the validity of the coefficients. They should be approximately below .05 to prove that the coefficients are valid. These are shown in Table 20 as values with 8 significant digits as output by Microsoft ® Excel.

<i>Processing Parameters</i>	<i>P-value</i>
Intercept	0.00164761
BP	0.63001931
TS	0.005281878
WF	0.749194793
BP*TS	0.382867512
BP*WF	0.046026994
TS*WF	0.789844986
BP^2	0.538989164
TS^2	0.199181048
WF^2	0.322350977

Table 20. P-Values for the BW Response Coefficients.

4.5 Math Models for Response Data

The coefficients from the regression analyses are shown in Table 21. Weight percent values are reduced to two significant digits and BH and BW values are reduced to

one significant digit. These become the variables in the quadratic equations used to compute RS equations. The strongest (s) and weakest effects (w) and interaction effects are ranked by absolute value and are highlighted in bold. The squared terms in bold show which factors had the greatest influence on the non-linearity of the data.

Factors	<i>Coefficients</i>		
	AL (Wt %)	BH (mm)	BW (mm)
Intercept	5.31	1.0	3.7
BP	0.09	0.2	0.2 (w)
TS	0.00 (w)	-0.8 (s)	-1.5 (s)
WF	0.16 (s)	-0.1 (w)	0.2
BP*TS	-0.21 (s)	-0.6	-0.5
BP*WF	-0.04 (w)	0.8 (s)	1.2 (s)
TS*WF	0.19	-0.1 (w)	0.2 (w)
BP^2	0.08	0.6 (s)	0.5
TS^2	0.13 (s)	0.2	1.1 (s)
WF^2	0.11	0.2	0.8

Table 21. Coefficients for AL, BH and BW Responses.

The coefficients derived from the ANOVA are plugged into the equation $Y=b_0+b_1BP+b_2TS+b_3WF+b_4BP*TS+b_5BP*WF+b_6TS*WF+b_7BP^2+b_8TS^2+b_9WF^2$, as shown below. The values 1 and -1 inside of the parenthesis indicate the processing level selected by Microsoft® Excel Solver and are discussed in the next section.

$$Y [AL] = 5.31+0.091(1) + 0.001 (-1) + 0.156 (-1) -0.214 (1) (-1)-0.035(1) (-1) + 0.193 (-1) (-1) + 0.084 (1) (1) + 0.132 (-1) (-1) + 0.106 (-1) (-1)$$

$$Y [BH] = 1.03+0.219 (1) -0.808 (-1) -0.122 (1) -0.596 (1) (-1) + 0.797 (1) (1) - 0.127 (-1) (1) + 0.634 (1) (1) + 0.169 (-1) (-1) + 0.243 (1) (1)$$

$$Y [BW] = 3.741+0.227 (1) -1.482 (-1) + 0.151 (-1) - 0.509 (1) (-1) + 1.222 (1) (-1) + 0.154 (-1) (-1) + 0.504 (1) (1) + 1.073 (-1) (-1) + 0.819 (-1) (-1)$$

Using Microsoft ® Excel Solver add-in, the Y (response) values were then optimized at processing levels recommended by the software. Solver maximizes the value of the target cell by changing the values in three cells that represent the coded processing levels for BP, TS and WF. Constraints are added to keep the levels as integers between low (-1) and high (1). The optimized values for all three factors are shown in Table 22.

Responses	AL (wt %)	BH (mm)	BW (mm)
Math Model	Y [AL] = 6.00	Y [BH] = 4.50	Y[BW] = 9.57

Table 22. Optimized Responses for AL, BH and BW.

4.6 Processing Levels for Response Data

Microsoft ® Excel Solver provided solutions for each response by selecting the optimum processing levels between -1 and 1. A summary of the processing levels used to obtain the optimized or maximum output responses are shown in Table 23. The prediction RS suggests that these levels resulted in the calculated optimized Y (response) values shown in Table 22.

Responses	AL	BH	BW
Processing Levels	BP = +1	BP = +1	BP = +1
	TS = -1	TS = -1	TS = -1
	WF = +1	WF = +1	WF = +1

Table 23. Processing Levels for BP, TS and WF Rate.

The processing levels for the optimized AL response reconciled with the processing levels used to produce Sample 9 as shown in Figure 42 of Appendix A. Sample 9 had an AL content of 5.87 wt % and good bead geometry. The recommendation of Sample 9 by the math model for AL was the cause for studying the BH and BW. The high heat of the BP and slow speeds of the TS and WF may compound the vaporization problem. It is suspected that running EBF³ at the processing levels of Sample 9 over time [BP = high, TS = low and WF = low] would subject the layers under the beam to too much heat. The processing levels for the optimized BH response reconciled with Sample 7 as shown in Figure 41 of Appendix A. The processing levels for the optimized BW also reconciled with Sample 7.

4.7 Contour Plots for Response Data

Using Design-Expert®, an optimization analysis was conducted generating contour plots for each of the responses to obtain graphical representation of the predictions.

AL – The optimization was constructed in Design-Expert® using options for building and viewing contour plots. The ‘in range’ option with the true AL response range of 4.96 wt % - 6.54 wt% was selected. The independent and interaction factors that

corresponded to the strongest coefficients [+] (WF) and [-] (BP*TS), as previously shown in Table 21, were selected for analysis. AL is maximized when BP = +1, TS = -1 and WF = -1 and the predicted response is approaching ~ 6.00 wt % as shown in the contour plot in Figure 13. The processing levels reconcile with the processing levels used to produce Sample 9 as was also predicted by the RS.

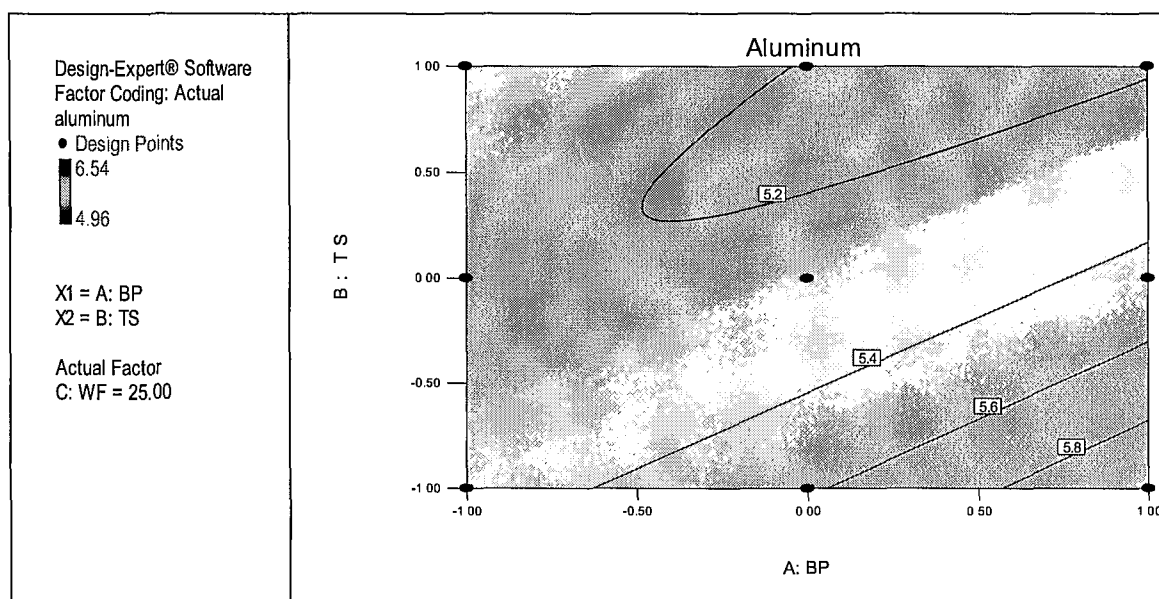


Figure 13. AL Response Data Evaluated Optimized When BP = +1, TS = -1, WF = -1.

BH - The optimization was constructed using the 'in range' option. The range of .2 mm – 5.2 mm represents the minimum and maximum height values to include the entire height range of the samples. The independent and interaction factors that corresponded to the strongest coefficients are [-] (TS) and [+] (BP*WF), as previously shown in Table 21, were selected for analysis. BH was maximized when BP = +1, TS = -1 and WF = +1 and the predicted response was approaching ~ 5.0 mm as shown in Figure 14. The processing levels reconcile with processing levels used to produce Sample 7 as was also predicted by the RS.

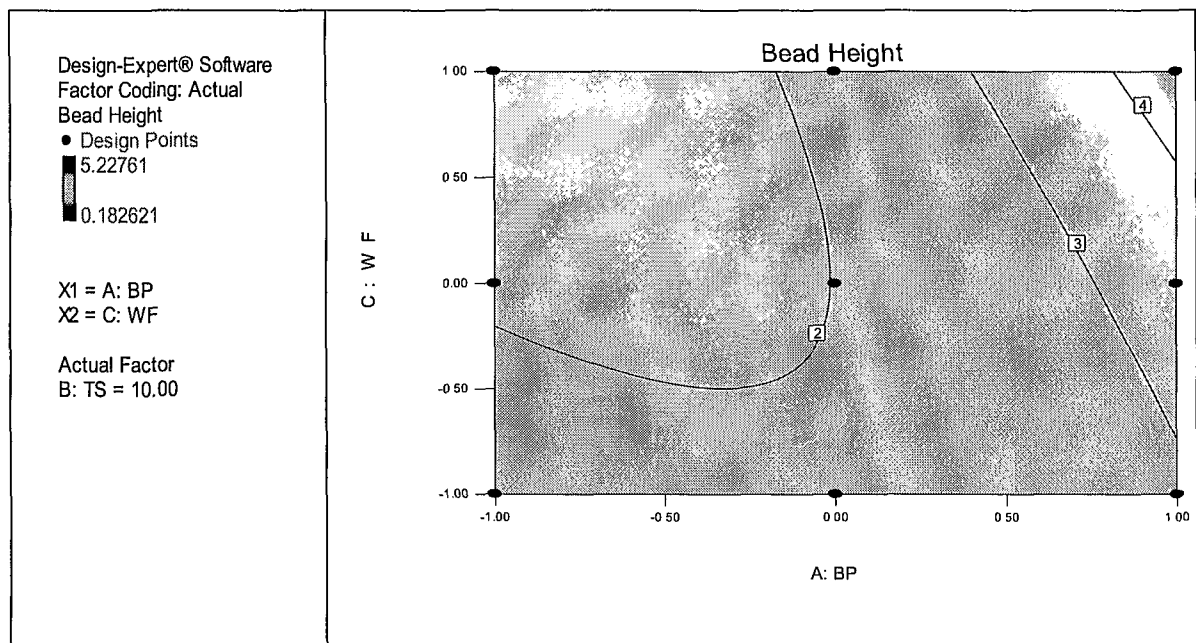


Figure 14. BH Response Data Optimized When BP = +1, TS = -1, WF = +1.

BW - The optimization was constructed using the 'in range' option in order to narrow the otherwise large measurement range. The range of .6 mm – 11.2 mm represents the minimum and maximum width values for all 27 samples. The independent and interaction factors that corresponded to the strongest coefficients [-] (TS) and [+] (BP*WF), as previously shown in Table 21, were selected for analysis. BW was maximized when BP = +1, TS = -1, and WF = +1 and the response was approaching ~ 10.0 mm as shown in Figure 15. The processing levels reconcile with processing levels used to produce Sample 7 as was also predicted by the RS.

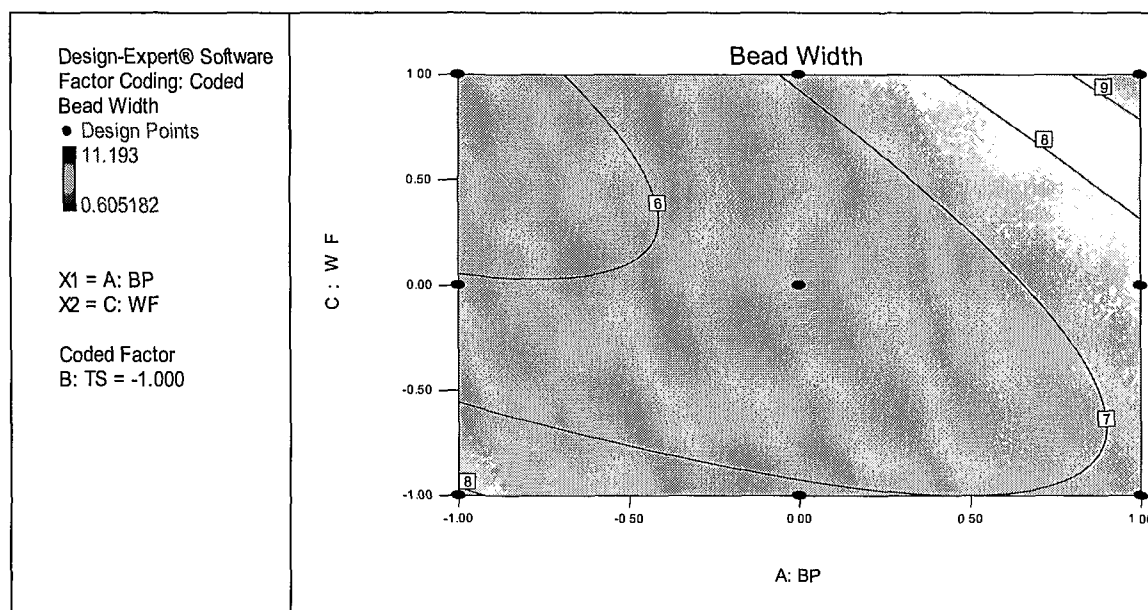


Figure 15. BW Response Data Optimized When BP = +1, TS = -1, WF = +1.

In summary, the optimized predicted processing levels are as follows:

- AL (wt %) reconciles with Sample 9 - [BP = +1, TS = -1, WF = -1]
- BH (mm) reconciles with Sample 7 - [BP = +1, TS = -1, WF = +1]
- BW (mm) reconciles with Sample 7 - [BP = +1, TS = -1, WF = +1]

4.8 Transformation Overview

Box-Cox plots were constructed in Design-Expert ® and evaluated to determine if a transformation of the response data was recommended. The diagnosis involves a check to see if the 95% confidence interval around a calculated best Lambda value, which is the natural log of the sum of squares of the residuals, includes the value 1. If the interval does not include 1, then a transformation is recommended (Stat-Ease ®, 2011).

Brooks@StatHelp (personal communication, July 19, 2012) provided an explanation for the calculation of the confidence intervals. The Ln(Res SS) for models is obtained after applying the transformation with Lambda values normally between -3 and 3.

Transformation of the AL response data is not recommended because the low confidence is -6.19 and the high confidence interval is 6.33. This range includes the value $\text{Lambda} = 1$. Transformation of the BW data is also not recommended because the value 1 is within the low confidence interval of 0.18 and the high confidence interval of 1.45 calculated around the best Lambda of 0.75. A transformation is recommended for the BH response data because the lower confidence interval is -0.12 and the high confidence interval is 0.84 making $\text{Lambda} = 1$ outside of the confidence interval range. Figures 16, 17 and 18 show the Box-Cox diagnostic plots for AL, BH and BW respectively.

Design-Expert® Software
aluminum

Lambda
Current = 1

Low C I = -6.31
High C I = 6.18

Recommend transform.
None
(Lambda = 1)

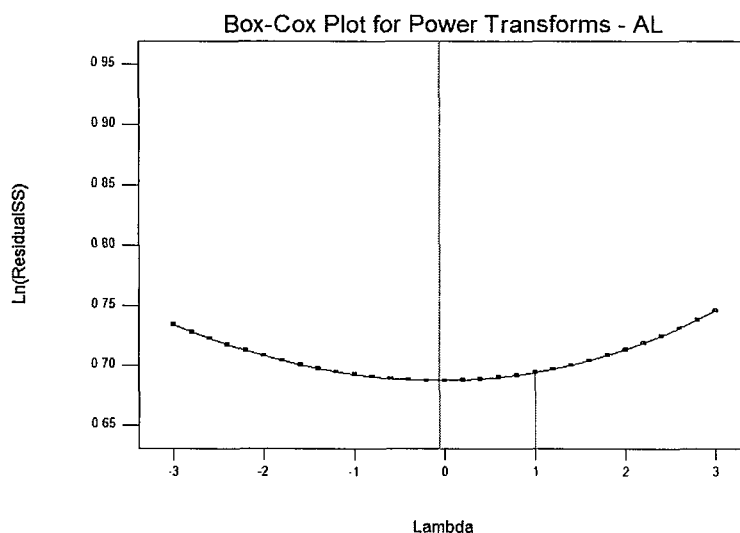


Figure 16. Box-Cox Plot for Power Transforms – AL Responses.

Design-Expert® Software
Bead Height

Lambda
Current = 1
Low C I = -0.12
High C I = 0.84

Recommend transform
Square Root
(Lambda = 0.5)

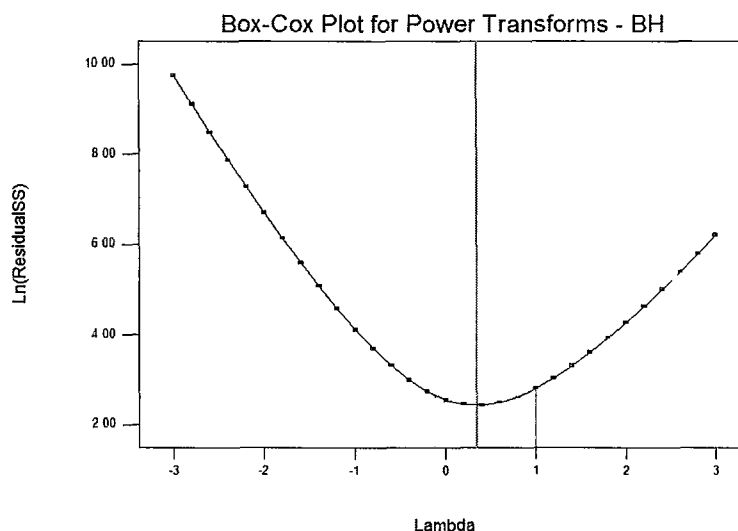


Figure 17. Box-Cox Plot for Power Transforms – BH Responses.

Design-Expert® Software
Bead Width

Lambda
Current = 1
Low C I = 0.18
High C I = 1.45

Recommend transform
None
(Lambda = 1)

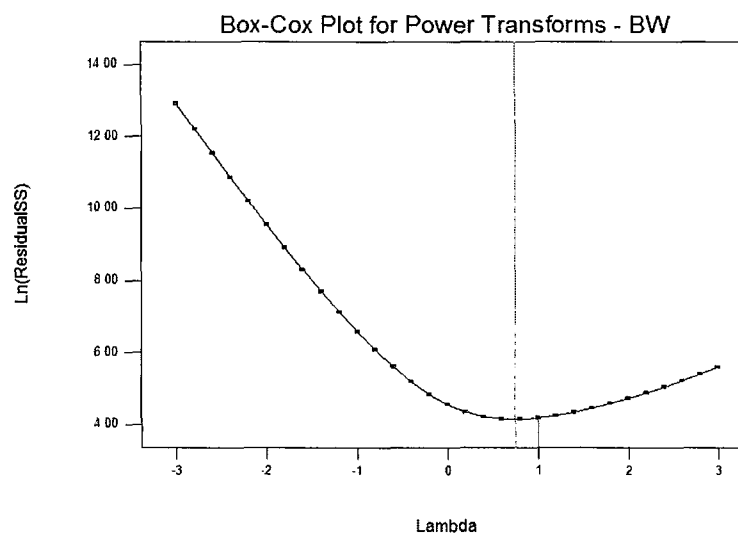


Figure 18. Box-Cox Plot for Power Transforms – BW Responses.

4.9 SQRT(x) Transformation and Regression of BH Response Data

As suggested by the Box-Cox diagnostic as shown in the legend of Figure 17, and indicated by the distribution curve improvement previously shown in Figure 9 (Distribution Curve for Square Root Transformed BH Responses), the square root

transformation was applied to the BH responses matrix in Design-Expert ® and the Box-Cox test conducted. Figure 19 shows that the calculated best Lambda is now equal to 1 which falls within the confidence interval range. Figure 20 shows the improved distribution of the data.

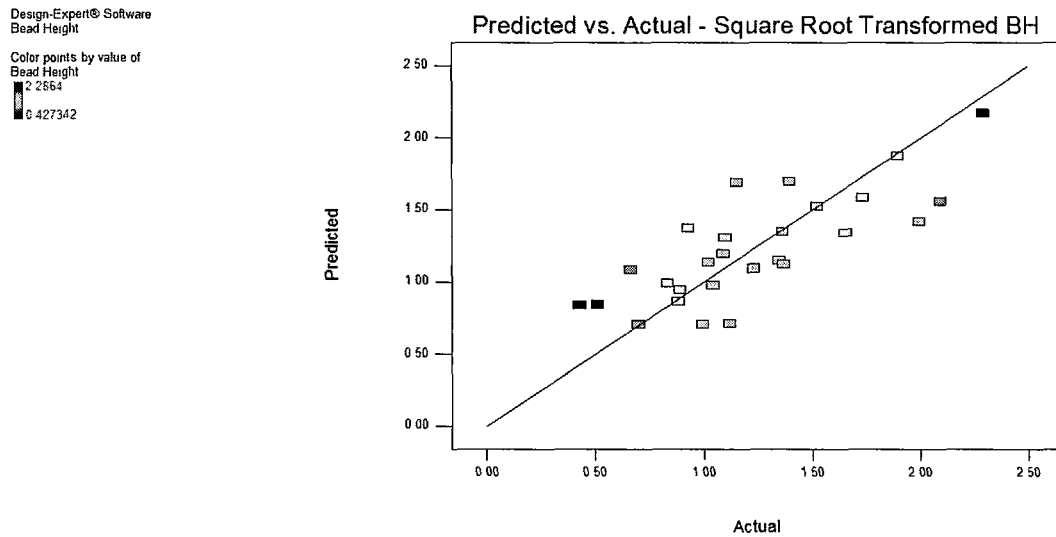


Figure 19. Box-Cox Plot for Power Transforms – BH Responses with Square Root Transformation Applied.

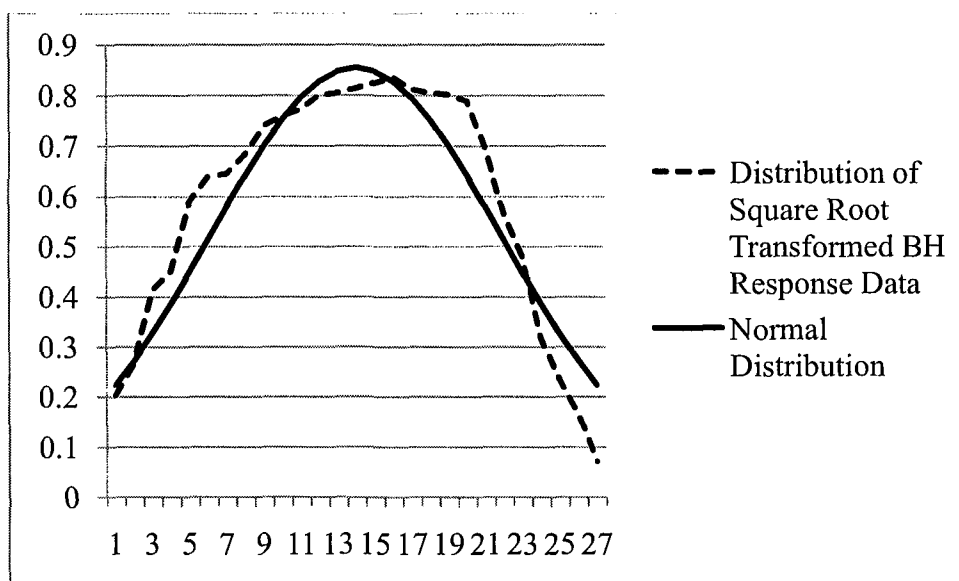


Figure 20. Distribution of the Square Root Transformed BH Responses.

A new regression was calculated for the square root ($\sqrt{}$) transformed BH response data. Table 24 shows the statistics culled from the Regression.

Response	R Square	F Statistic	Stdev
BH (Non-Transformed)	0.63	3.17	1.31
BH ($\sqrt{}$ Transformation)	0.62	3.08	0.48

Table 24. Summary of Statistics for BH before and after SQRT Transformation.

The R Square value and F Statistic were not improved by the square root transformation. Figures 21 and 22 show the predicted vs. actual BH responses for non-transformed and square root transformed responses. The transformed plot shows only marginal improvement of the fit.

Design-Expert® Software
Bead Height

Color points by value of
Bead Height
5.22761
0.162621

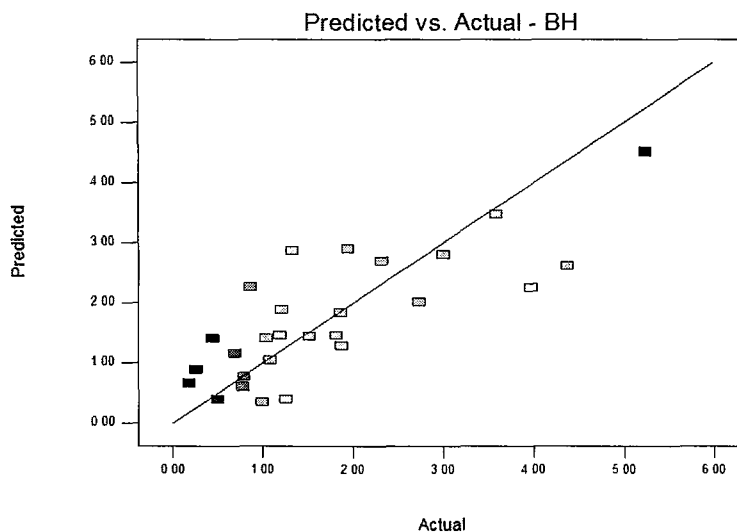


Figure 21. Predicted vs. Actual Values for Non-Transformed BH Responses.

Design-Expert® Software
Bead Height

Color points by value of
Bead Height
2.2864
0.427342

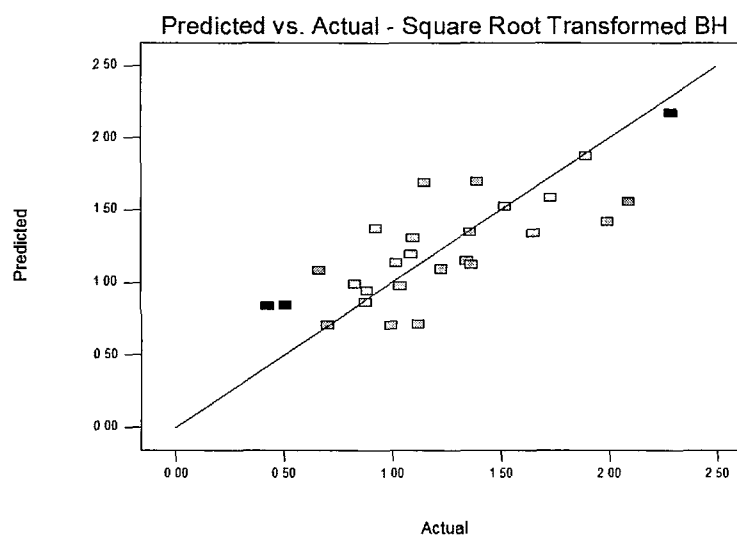


Figure 22. Predicted vs. Actual Values for Square Root Transformed BH Responses.

A math equation was derived next, computed using the new transformed coefficients from the ANOVA statistics shown in Table 25. The values were reduced to two significant digits. Strongest (s) and weakest (w) main and interaction effects are

ranked by absolute value and are shown in bold. The squared terms show which factors had the greatest influence on the non-linearity of the data. As with non-transformed BH responses, the squared BP had the strongest influence.

<i>Factors</i>	<i>Coefficients</i>
Intercept	0.98
BP	0.06
TS	-0.31(s)
WF	-0.05(w)
BP*TS	-0.21
BP*WF	0.26(s)
TS*WF	-0.02(w)
BP^2	0.27 (s)
TS^2	0.05
WF^2	0.06

Table 25. Coefficients for Square Root Transformed BH Responses.

The strongest interactions are the TS for the independent variable and BP*WF for the interaction variables. WF is the weakest independent factor and TS*WF is the weakest interaction. The math equation was constructed using the Microsoft ® Excel Solver with recommended processing levels for optimized output response as shown in Table 26.

SQRT Transformation	BH
Processing Levels	BP=1 TS= -1 WF= 1

Table 26. Processing Levels for Square Root Transformed BH Responses.

4.10 Math Model for SQRT Transformed BH Response Data

$$Y [BH] = 4.71 \text{ mm}$$

4.11 Processing Levels for Square Root Transformed BH Response Data

Processing levels of BP = +1, TS = - 1 and WF = +1 reconcile with the processing levels used to produce Sample 7. BH was maximized at 4.7 mm. The results of transforming the BH with square root actually had no effect on the outcome of the prediction model, except for increasing the predicted response from 4.5 mm to 4.7 mm.

4.12 Contour Plot for Square Root Transformed BH Response Data

Using Design-Expert®, an optimization analysis was conducted for each of the three factors to produce the graphical representation of the predictions.

The optimization was constructed using the 'in range' option. The range of .2 mm – 5.2 mm represents the minimum and maximum height values to include the entire height range of the samples. The independent and interaction factors that corresponded to the strongest coefficients [-] (TS) and [+] (BP*WF), as previously shown in Table 25, were selected to produce the contour plot as shown in Figure 23. Given that the inverse of the transformation is taken into consideration, BH was maximized when BP = +1, TS

= -1 and WF = +1 when the predicted response was approaching levels greater than 2.2 or the inverse of the square root transform, $(2.2)^2 \sim 4.0$ mm. The processing levels reconcile with processing levels used to produce Sample 7.

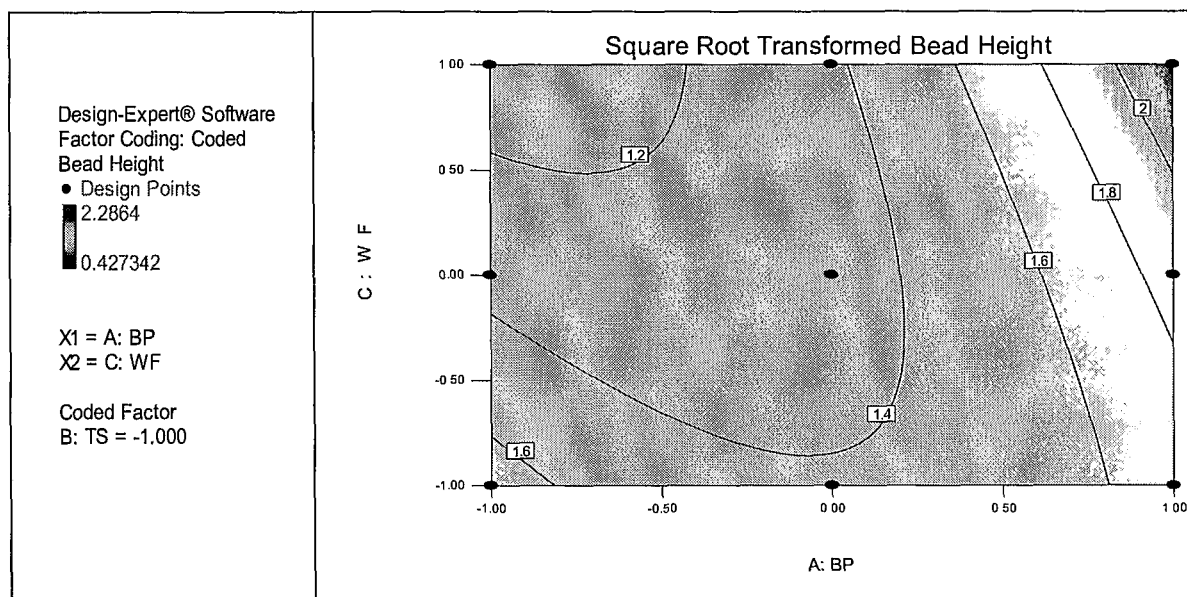


Figure 23. BH with SQRT Transformation Optimized BP = +1, TS = -1 and WF = +1.

4.13 Log(x) Transformation and Regression of Response Data

To test the hypothesis that a Log(x) transformation may produce usable predictions, the Log(x) transformation was applied to all of the response sets. This transformation improved the shape of the data for BH, but did not improve the shape for AL or BW as shown in Figures 24, 25 and 26.

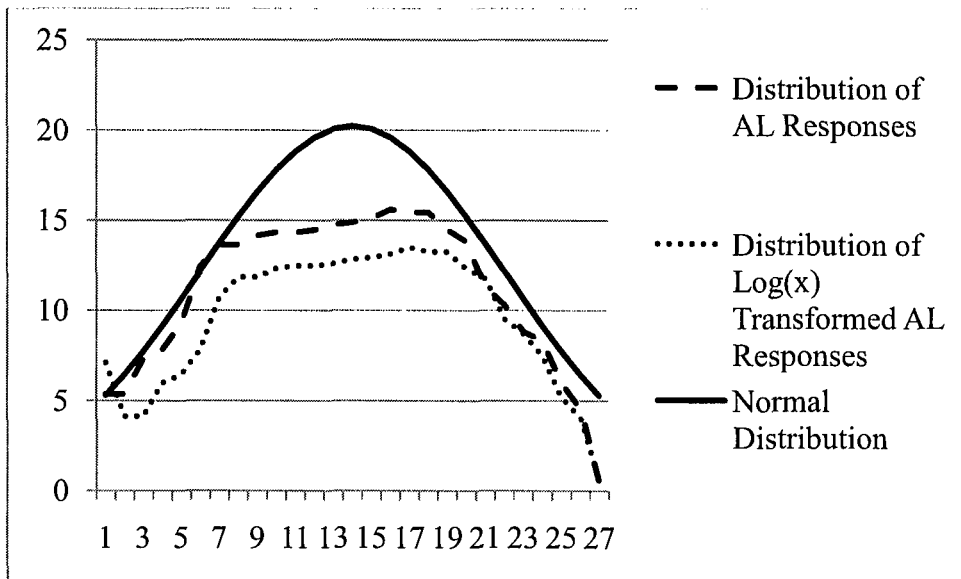


Figure 24. AL Responses Transformed with Log(x).

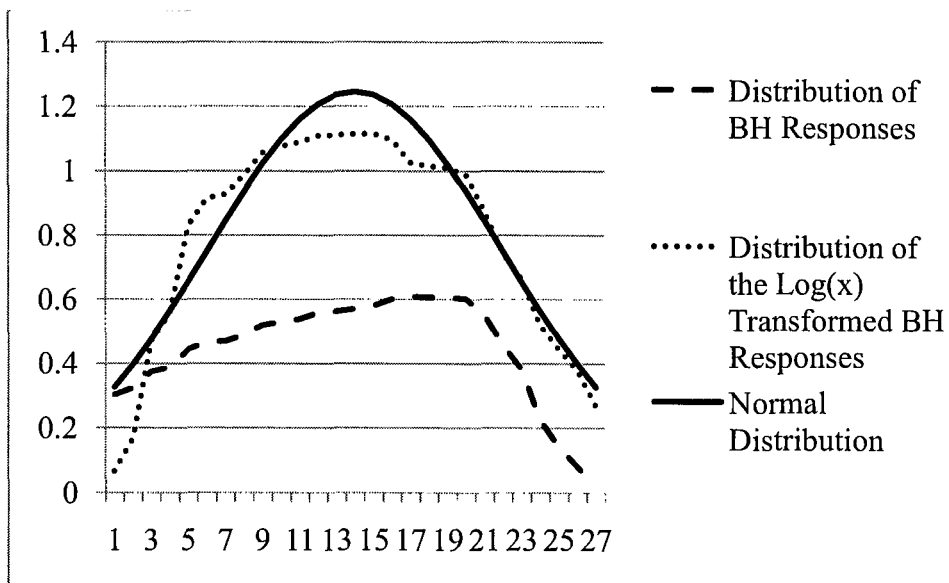


Figure 25. BH Responses Transformed with Log(x).

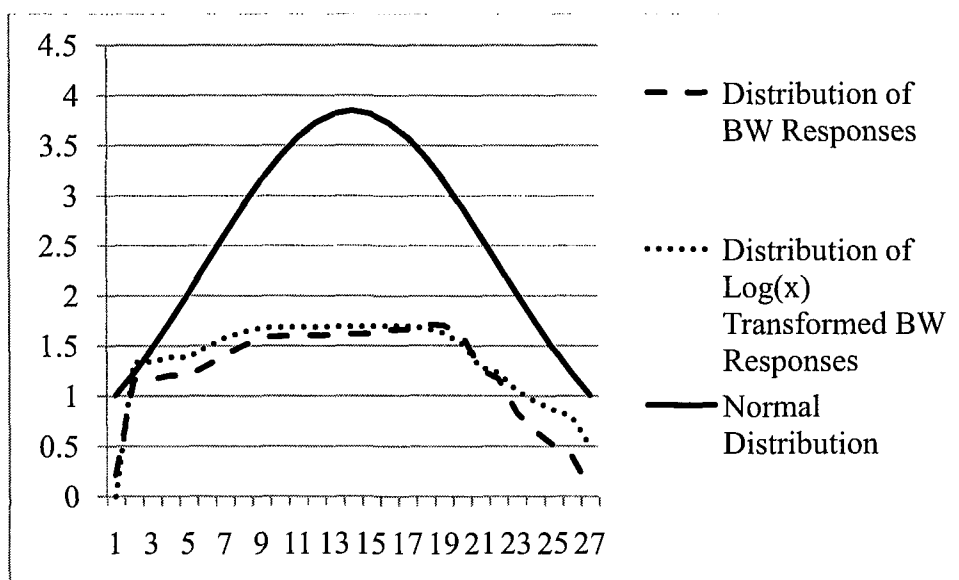


Figure 26. BW Responses Transformed with Log(x).

A regression analysis was conducted for the Log(x) transformed AL, BH and BW response data. The statistics for non-transformed and Log(x) transformed responses are summarized in Table 27.

Factors	R Square	F Statistic	Standard Deviation
AL (non-transformed)	0.47	1.71	0.38
AL (log(x))	0.45	1.59	0.03
BH (non-transformed)	0.63	3.17	1.31
BH (log(x))	0.57	2.47	0.35
BW (non-transformed)	0.53	2.14	2.32
BW (log(x))	0.45	1.52	0.23

Table 27. Statistics and ANOVA Results for Non-Transformed and Log(x) Transformed Responses.

The R Square and F Statistic values show even greater probability that the model does not explain the variation in Y. Figures 27, 28 and 29 show the predicted vs. actual plots for Log(x) transformed response data. The only improvement was seen in the BH Log(x) transformed response data.

Design-Expert® Software
aluminum

Color points by value of
aluminum
0.816578
0.695482

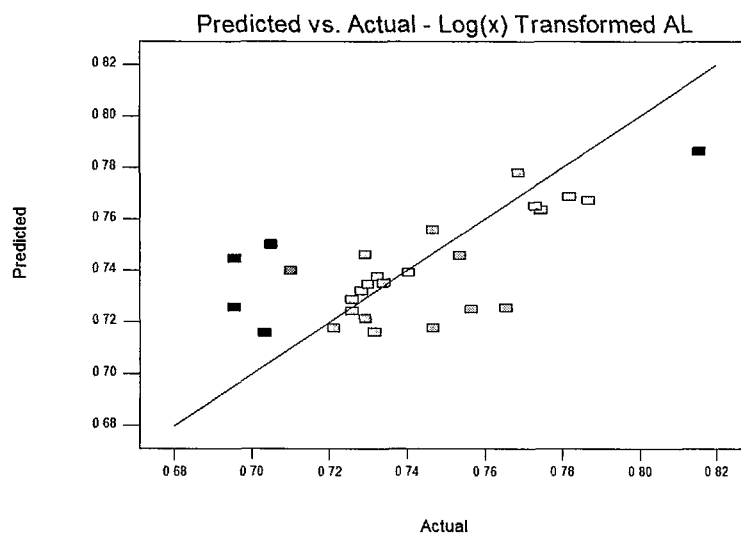


Figure 27. Predicted vs. Actual Values for Log(x) Transformed AL Responses.

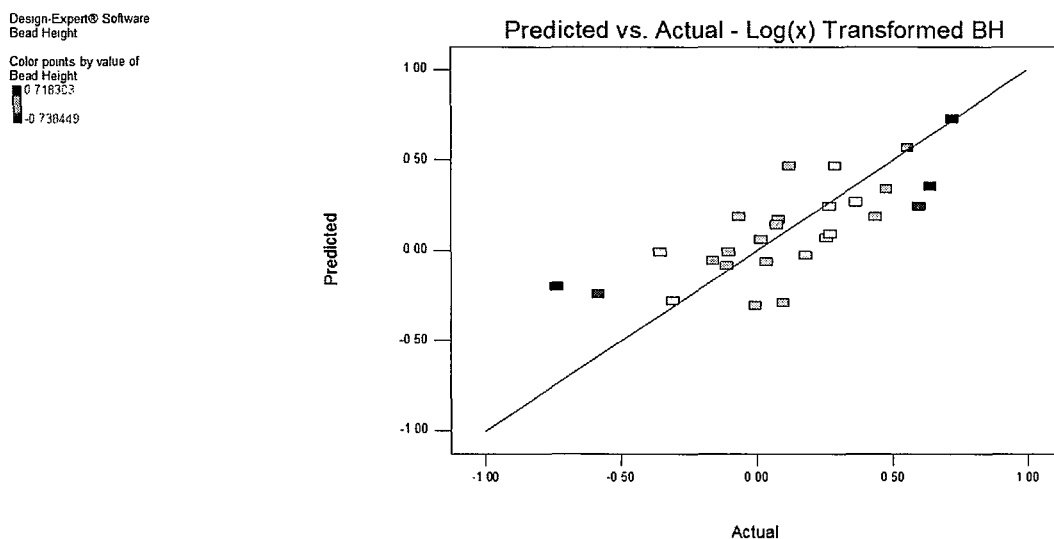


Figure 28. Predicted vs. Actual Values for Log(x) Transformed BH Responses.

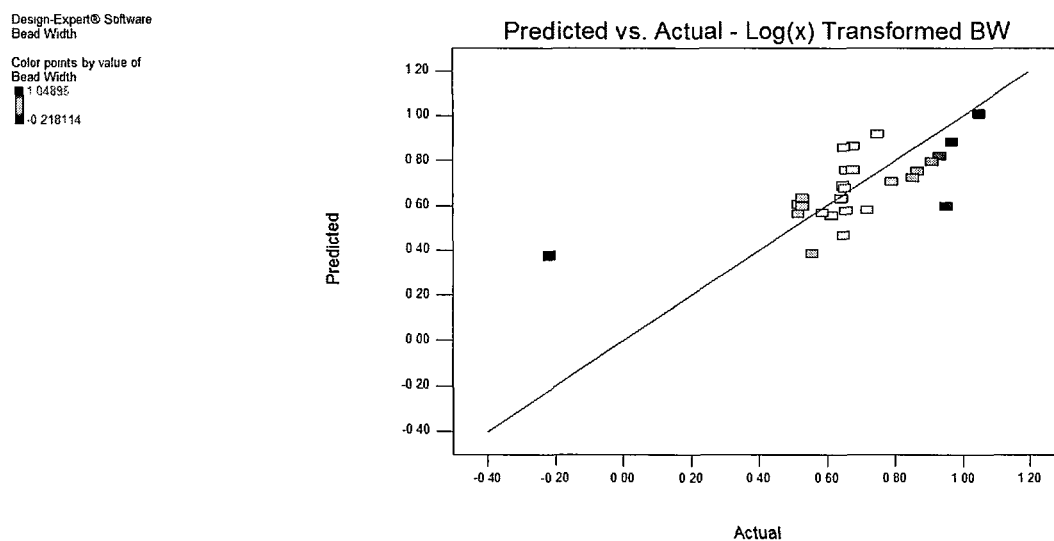


Figure 29. Predicted vs. Actual Values Log(x) Transformed BW Responses.

4.14 Math Models for Log(x) Transformed Response Data

The coefficients from the transformed regression analysis are reduced to two significant digits and shown in Table 28. Strongest (s) and weakest (w) interactions are ranked by absolute value and are shown in bold. The squared terms that had the strongest

effect on the non-linearity are shown in bold. In the case of AL, rounding to two significant digits reduces the accuracy of the original values [BP = 0.006258, TS = 0.009577, WF = 0.007594].

<i>Factors</i>	<i>Coefficients</i>		
	AL (Wt %)	BH (mm)	BW (mm)
Intercept	0.73	-0.06	0.57
BP	0.01	0.02 (w)	-0.02
TS	-0.00 (w)	-0.24 (s)	-0.14 (s)
WF	0.01 (s)	-0.02	0.00 (w)
BP*TS	-0.02 (s)	-0.14	-0.08 (w)
BP*WF	-0.00 (w)	0.16 (s)	0.09 (s)
TS*WF	0.02	0.01 (w)	0.02
BP^2	0.01	0.22 (s)	0.01
TS^2	0.01(s)	0.01	0.04
WF^2	0.01	0.03	0.12(s)

Table 28. Coefficients for Log(x) Transformed AL, BH and BW Responses.

Math models were derived from the coefficients based on the quadratic equation:

$$Y = b_0 + b_1BP + b_2TS + b_3WF + b_4BP*TS + b_5BP*WF + b_6TS*WF + b_7BP^2 + b_8TS^2 + b_9WF^2.$$

Using Microsoft ® Excel Solver add-in, the responses (Y), were optimized.

$$Y [AL] = 5.85$$

$$Y [BH] = 5.34$$

$$Y [BW] = 10.21$$

4.15 Processing Levels for Log(x) Transformed Response Data

Microsoft ® Excel Solver examines all possible combinations of the processing levels for each of the processing levels for each response. The best processing levels are used to obtain the optimized output response above and are shown in Table 29.

Log (x)	AL	BH	BW
Processing Levels	BP = 1	BP = 1	BP = 1
	TS = -1	TS = -1	TS = -1
	WF = 1	WF = 1	WF = 1

Table 29. Processing Levels for Log(x) Transformed BP, TS and WF Responses.

The processing levels for AL reconciled with processing levels used to produce Sample 7 for AL, BH and BW. The analysis suggests that the Log(x) transformation aligned the processing levels with the most visually appealing and chemically desired sample.

4.16 Box-Cox Plots for Log(x) Transformed Response Data

The Box-Cox diagnosis shows Lambda = 1 is within range for AL and BH as shown in Figures 30 and 31.

Design-Expert® Software
aluminum

Lambda
Current = 1

Low C I = -9.98
High C I = 11.65

Recommend transform
None
(Lambda = 1)

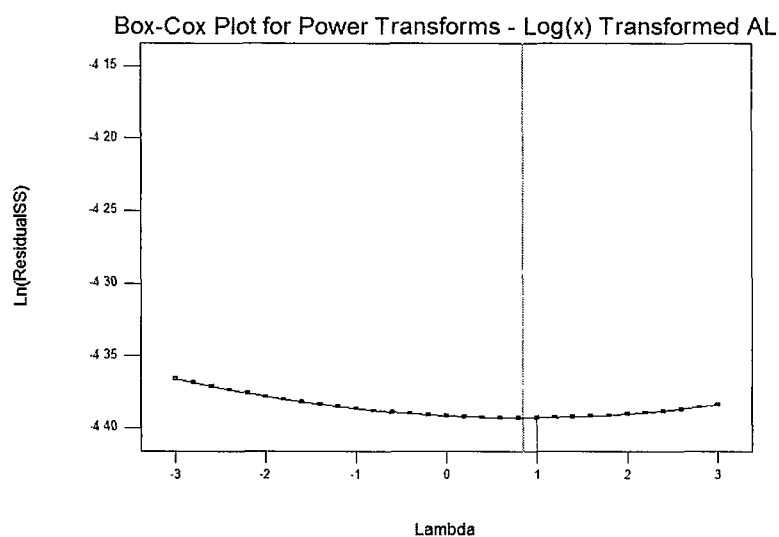


Figure 30. Log(x) Transformed Box-Cox Plot for AL.

Design-Expert® Software
Bead Height

Lambda
Current = 1
Low CI = 0.72
High CI = 2.34

Recommend transform
None
(Lambda = 1)

k = 0.812294
(used to make
response values
positive)

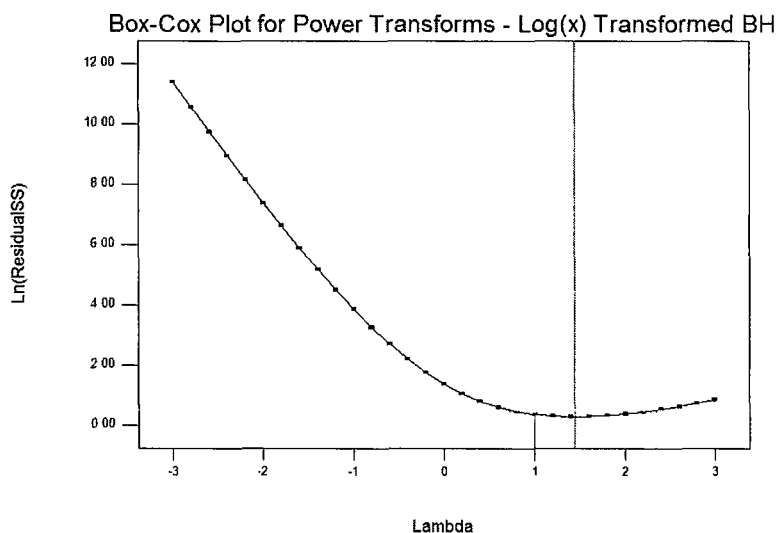


Figure 31. Log(x) Transformed Box-Cox Plot for BH.

The Box-Cox plot shown in Figure 32 recommends a power transformation. The power transformation was applied to the non-transformed BW response values using the recommended constant K of 0.239925. The Lambda = 1 was then within the confidence interval range, but the statistics and results of the analysis were the same as for the Log(x) transformation. A contour plot will be shown subsequently for illustration.

Design-Expert® Software
Bead Width

Lambda
Current = 1

Low CI = 1.11
High CI = 2.93

Recommend transform
Power
(Lambda = 1.86)

k = 0.239925
(used to make
response values
positive)

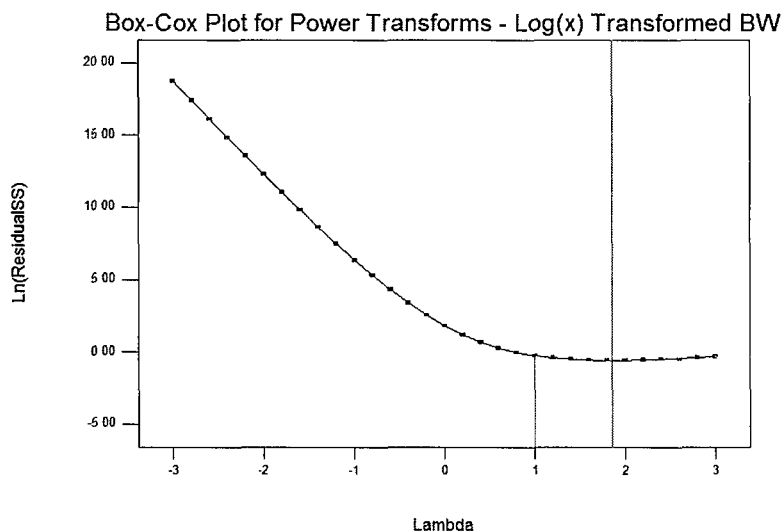


Figure 32. Log(x) Transformed Box-Cox Plot for BW.

4.17 Contour Plots for Log(x) Transformed Response Data

Using Design-Expert®, an optimization analysis was conducted for each of the three factors to produce a graphical representation of the predictions:

AL – The optimization was constructed using the ‘in range’ option with a Log(x) inverse transformed AL response range of 4.96 wt % - 6.54 wt%. The independent and interaction factors that corresponded to the strongest coefficients [+] (WF) and [-] (BP*TS), as previously shown in Table 28, were selected to produce the contour plot shown in Figure 33. AL was maximized when BP = +1, TS = -1 and WF = +1 when AL was approaching .77 or the inverse of the Log(x) transform, $10^{.77} \sim 5.85$ wt %. The processing levels reconcile with the processing levels used to produce Sample 7.

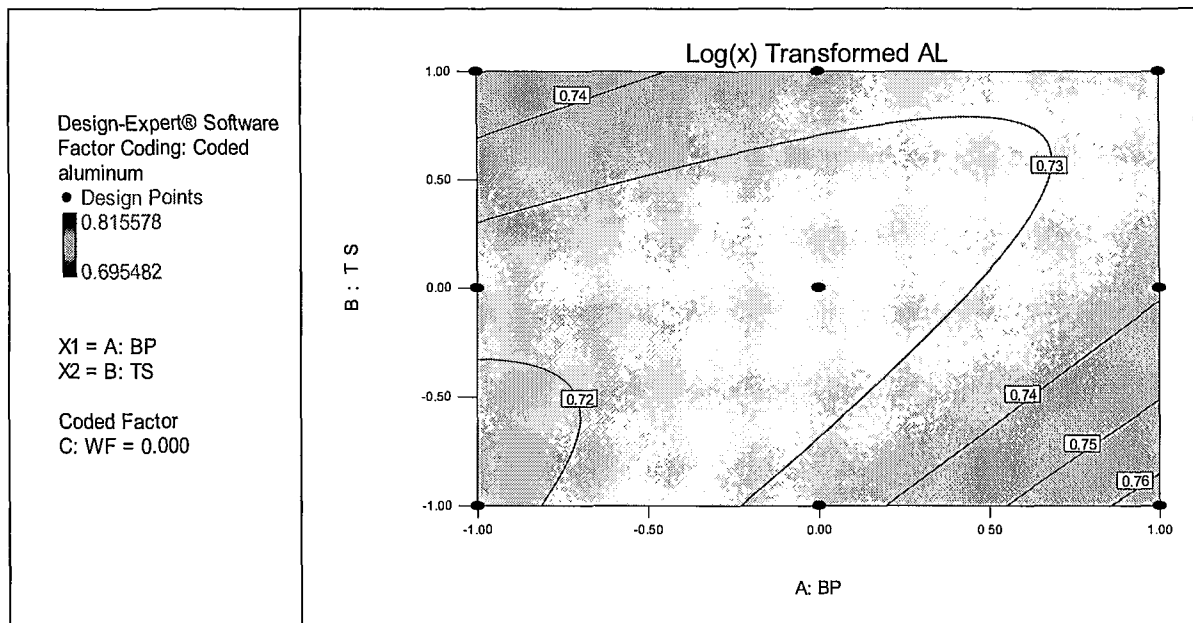


Figure 33. Log(x) Transformed AL Response Data Optimized when BP = +1, TS = -1 and WF = +1.

BH - The optimization was constructed using the 'in range' option in order to narrow the otherwise large range. The inverse Log(x) range of 1.5 mm – 5.2 mm was input to represent the minimum and maximum height values of the twelve visually acceptable samples. The independent and interaction factors that corresponded to the strongest coefficients [-] (TS) and [+] (BP*WF), as previously shown in Table 28, were selected to produce the contour plot as shown in Figure 34. BH was maximized when BP = +1, TS = -1, and WF = +1 and BH was approaching .73 or the inverse of the Log(x) transform, $10^{-.73} \sim 5.3$ mm. These processing levels reconcile with the processing levels used to produce Sample 7.

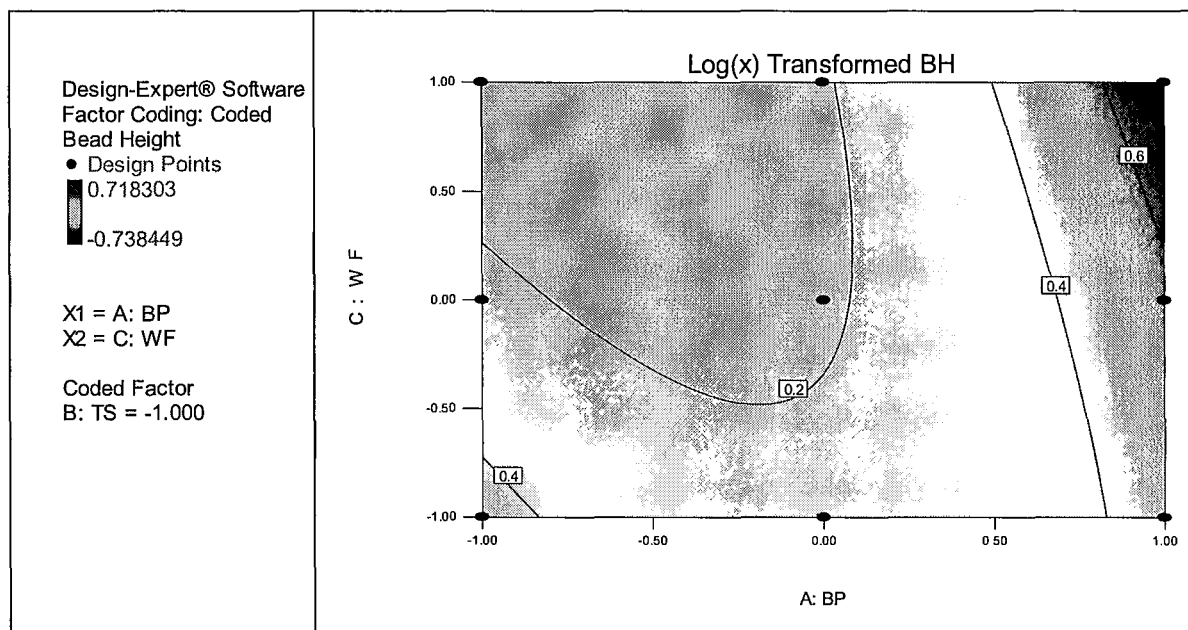


Figure 34. Log(x) Transformed BH Response Data Optimized when BP = +1, TS = -1, and WF = +1.

BW - The optimization was constructed using the 'in range' option in order to narrow the otherwise large range. The inverse Log(x) range of 4.6 mm – 11.2 mm was input to represent the minimum and maximum width values of the twelve visually acceptable samples. The independent and interaction factors that corresponded to the strongest coefficients [-] (TS) and [+] (BP*WF), as previously shown in Table 28, were selected to produce the contour plot as shown in Figure 35. BW was maximized when BP = +1, TS = -1 and WF = +1 and BW was approaching 1.0 or the inverse of the Log(x) transform, $10^{1.0} \sim 10.2$. These processing levels reconcile with the processing variables used to produce Sample 7. Figure 36 shows no difference in the contour of the Log(x) transformation and the power transformed.

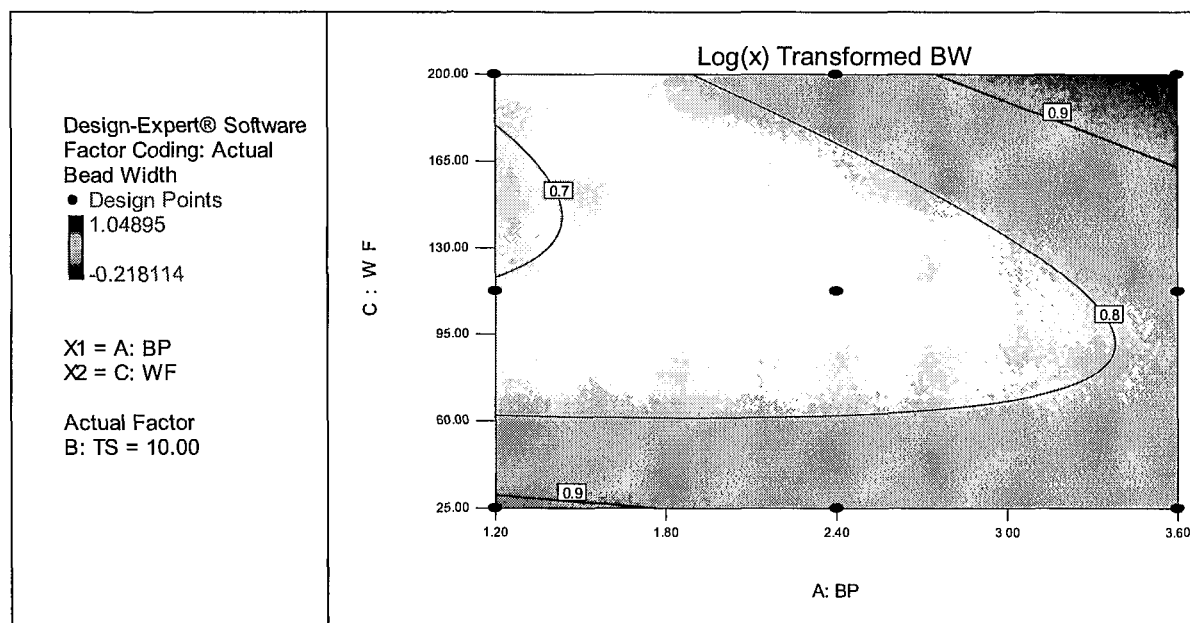


Figure 35. Log(x) Transformed BW Response Data Optimized when BP = +1, TS = -1 and WF = +1.

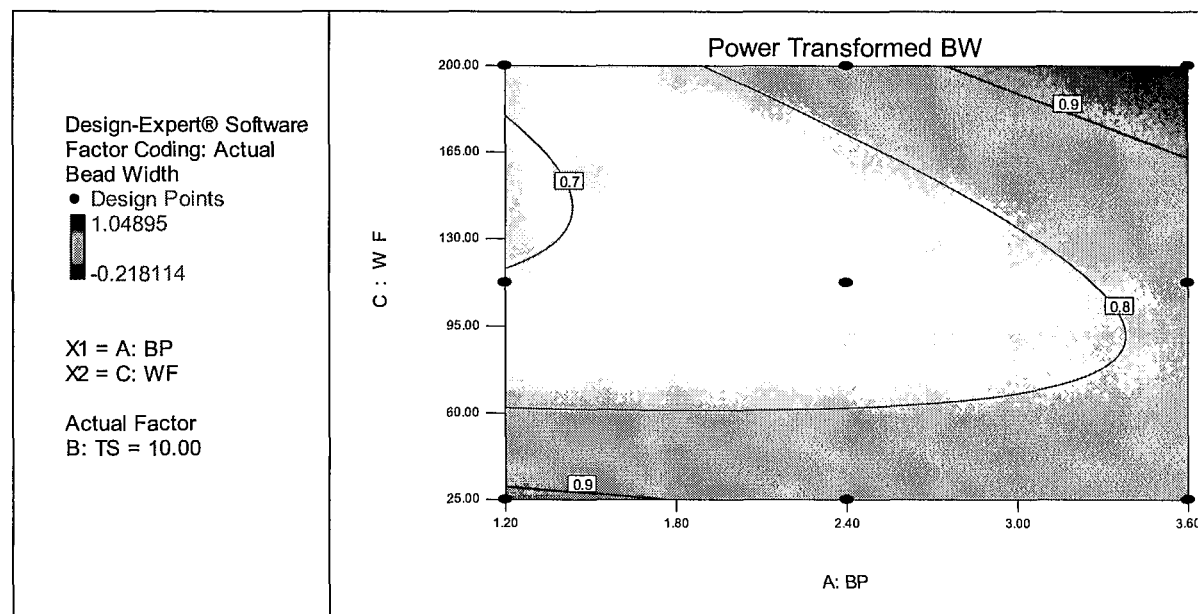


Figure 36. Power Transformed BW Response Data Optimized when BP = +1, TS = -1 and WF = +1.

4.18 Analysis Conclusion

A full factorial design enabled processing levels for BP, TS and WF to be calculated from a regression analysis. The analysis of the non-transformed AL response data created an RS which predicted processing levels for BP, TS and WF that reconciled with the processing levels [BP = +1, TS = -1, WF = -1] that produced Sample 9. This was not ideal as the high beam power, and low translation speed and wire feed rate may cause the substrate and deposit to retain too much heat during passes. This would cause the undesired AL vaporization that will compromise the chemical integrity. The analysis of the non-transformed BH response data created an RS which predicted processing levels which reconciled with the processing levels [BP = +1, TS = -1, WF = +1] that produced Sample 7. The analysis of the non-transformed BW response data created an RS which predicted processing levels that also reconciled with the processing levels that produced Sample 7. Microsoft ® Excel Solver optimized the response values as AL = 6.00, BH = 4.5 and BW = 7.1. These values match most closely with the response values for Sample 7 where AL = 6.12, BH = 5.2 and BW = 11.2. The non-transformed response data was analyzed in Design-Expert ® and contour plots were constructed for all three response variables. The contour plots predicted processing levels that reconciled with processing levels used to produce Sample 7 for BH and BW and Sample 9 for AL.

A square root transformation was recommended by the Box-Cox test for the BH data as the value $\Lambda = 1$ was not within the low and high confidence interval of -0.12 to 0.84. The transformation improved the shape of the normal distribution curve, but did not improve the statistics or prediction plots. The transformation did not predict different processing levels from what was predicted for the non-transformed BH data, but

the response Y was higher at 4.7 mm as compared with 4.5 mm when optimized by the Microsoft ® Excel Solver. The contour plot predicted processing levels that reconciled with processing levels used to produce Sample 7. There was no significant benefit to a square root transformation of the BH response data. The square root transformation was not recommended for AL and BW.

It was hypothesized that transforming the data using Log(x) may improve the fit of the data and may yield better optimized responses and processing levels. The analysis of the transformed AL response data provided an RS which predicted processing levels for BP, TS and WF that reconciled with processing levels use to produce Sample 7. The analysis of the transformed BH response data provided an RS which predicted processing levels that reconciled with processing levels used to produce Sample 7. The analysis of the transformed BW response data provided an RS which predicted processing levels which reconciled with processing levels used to produce Sample 7.

The Log(x) did not significantly improve the residual SS and standard deviation of all three factors. The F Statistic only slightly improved in some cases and the R Square value was slightly degraded for all of the responses. The shape of the data and the predicted vs. actual plot for AL and BW was not improved, but improvement was seen in the normality of the distribution and the predicted vs. actual plots for the square root and the Log(x) transformed BH. Microsoft ® Excel Solver optimized response values for AL = 5.85, BH = 5.3 and BW = 10.2 match most closely with response values for Sample 7 where AL = 6.12, BH = 5.2 and BW = 11.w. The transformed response data was analyzed in Design-Expert ® and contour plots were constructed for all three response variables. All of the contour plots predicted processing levels that reconciled with the

processing levels used to produce Sample 7. Sample 7 was also ranked highest in the visual observation analysis. Figure 37 shows an enlarged view of Sample 7.



Figure 37. EBF³ Ti-6Al-4V - Sample 7 [BH = +1, TS = -1, BW = +1].

5. CONCLUSION

5.0 Conclusion of Visual Examination

The visual inspection of the 27 deposits extracted 12 samples of the 27 as having the desired symmetry, BH and BW needed for the layer additive process to produce a finished part that has the potential to conform to the precise specifications of the computer driven design. These samples were then sorted in order of maximum to minimum AL content. It was observed that sample 7 ranked the highest with an AL content of 6.12 Wt %. The samples were then sorted by maximum to minimum BH. Sample 7 was measured as the tallest with a BH of 5.2. A tall bead is indicative of ideal layering conditions for developing the design structure. Finally the samples were sorted by maximum to minimum BW. Uniformity is critical to consistent bead morphology. Sample 7 ranked highest with a width of 11.2.

Reconciling sample 7 to the calculation matrix indicated the optimum processing level for BP as high, TS as low and WF rate as high (BP (+1), TS (-1), WF (+1)).

5.1 Conclusion of Regression Analyses

The regression analyses for each response enabled math models to be constructed. The analysis of the BH and BW response data resulted in a prediction RS with the same processing levels (BP = +1, TS = -1, WF = +1) as those used to produce Sample 7. The AL analysis resulted in a prediction RS with the same processing levels (BP = +1, TS = -1, WF = +1) as those used to produce Sample 9. Sample 9 may be excluded for high heat and slow travel speeds. Contour plots generated by Design-Stat ® illustrated the prediction RS for each of the responses.

5.2 Summary of Transformation

A square root transformation was recommended for the BH response data by Design-Expert ® software. This was applied and a closer approximation to the normal distribution curve was observed, but with no significant changes in the model or the prediction RS. The mathematical approximation predicted processing levels that reconciled with those used to produce Sample 7. The contour plot for BH illustrated the prediction RS. No transformation was recommended for AL or BW.

A Log(x) transformation was applied to all responses and the results analyzed. As with the square root transformation, the Log(x) transformation improved the distribution curve for BH, but no significant changes were observed in the analysis. The RS for AL, BH and BW predicted processing levels that reconciled with those used to produce Sample 7.

A Box-Cox diagnosis suggested a power transformation be applied to the Log(x) transformed BW response values. This was applied with no change observed in the prediction RS.

5.3 Summary of Optimization

The objective in this experiment was to maximize the AL content to maintain the chemical integrity of the finished product. The AL content of the final deposition must be between 5.50 wt % and 6.75 wt% or it can no longer be considered Ti-6Al-4V. The predicted optimized processing variables with a Log(x) transformation applied reconciled with those used to produce Sample 7. BH and BW optimized processing variables reconciled with those levels used to produce Sample 7. The Log(x) transformed responses yielded processing levels consistent with the visual observation and chemical

content TPM. Bead morphology was also considered and agreed with the computational analysis. Processing levels for Sample 7 could be further explored in validation testing.

Even though the prediction RS quantified the visual observation analysis, the model was not a good fit for the data. This detracts from the credibility of the prediction RS for each test and may indicate that other factors are more significant to the build process than the BP, TS and WF. Other factors such as the beam focus may also be studied as well as other considerations:

- Height increase each pass – bead height
- Width increase each pass – bead width
- Part surface condition each pass and total number of layers
- Consistency of height at each coordinate
- Temperature part and substrate
- Density of previous layers
- Platform position due to vibration
- Warping of platform
- Warping of part
- Distance of part from beam as part height increases
- Time each pass
- Time start to completion
- Ambient temperature during processing
- Part temperature
- Wire feed from ambient temperature
- Humidity
- Wire temperature
- Reflectivity of new material
- Beam intensity
- Beam focus
- Progressive contamination of beam source from debris feedback
- Power surge
- Warping of platform
- Debris on part or platform from previous pass
- Volume of material
- Microstructure changes of each layer and in substrate [HAZ, mixing zone, etc.]
- Depth of penetration into substrate

5.4 Validation Testing

A Box-Behnken Design is recommended for validation testing for its robust capability of studying points in between the vertices and end points of the design. This is not possible with the full factorial design. Refer to Figure 4 which is the cubic representation of the full factorial design. The Box-Behnken design, however, does not evaluate extreme responses located on the vertices of the cube (Ferreira, et al., 2007). The Box-Behnken design is a space filling, rotatable design with multiple center points. An example of this design was generated in Design-Stat ® and is shown in Figure 38. Multiple center points yield better statistics because variability can be tested. A major consideration for choosing Box-Behnken over a full factorial design is the capability to run fewer experiments.

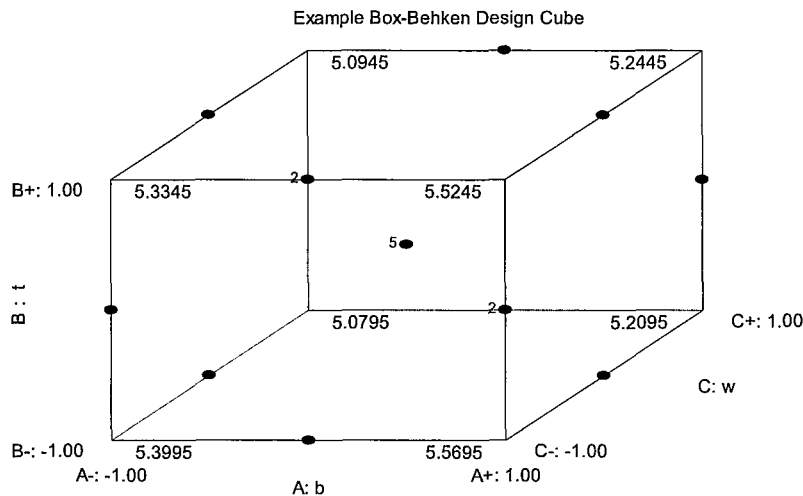


Figure 38. Example Box-Behnken Design Cube.

The design matrix for the Box-Behnken design is set up using the formula

$N = 2k(k-1) + C_0$ where k is equal to the number of factors and C_0 is equal to the number

of midpoints. If only the BP, TS and WF are used for validation testing, the number of factors is three. The number of midpoints has been suggested to be five, so $N = 17$. The factors and midpoints were input into Design-Expert ® which constructed the design matrix as shown in Appendix D. Run order was also suggested, but may be varied by engineers to maximize stability in processing conditions. The processing variables could be tightly refined about the levels used in Sample 7 to build 17 linear Ti-6Al-4V deposits.

The Box-Behnken design claims increased efficiency using the efficiency formula. This is the number of coefficients divided by the number of experiments (Ferreira et al., 2007). The calculated efficiency for the full factorial in this study was $10/27$ or .37. The calculated efficiency for the Box-Behnken is $10/17$ or .58.

5.5 Future Work

Optimization of the EBF³ for the Ti-6Al-4V alloy will afford the potential for further experimentation for various aerospace components and has served as a spring board for trials with other metals. In April 2012, a stainless steel screening DOE was conducted using EBF³. Three replicates were run at the midpoint processing levels. A Box-Behnken design was planned using 13 runs with 4 center point runs. Plans are being considered for AL and more Ti-6Al-4V analyses.

5.6 Applications in Aerospace

The EBF³ process is at the forefront of technology. Optimization would enable NASA to forge paths and sustain a leading edge in innovation. There are many benefits and applications of EBF³. EBF³ technology is prescribed for use in government and commercial applications in areas of land, sea, and air. Aircraft weight reduction is realized through advanced fabrication techniques. The time consuming manufacture of

conventional landing gear consists of forging high strength alloys in dies to produce a general shape. Parts are then transported to another facility where they are machined to net shape and then heat treated. The heat treatment causes distortion in the shape which results in an iterative process of inspections and machining before being honed and finally surface coated (MacKenzie, 2008). In addition, the current ratio of composite material to aluminum/titanium results in increased weight. EBF³ components of aluminum and titanium weigh less than those of composite making it ideal for wing stiffener production. The additive layering capability of EBF³ also will enable fewer parts in this intricate assembly. “Typically, the construction of a traditional metallic wing panel will comprise several panels joined by conventional fasteners, whilst the wing skins themselves are often complex subassemblies made of many panels with the stringers and stiffeners attached to the wing skin panels separately” (Richardson, 2009, p1).

Corrosion is the result of a chemical reaction known as oxidation. Some metals are more corrosive than others. Corrosion is a huge problem in jet aircraft due to condensation from environmental control apparatuses and weather. Water accumulates in the multitude of crevices caused by the juncture of parts, especially in wing panels. Three factors must be present for oxidation to take place; metal, oxygen and an electrolyte such as water. Small amounts of water reacting with metallic structures can cause corrosion. Care must be taken to inspect every minute area to spot and evacuate water and moisture buildup. This takes valuable time and resources. Aircraft parts made with the EBF³ system, and specifically with Ti-6Al-4V for its good corrosion properties, would produce components such as wing stiffeners and panels, landing gear and many more structures with fewer parts and fewer joints to discourage corrosion (USAF, 2007).

5.7 Future Work Potential

EBF³ has a promising future in aviation, spaceflight and the medical community with the capability to build large structural parts. The EBF³ is currently being used to manufacture titanium spars for vertical tails of the F-35 Joint Strike Fighter. It is also predicted that this process will serve to enhance aircraft performance (NASA, 2011).

Because the EBF³ process can use more than one type of metal by feeding in different wire combinations, it is even possible to embed fiber optic glass strands inside of aluminum parts (NASA, 2009). “While initial parts for the aviation industry will be simple shapes, replacing parts already designed, future parts designed from scratch with the EBF³ process in mind could lead to improvements in jet engine efficiency, fuel burn rate and component lifetime” (NASA, 2009, p1).

Explorers of other planets will benefit from the EBF³ system as parts can be manufactured as needed, saving time and money that would be spent launching heavy cargo from Earth. “But the immediate and greatest potential for the process is in the aviation industry where major structural segments of an airliner, or casings for a jet engine, could be manufactured for about \$1,000 per pound less than conventional means, Karen Taminger said. It is hoped that a scaled down version of the hardware can be tested on the International Space Station (NASA, 2009, p1).”

BIBLIOGRAPHY

- Alimardani, M., Toyserkani, E., Huissoon, J.P., & Paul, C.P. (2009, July 22). *On the delamination and crack formation in a thin wall fabricated using laser solid freeform fabrication process: An experimental-numerical investigation*. Science Direct. Optics and Lasers in Engineering 47 (2009) 1160-1168.
- Azom (2002, July 30). *Titanium alloys – Ti64Al4V grade 5*. Retrieved from <http://www.azom.com/article.aspx?ArticleID=1547> on July 22, 2012.
- Blanchard, B.S. & Fabrycky, W.J. (2001). *Systems Engineering and Analysis Fifth Edition*. Prentice Hall, 2001.
- Domack, M., Taminger, K. & Begley, M. (2006, July 10-14). *Metallurgical mechanisms controlling mechanical properties of aluminum alloy 2219 produced by electron beam freeform fabrication*.
- Ek, L.T. (2005). *Quality improvement using factorial design*. Pakistan's 9th International Convention on Quality Improvement.
- Ferreira, S.L.C, Bruns, R.E., Ferreira, H.S., Matos, G.D., David, J.M., Brandao, G.C, daSilva, E.G.P, Portugal, L.A., dos Reis, P.S., Souza, A.S., & dos Santos, W.N.L. (July 23, 2007). *Box=Behnken design: An alternative for the optimization of analytical methods*.
- Francedschini, G. & Macchietto, S. (2007, December 4). *Model-based design of experiments for parameter precision: State of the art*.
- Ghasemi, F.A., Malekzadeh, K. & Raissi, S. (2008, February 27). Thin-Walled Structures. Retrieved June 26, 2012 from <http://www.referencerepository.com/homes/tagsearch/page:5/jrnl:Thin-Walled%20Structures/tag:method>
- Hague, R., Campbell, I. & Dickens, P. (2003, January 1). *Implications on design of rapid manufacturing*.
- Helton, J. & Davis F. (2003, February 28). *Latin hypercube sampling and the propagation of uncertainty in analysis of complex systems*.
- Hillier, C. & Liu, S. (2009, February 15-19). Powder-Cored Tubular Wire Manufacturing for Electron Beam Freeform Fabrication. TMS Annual Meeting & Exhibition *Materials Issues in Additive Powder-Based Manufacturing Processes* San Francisco, CA
- Lach, C. (2007, June 27). Effect of Electron Beam Freeform Fabrication (EBF³) Processing Parameters on Composition of Ti-6-4. Aeromat18th clLach2007_compressed.pdf.

- Lach C.L., Green L. & Quigley, P.A. (2012). *Process variable equations to control electron beam freeform fabrication [EBF³] bead geometry*. Personal communication for professional paper.
- Levy, G. N., Schindel, R. & Kruth, J.P. (2007, June 26). *Rapid Manufacturing and rapid tooling with Layer Manufacturing (LM) technologies, state of the art and future perspectives*.
- Lin, S., Hoffman, E. & Domack M. (2007, June 27). *Distortion and residual stress control in integrally stiffened structure produced by direct metal desposition*.
- MacKenzie, D.S. (2008, June). Heat treatment of landing gear. [Electronic version]. *ASM International Publication. Heat Treatment Progress*, 8(31).
- Manivannan, S., Arumugam, R., Sudharsan, N.M. & Prasanna Devi, S. (2010). *Taguchi based linear regression modeling of flat plate heat sink*. Journal of Engineering and Applied Sciences, 5(1)36-44. Retrieved December 23, 2011 from <http://www.medwelljournals.com/fulltext/?doi=jeasci.2010.36.44>
- Marengo, E., Gennaro, M.C., & Abrigo, C. (1995). *Investigation by experimental design and regression models of the effect of five experimental factors on ion-interaction high-performance liquid chromatographic retention*. Dipartimento di Chimica Analitica, Universita di Torino, via P. Giuria, 5, 10125 Turin, Italy.
- Matusiewicz, H. & Barnes, R.M. (1984). *Determination of aluminum and silicon in biological materials by inductively coupled plasma atomic emission spectrometry with electrothermal vaporization*. Spectrochimica Acta Part B: Atomic Spectroscopy, Volume 39, Issue 7, 1984, Pages 891–899. Department of Chemistry, GRC Towers, University of Massachusetts, Amherst, MA 01003-0035
- Microsoft ® Excel (2007). Microsoft ® Office 2007.
- Monroe, R.W., Lepsch, R.A. Jr., & Unal, R. (1998). *Using expert judgment methodology to address uncertainty in launch vehicle weight estimates*.
- Montgomery, D.C. (2009). *Introduction to Statistical Quality Control 6th Edition*. John Wiley & Sons, Inc.
- Myers, R. H., Montgomery, D.C. & Anderson-Cook, C. M. (2009). *Response Surface Methodology: Process and Product Optimization Using Designed Experiments, 3rd Edition*. John Wiley & Sons, Inc. Retrieved July 7, 2012 from http://books.google.com/books?hl=en&lr=&id=89oznEFHF_MC&oi=fnd&pg=PR11&dq=response+surface+methodology&ots=Dhwe09nThU&sig=HAhLGltRSR7xvk8I_j7S3LlhNhs#v=onepage&q=response%20surface%20methodology&f=false

- Myers, W. R., Khuri, A., Carter & W.H. Jr. (1989, May). Response Surface Methodology: 1966-1988. *Technometrics* 31(2). Retrieved December 23, 2011 from <http://www.jstor.org/pss/1268813>
- National Aeronautics and Space Administration (NASA). (2009, March 03). *NASA's EBF3: The future of art-to-part manufacturing*. Retrieved December 15, 2011 from <http://technologygateway.nasa.gov/docs/EBF3.pdf>
- National Aeronautics and Space Administration (NASA). (2009, September 23). *From nothing, something: one layer at a time*. Retrieved June 24, 2012 from http://www.nasa.gov/topics/aeronautics/features/electron_beam.html
- National Aeronautics and Space Administration (NASA). (2012). *NASA's EBF3: The Future of Art-to-Part Manufacturing For reduced fatigue, improved safety, and greater efficiency*. Retrieved April 22, 2012 from <http://www.fuentek.com/technologies/EBF3.htm>
- National Aeronautics and Space Administration (NASA). (2011, June 22). *Electron Beam Freeform Fabrication*. Retrieved June 24, 2012 from <http://www.nasa.gov/topics/technology/features/ebf3.html>
- Nguyen, T.N & Wahab, M.A. (1998, January 10). *The effect of weld geometry and residual stresses on the fatigue of welded joints under combined loading*. *Journal of Materials Processing Technology*, Volume 77, Issues 1–3, 1 May 1998, Pages 201-208. Retrieved June 29, 2012 from <http://www.sciencedirect.com/science/article/pii/S0924013697004184>
- Quigley, P.A. (2012, April 27). *Electron Beam Freeform Fabrication Optimization Analysis*. Old Dominion University, Engineering Management 863.
- Ratnadeep, P. (2011, July 19). *Optimal part orientation in rapid manufacturing process for achieving geometric tolerances*.
- Richardson, M. (2009). *Greater than the sum of its parts*. Retrieved June 28, 2012 from *Aerospace Manufacturing* <http://www.aero-mag.com/features/19/20099/105>
- SAE Aerospace (2002). *Titanium alloy direct deposited products, 6Al – 4V annealed*. Aerospace material specification (AMS4999, Rev. A) Issued 2002-02.
- SAI Titanium Specialists. Supra Alloys Inc. <http://www.supraalloys.com/titanium-grades.php>
- Schmider, E., Ziegler, M., Danay, E., Beyer, L. & Buhner, M. (2010, October 7). *Is it really robust? Reinvestigating the robustness of ANOVA against violations of the normal distribution assumption*.

- Sankararaman, S. & Mahadevan, S. (2011). *Likelihood-based representation of epistemic uncertainty due to sparse point data and/or interval data*.
- Simpson, M.L & Unal, R. (2010). *Using response surface methodology as an approach to understand and optimize operational air power*. The International Journal, Vol. 4, No 3, 2010. Retrieved April 24, 2012 from <http://www.dtic.mil/cgi-bin/GetTRDoc?Location=U2&doc=GetTRDoc.pdf&AD=ADA526458>
- Stat-Ease ®. (December 30, 2011). Design-Expert ® 8.0.7.1. (<http://www.statease.com/>).
- Tamminger, K., Hafley, R. & Domack M. (2002). *Evolution and control of 2219 aluminum microstructural features through electron beam freeform fabrication*.
- Tamminger, K., Hafley, R. Fahringer, D., and Martin, R. (2004, August 4). *Effect of surface treatments on electron beam freeform fabricated aluminum structures*.
- Touzik, A., Hermann, H. & Wetzig, K. (2003, September 11). *General-purpose distributed software for Monte Carlo simulations in materials design*.
- Unal, R. (2012). Robust Engineering Design. ENMA 863. Old Dominion University.
- Unal, R. & Yeniay, O. (2003, March). Reducing design risk using robust design Methods: A dual response surface approach. ODU Project No:113091. NASA Grant No: NAG-1-01086
- Unal, R. (2012). Robust Engineering Design Course, Old Dominion University.
- Unal, R. (April 11, 2006). *Optimization on cost basis and robust design approaches for reducing risk*. Slide presentation for Engineering Management and Systems Engineering, Old Dominion University, Norfolk, VA.
- Usunoff, E., Carrera, J. & Mousavi, S.F. (1992). *Approach to the design of experiments for discriminating among alternative conceptual models*. Advances in Water Resources 15 (1992) 199-214.
- Van Albada, S.J. & Robinson, P.A. (2006, August 18). *Transformation of arbitrary distributions to the normal distribution with application to EEG test-retest reliability*. Journal of Neuroscience Methods 161 (2007) 205-211.
- Wang, X.D, Shi Q. & Wang, X. (2009). *New vacuum electron beam processing method based on temperature closed-loop control*. Retrieved July 3, 2012 from <http://www.sciencedirect.com/science/article/pii/S0042207X08004491>
- Wanjara, P., Brochu, M. & Jahazi, M. (2006, March 17). *Electron beam freeforming of stainless steel using solid wire feed*. Science Direct. Materials and Design 28 (2007) 2278-2286.

Single Bead DOE Experiments – Macro Images of Ti-6Al-4V Deposits

Sample 2 is not available as a macro image.

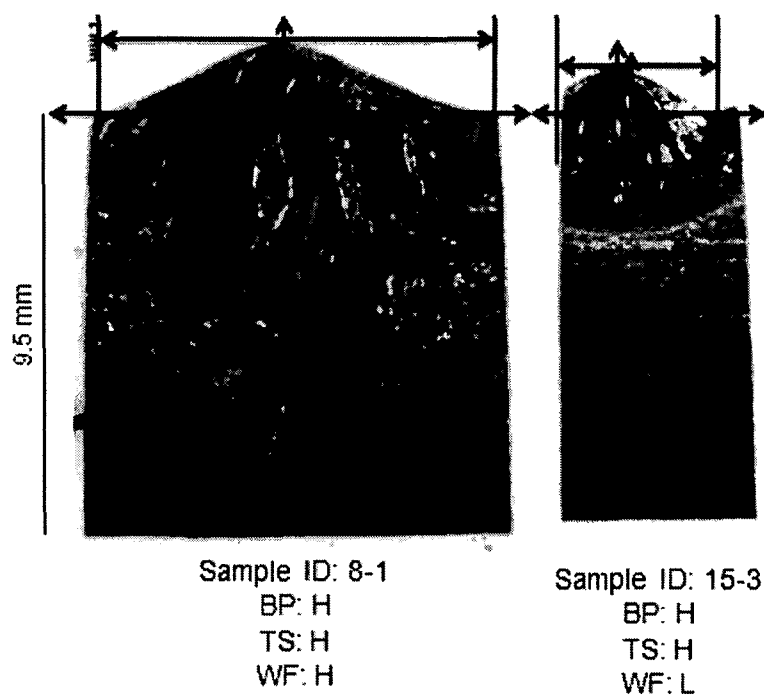


Figure 39. EBF³ Ti-6Al-4V - Sample 1 (left) and Sample 3 (right).

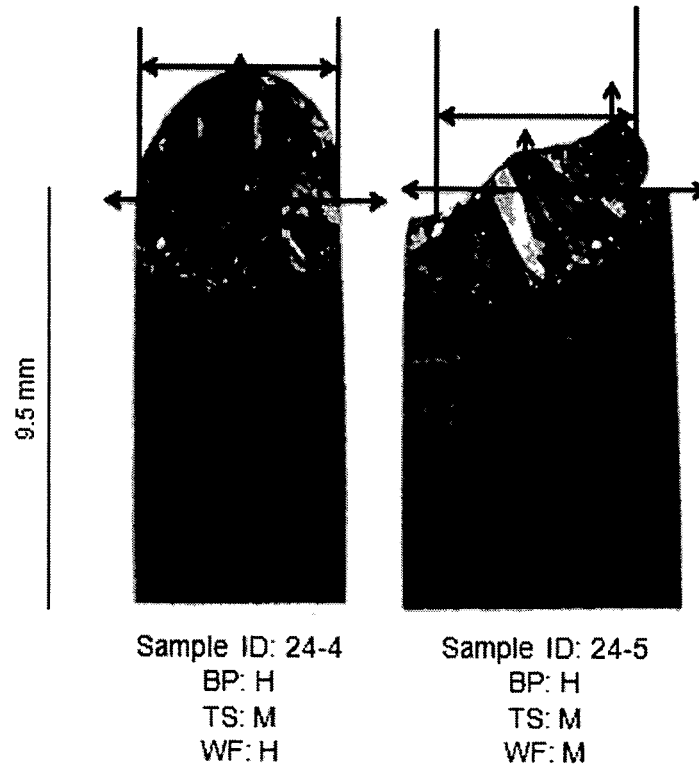


Figure 40. EBF³ Ti-6Al-4V - Sample 4 (left) and Sample 5 (right).

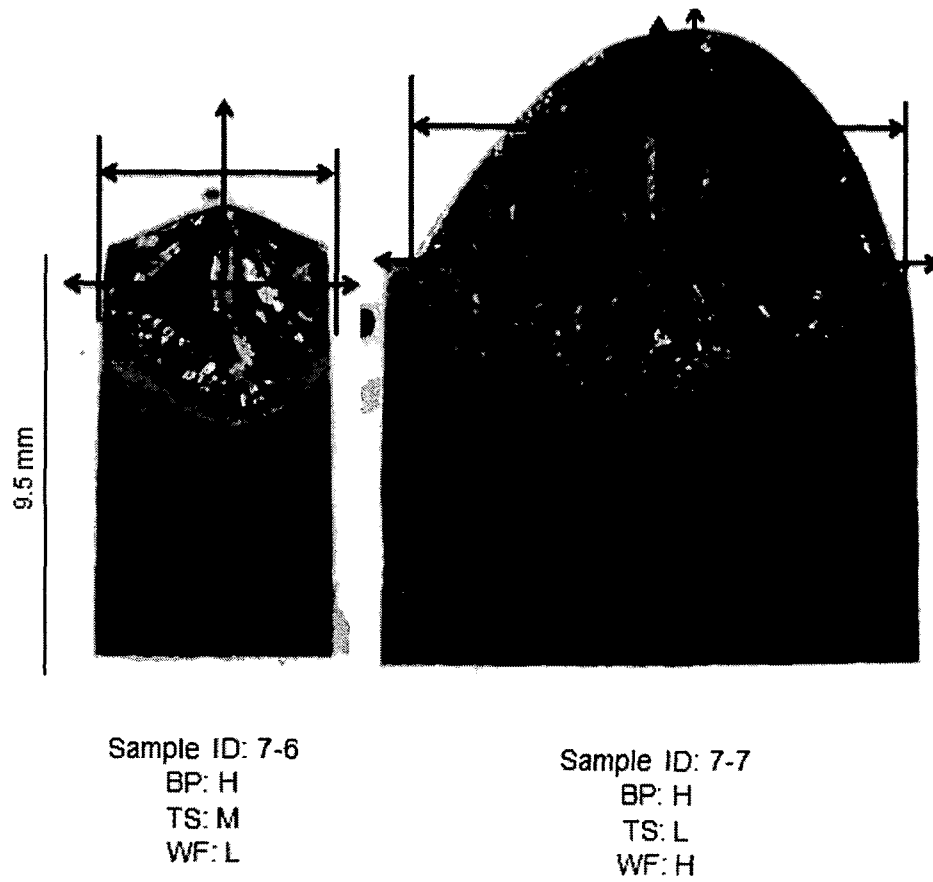


Figure 41. EBF³ Ti-6Al-4V - Sample 6 (left) and Sample 7 (right).

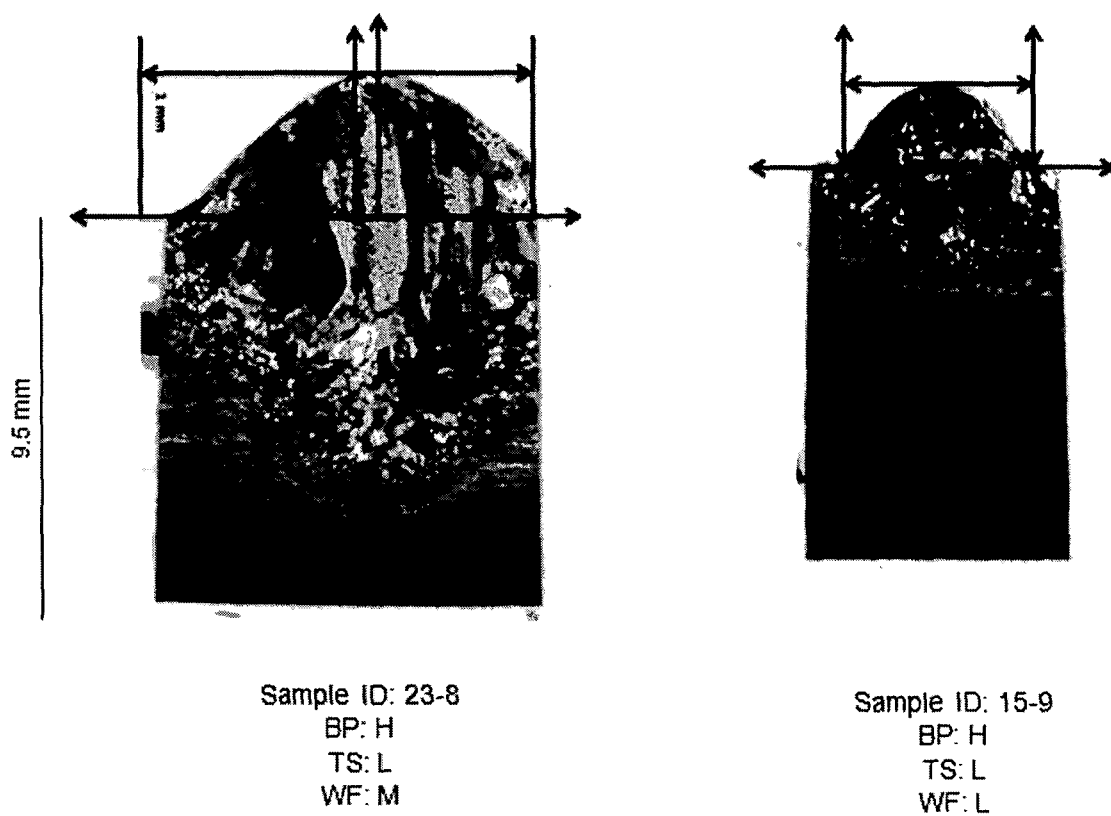


Figure 42. EBF³ Ti-6Al-4V - Sample 8 (left) and Sample 9 (right).

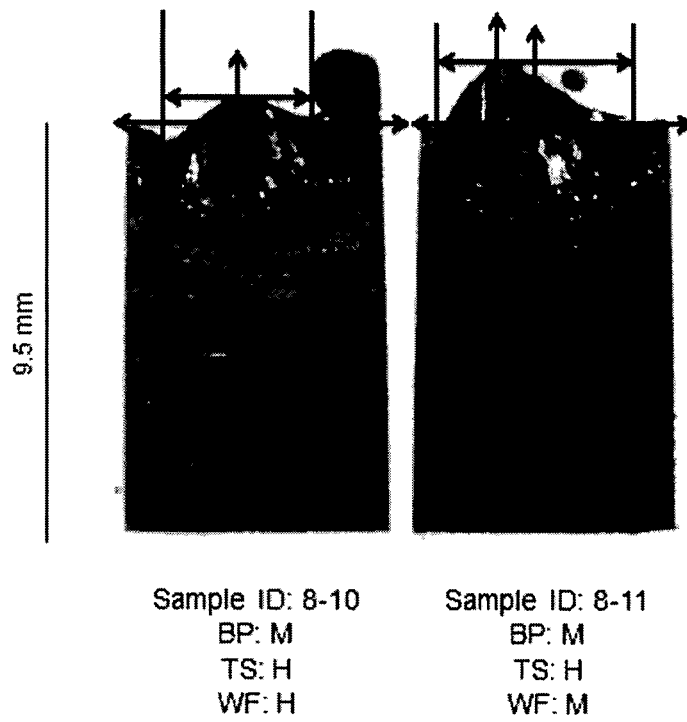


Figure 43. EBF³ Ti-6Al-4V - Sample 10 (left) and Sample 11 (right).

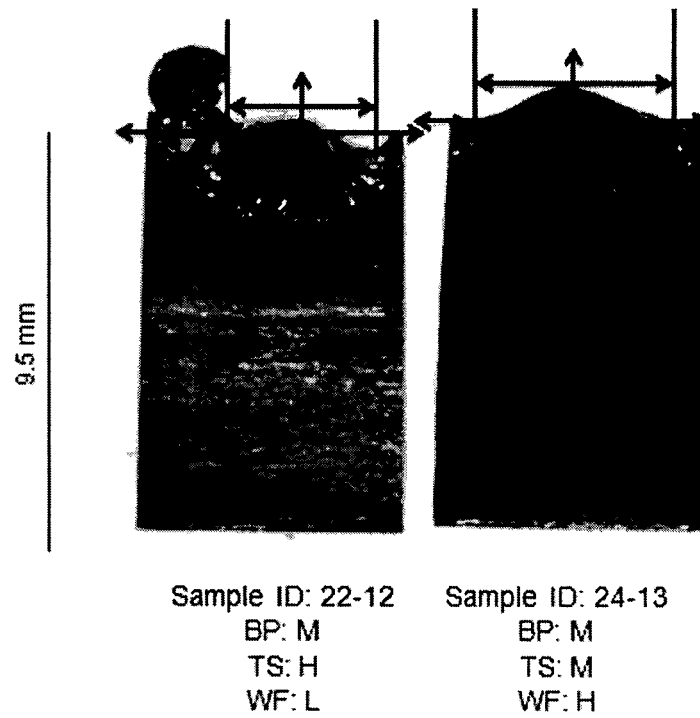


Figure 44. EBF³ Ti-6Al-4V - Sample 12 (left) and Sample 13 (right).

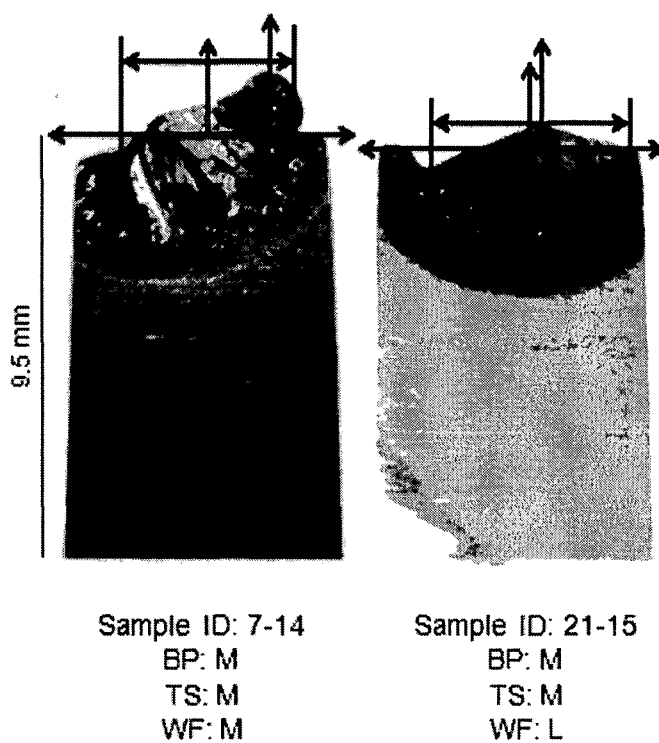


Figure 45. EBF³ Ti-6Al-4V - Sample 14 (left) and Sample 15 (right).

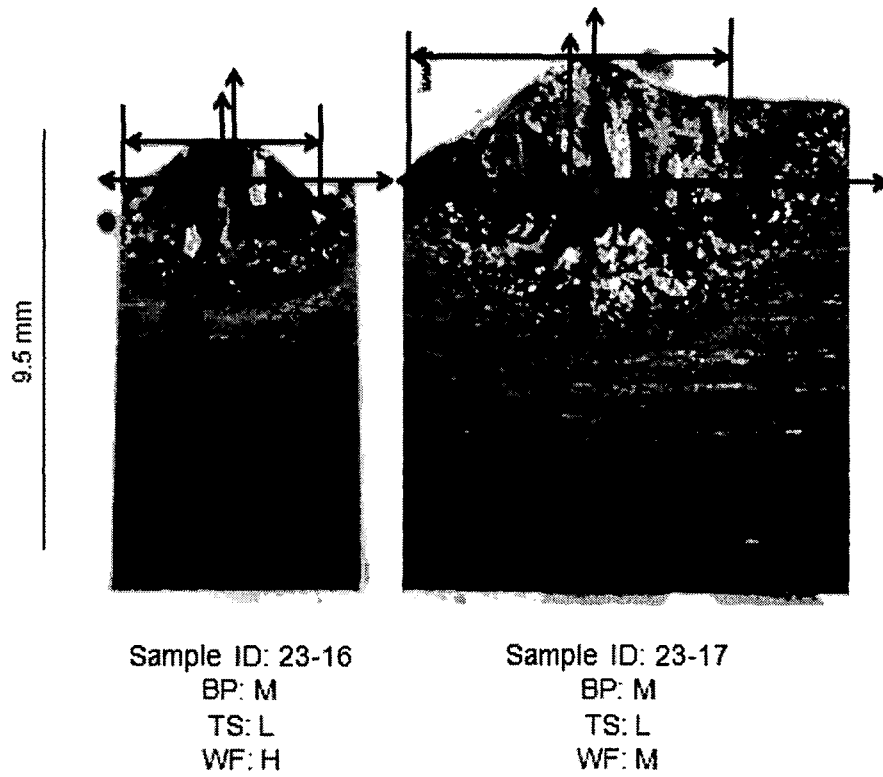


Figure 46. EBF³ Ti-6Al-4V - Sample 16 (left) and Sample 17 (right).

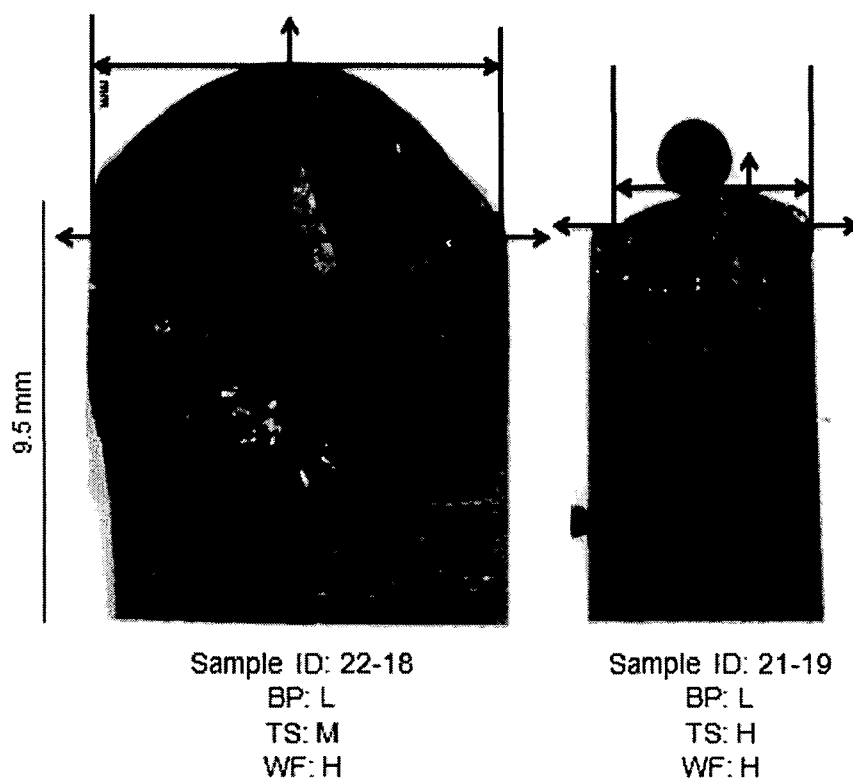


Figure 47. EBF³ Ti-6Al-4V - Sample 18 (left) and Sample 19 (right).

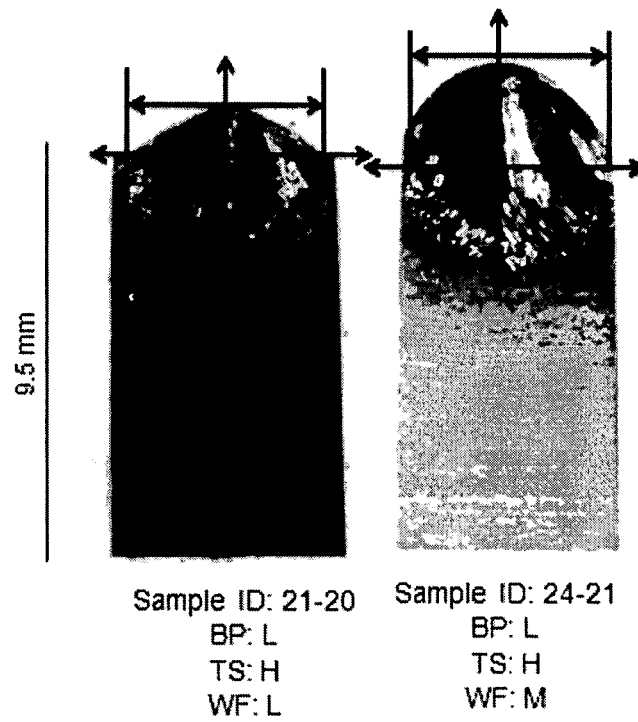


Figure 48. EBF³ Ti-6Al-4V - Sample 20 (left) and Sample 21 (right).

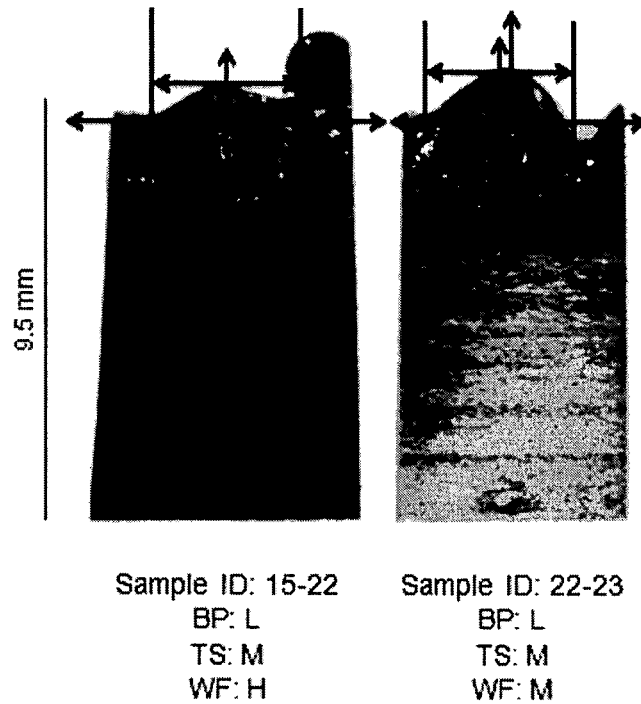


Figure 49. EBF³ Ti-6Al-4V - Sample 22 (left) and Sample 23 (right).

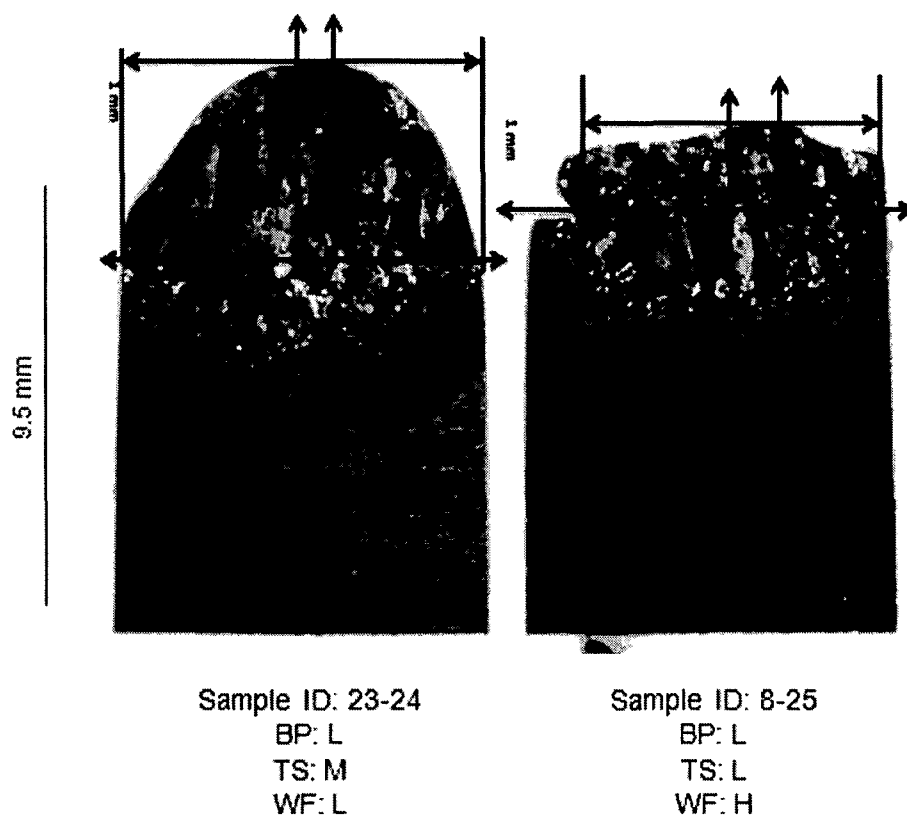


Figure 50. EBF³ Ti-6Al-4V - Sample 24 (left) and Sample 25 (right).

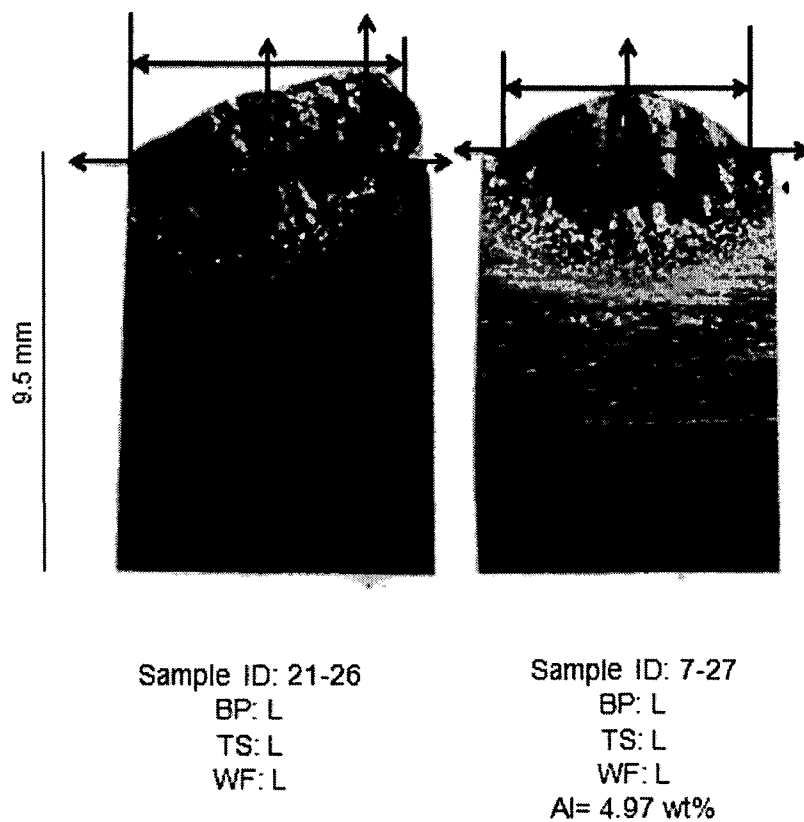


Figure 51. EBF³ Ti-6Al-4V - Sample 26 (left) and Sample 27 (right).

Calculation Matrix for Aluminum, Bead Height
and Bead Width Response Data

RUN	BP	TS	WF	BP * TS	BP * WF	TS * WF	BP ²	TS ²	WF ²	AL (wt%)	BH (mm)	BW (mm)
1	+1	+1	+1	+1	+1	+1	+1	+1	+1	5.95	1.5	9.0
2	+1	+1	0	+1	0	0	+1	+1	0	5.35	0.2	0.6
3	+1	+1	-1	+1	-1	-1	+1	+1	+1	5.05	1.0	3.6
4	+1	0	+1	0	+1	0	+1	0	+1	5.58	3.0	4.6
5	+1	0	0	0	0	0	+1	0	0	5.50	1.2	4.1
6	+1	0	-1	0	-1	0	+1	0	+1	5.40	1.8	5.2
7	+1	-1	+1	-1	+1	-1	+1	+1	+1	6.12	5.2	11.2
8	+1	-1	0	-1	0	0	+1	+1	0	5.93	3.6	8.6
9	+1	-1	-1	-1	-1	+1	+1	+1	+1	5.87	1.9	4.8
10	0	+1	+1	0	0	+1	0	+1	+1	6.05	0.5	3.3
11	0	+1	0	0	0	0	0	+1	0	5.37	1.3	4.5
12	0	+1	-1	0	0	-1	0	+1	+1	5.39	0.3	3.3
13	0	0	+1	0	0	0	0	0	+1	4.96	0.7	4.4
14	0	0	0	0	0	0	0	0	0	5.83	1.1	3.9
15	0	0	-1	0	0	0	0	0	+1	5.36	0.4	4.5
16	0	-1	+1	0	0	-1	0	+1	+1	5.13	0.9	4.5
17	0	-1	0	0	0	0	0	+1	0	5.42	2.7	7.4
18	0	-1	-1	0	0	+1	0	+1	+1	5.67	4.0	9.3
19	-1	+1	+1	-1	-1	+1	+1	+1	+1	6.54	0.8	4.4
20	-1	+1	0	-1	0	0	+1	+1	0	5.07	1.0	4.5
21	-1	+1	-1	-1	+1	-1	+1	+1	+1	5.32	2.3	4.8
22	-1	0	+1	0	-1	0	+1	0	+1	5.36	0.8	3.4
23	-1	0	0	0	0	0	+1	0	0	5.32	1.2	3.4
24	-1	0	-1	0	+1	0	+1	0	+1	5.58	4.4	8.1
25	-1	-1	+1	+1	-1	-1	+1	+1	+1	5.71	1.9	7.2
26	-1	-1	0	+1	0	0	+1	+1	0	5.26	1.9	6.2
27	-1	-1	-1	+1	+1	+1	+1	+1	+1	4.96	1.3	5.6

Log (x) and Square Root Transformed Aluminum, Bead Height
and Bead Width Response Data

LOG (x) AL Response	LOG (x) BH Response	LOG (x) BW Response	SQRT AL Response	SQRT BH Response	SQRT BW Response
0.77	0.2	1.0	2.44	1.2	3.0
0.73	-0.7	-0.2	2.31	0.4	0.8
0.70	0.0	0.6	2.25	1.0	1.9
0.75	0.5	0.7	2.36	1.7	2.1
0.74	0.1	0.6	2.35	1.1	2.0
0.73	0.3	0.7	2.32	1.3	2.3
0.79	0.7	1.0	2.47	2.3	3.3
0.77	0.6	0.9	2.44	1.9	2.9
0.77	0.3	0.7	2.42	1.4	2.2
0.78	-0.3	0.5	2.46	0.7	1.8
0.73	0.1	0.7	2.32	1.1	2.1
0.73	-0.6	0.5	2.32	0.5	1.8
0.70	-0.2	0.6	2.23	0.8	2.1
0.77	0.0	0.6	2.41	1.0	2.0
0.73	-0.4	0.7	2.32	0.7	2.1
0.71	-0.1	0.7	2.26	0.9	2.1
0.73	0.4	0.9	2.33	1.7	2.7
0.75	0.6	1.0	2.38	2.0	3.0
0.82	-0.1	0.6	2.56	0.9	2.1
0.71	0.0	0.7	2.25	1.0	2.1
0.73	0.4	0.7	2.31	1.5	2.2
0.73	-0.1	0.5	2.32	0.9	1.8
0.73	0.1	0.5	2.31	1.1	1.8
0.75	0.6	0.9	2.36	2.1	2.8
0.76	0.3	0.9	2.39	1.4	2.7
0.72	0.3	0.8	2.29	1.4	2.5
0.70	0.1	0.7	2.23	1.1	2.4

Box-Behnken Design Matrix

STD	RUN	BP	TS	WF
17	1	0	0	0
3	2	-1	1	0
9	3	0	-1	-1
16	4	0	0	0
8	5	1	0	1
1	6	-1	-1	0
14	7	0	0	0
10	8	0	1	-1
7	9	-1	0	1
2	10	1	-1	0
13	11	0	0	0
11	12	0	-1	1
6	13	1	0	-1
5	14	-1	0	-1
4	15	1	1	0
12	16	0	1	1
15	17	0	0	0

VITA

PATRICIA A. QUIGLEY

EDUCATION:

Old Dominion University – Department of Engineering Management, 5115 Hampton Boulevard, Norfolk, VA 23529

Old Dominion University – Ph.D. Engineering Management Courses:

Robust Engineering Design, Research Methods, Methods for Rational Decision Making, Systems Analysis

Old Dominion University – M.S Engineering Management (12/12)

Strayer University – B.S. Computer Information Systems (3/07)

Community College Air Force - A.A.S. Aerospace Control & Warning Systems (5/85)

Thomas Nelson Community College - A.A.S. Mechanical Engineering (5/92)

Community College of the Air Force - A.A.S. Avionics Systems (7/11)

EMPLOYMENT HISTORY:

Company: NASA/CSC/SAIC/SSAI - FEB 1998 to present

Position: Functional Test Engineer/Computer Programmer/Analyst/System Administrator

Company: NASA/Analytical Services and Materials - SEP 1995 to FEB 1998

Position: Assistant Research Scientist

Company: Lockheed Engineering and Science Corporation - OCT 1992 to SEP 1995

Position: Engineer Aide

MILITARY EXPERIENCE:

Active duty Air Force – 1979 – 1987 – Aerospace Control and Warning Systems

Army National Guard – JAN 87 – JAN 90 – Artillery Unit

Air National Guard – 19 FEB 08 – PRESENT (F22 Avionics)